Wind Turbine Sizing For Offshore Wind Farms

Mehta, M.K.

DOI
10.4233/uuid:4daa4406-74a2-468b-9753-d49f6aef718c

Publication date
2025

Document Version
Final published version

Citation (APA)
Mehta, M. K. (2025). *Wind Turbine Sizing For Offshore Wind Farms*. [Dissertation (TU Delft), Delft University of Technology]. https://doi.org/10.4233/uuid:4daa4406-74a2-468b-9753-d49f6aef718c

Important note
To cite this publication, please use the final published version (if applicable).
Please check the document version above.

WIND TURBINE SIZING FOR OFFSHORE WIND FARMS

MIHIR MEHTA

Propositions

accompanying the dissertation

Wind turbine sizing for offshore wind farms

by

Mihir Kishore Mehta

1. From an economic perspective for wind farm developers, the benefits of further turbine up-scaling are marginal. (*This proposition pertains to this dissertation*)
2. Levelized Cost of Energy (LCoE) remains the best metric for turbine design at the wind farm level. (*This proposition pertains to this dissertation*)
3. The mechanics that drive turbine sizes towards low-specific power for low wind speed regions, profitability, or for hydrogen production are effectively the same. (*This proposition pertains to this dissertation*)
4. For turbine sizing, uncertainties arising from the use of low-fidelity models may affect the absolute value of the optimum but do not significantly alter overall trends. (*This proposition pertains to this dissertation*)
5. Addressing climate change requires fixing policies and markets, not inventing new technology.
6. The value of research on climate change lies more in its practical relevance than in its pursuit of scientific understanding.
7. Given the evident positive bias in published research, there should be journals for reporting negative or null results.
8. The ability to formulate an opinion is more valuable than merely holding one.
9. Personal experiences or observations should serve as catalysts for further inquiry rather than as bases for generalized conclusions.
10. Most arguments against veganism contain logical fallacies or are factually inaccurate.

These propositions are regarded as opposable and defendable, and have been approved as such by the promotors Prof.dr. D.A. von Terzi, Prof.dr. S.J. Watson, and the copromotor Dr.ir. M.B. Zaayer.

Wind Turbine Sizing for Offshore Wind Farms

Wind Turbine Sizing for Offshore Wind Farms

Dissertation

for the purpose of obtaining the degree of doctor
at Delft University of Technology,
by the authority of the Rector Magnificus, prof.dr.ir. T.H.J.J. van der Hagen,
chair of the Board of Doctorates,
to be defended publicly on Tuesday 28 October 2025 at 15.00

by

Mihir Kishore MEHTA

Master of Science in Sustainable Energy Technology,
Delft University of Technology, the Netherlands,
born in Vadodara, Gujarat, India.

This dissertation has been approved by the candidate's promotors.

Composition of the doctoral committee:

Rector Magnificus,	chairperson
Prof.dr. D.A. von Terzi,	Delft University of Technology, promotor
Prof.dr. S.J. Watson,	Delft University of Technology, promotor
Dr.ir. M.B. Zaayer,	Delft University of Technology, copromotor
Independent members:	
Prof. dr. ir. J.W. van Wingerden,	Delft University of Technology
Prof. dr. C.L. Bottasso,	Technical University of Munich, Germany
Prof. dr. M. Kühn,	University of Oldenburg, Germany
Prof. dr. M. Muskulus,	Norwegian University of Science and Technology, Norway
Prof. dr. ir. L.L.M. Veldhuis,	Delft University of Technology, reserve member

Keywords: Offshore wind farms, wind turbine sizing, techno-economic analysis of offshore wind

Front: Photo by Mihir Mehta

ISBN 978-94-6518-127-1
An electronic version of this dissertation is available at
http://repository.tudelft.nl/.

Contents

Acknowledgments

Earning a doctorate can sometimes appear to be the achievement of an individual alone. In reality, countless people, knowingly or unknowingly, have contributed to this milestone. Of course, luck and privilege also played a role along the way!

In shaping both this thesis and me, my supervisors, Michiel Zaaijer and Dominic von Terzi, played the most pivotal roles. After completing my master's thesis on rotor optimization with Michiel, I knew that if I chose to remain in academia, I would not find a mentor better suited for me. Your profound understanding of every aspect of the wind energy domain, combined with your patience in explaining even the most intricate details, makes you not only an exceptional researcher, but also a remarkable teacher and a generous human being.

Dominic, it has been a true pleasure to have you as my mentor. Your vision and your ability to connect countless dots have consistently ensured that my research remained relevant and impactful. Your insights, whether on the finer details of the content or the overarching storyline, have always been invaluable. Transitioning from a broad, open-ended topic on hybrid systems to the depth of wind turbine sizing, while achieving results that hold practical significance, would not have been possible without the guidance and support of both of you.

Simon, thank you for helping to improve the quality of this thesis. I have always enjoyed our conversations about wind energy and its wider implications for the energy system, and I am grateful for the opportunities you have provided. A special thanks to Sebastian Moreno for developing the Python-based MDAO framework that formed the foundation of my work, and to Tanuj for extending it further. Let's make WINDOW great again! Sylvia, thank you for being the backbone of the department and for always ensuring that processes ran smoothly for us.

Starting my PhD in the wind energy group while most others were finishing theirs was an interesting experience. The initial spark of excitement was quickly met with a dose of realism. Nevertheless, it was a truly rewarding beginning, and I definitely missed the post-lunch card game sessions. Thanks to Sebastian, Mikko, Bedassa, Navi, Vinit, Christopher, Mark, and Ashwin for making the first year so memorable. Jingna, it was wonderful to begin this journey alongside you. Rishi and Deepali, this PhD would not have been half as enjoyable without your company—cheers to many more laughs at Bombay Corner. Nils, I am glad to have shared this entire journey with you. Matteo, thank you for being my MDAO sparring partner and so much more. David, your humor will be missed-

keep those memes coming! Kiran, your company was always a delight—thank you also for the small talk lessons. Erik, you continue to be an inspiration. Adhyanth, Shyam, and Simone, thank you for keeping my Instagram content in check. Anand, I will always value our deep discussions. Finally, to everyone who made the office commute worthwhile—Mehtab, Likhita, Guanqun, Abhyuday, Jelle, Livia, Ali, Ricardo, Abhratej, and many others—thank you for being part of this journey.

Most of my PhD years unfolded during the Covid period, and I would not have made it through without the support of my close friends from graduation, Neel and Nilay. Thank you for always being there—for both the tech talks and the trash talks. I am also grateful to Husain and Sakina for all the memorable times we shared, and to Kaushal, Aditi, and Arundhati for the fun evenings and deep discussions. Arvind, thank you for being my tax consultant, Apple salesman, and, above all, a wonderful friend. And to Asvin, Lakshmi, and Riya, thank you for all the game nights—we definitely need more of those! Jeevan and Suhasini, thank you for making life in Delft fun and happening.

Dance has always been an important part of my life, and teaching workshops across the Netherlands allowed me to meet one of the best dancers I know—Prachi. Thank you for all the inspiration. Piyush, Prachi, and little Maahi, thank you for being friends who feel like family. Nikhita and Preeti, thank you for all the quirks, the chai sessions, the trash talks—and for letting me be a part of them.

I was also fortunate to work at one of Europe's leading wind farm developers in the period following the four years of my PhD, leading up to my defense. José, thank you for placing your trust in me. Your curiosity, depth of knowledge, and ability to communicate with clarity have been truly inspiring. To my Vattenfall colleagues—Emiel, Kirsten, Sylvie, Benjamin, Yannan, Lasse, Flavio, Ritika, Jan, Al, Hans, Joram, Jean-Luc, Siddharth and Helena—thank you for constantly motivating me and making life at Vattenfall both meaningful and enjoyable. A special thanks to Michiel for being my sparring partner in all discussions related to the energy transition.

A strong structure rests on a solid foundation, and for me, that foundation has always been my family. I cannot thank my parents enough for their unwavering support, their trust in every major life decision, and their constant effort in making it all possible. Thank you to Dadu and the rest of my family for always being there for me. I am equally grateful to my in-laws for their constant encouragement, support, and care throughout this journey. And finally, to my life partner and dance partner, Reshma—thank you for standing by my side through every high and low. This achievement would not have been possible without you. Lovey!

Mihir
Delft, October 2025

Summary

Offshore wind is poised to become a major source of electricity in a decarbonized future. However, one of the key challenges in achieving offshore wind targets is its high cost of energy. Advances in turbine scaling, along with technological innovations and economies of scale, have led to significant cost reductions. Additionally, the focus of design optimization has shifted from solely refining rotor design to minimizing the Levelized Cost of Electricity (LCoE) at the wind farm level. To assess whether further upscaling of the turbine is beneficial, it is essential to first understand the key drivers of turbine sizing and evaluate their impact on LCoE of the wind farm. In a subsidy-free market, the value of each kilowatt-hour varies, requiring developers to design turbines and farms that maximize revenue. For wind farms dedicated to hydrogen production, the objective shifts to minimizing the Levelized Cost of Hydrogen (LCoH). This research first identifies the factors that influence turbine size from an LCOE perspective and establishes a methodology to assess its impact on wind farms. It then explores how turbine sizing differs when optimizing for revenues and hydrogen production compared to a turbine sized for LCoE. The main research question that the thesis tries to answer is the following:

'What drives the optimal size of wind turbines for future offshore wind farms?'

To answer this question, the research uses a Multi-Disciplinary Design Analysis and Optimization (MDAO) based framework where various disciplines of the wind farm are modeled and coupled. A change in turbine size has major implications at the farm level as it impacts turbine costs, support structure costs, operations and maintenance costs, gross production, wake losses, etc. The framework captures the variations in costs and production or revenue with the design variables, while also accounting for all the interactions between the various disciplines. The two primary design variables for turbine sizing are rated power and rotor diameter. The framework is executed as an analysis block across a discrete set of rotor diameter and rated power values. As a case study, a hypothetical wind farm in the North Sea is analyzed, with an equality constraint applied to both the farm area and the farm rated power. Additionally, a sensitivity analysis is conducted to assess the impact of different modeling assumptions, constraint values, and constraint formulations.

The framework is initially applied to optimize turbine sizing to minimize the Levelized Cost of Electricity (LCoE) of the wind farm. The results show that turbines with a higher rating and a smaller rotor (high specific power) reduce overall costs by

requiring fewer turbines (due to the farm power equality constraint) and lowering per-turbine costs. In contrast, turbines with a lower rating and a larger rotor (low specific power) enhance Annual Energy Production (AEP) by increasing output in the partial load region. LCoE exhibits significant variation along the direction of changing specific power, whereas changes in LCoE remain minimal along the direction of constant specific power. For the baseline assumptions, the optimum turbine size w.r.t. LCoE is found to have a rating of around 15-16 MW with a rotor size of about 230 m. A sensitivity analysis is conducted on key assumptions such as wind speed, farm power density, model parameters, etc. The findings reveal that LCoE and optimal turbine size are most sensitive to wind speeds, while modeling assumptions tend to shift the optimal design in the constant specific power direction, where LCoE variations are negligible.

To simulate a subsidy-free scenario in which the value of each kWh produced is not the same, a simplified market model is coupled to the framework. The simplified market model takes the following inputs: mean spot price, standard deviation, and expected correlation between wind speeds and spot price. Given a set of wind speed values, the model samples spot prices from a normal distribution, using the mean and standard deviation provided, while maintaining the specified correlation between wind speeds and prices. The optimization problem is formulated for revenue-based objectives, such as Modified Internal Rate of Return (MIRR), Profitability Index (PI), and Net Present Value (NPV), while maintaining the same design variables and constraints as that of the LCoE optimisation. The response surface for MIRR and PI is found to be similar to those of LCoE. It is seen that a variation in the mean spot price pushes the optimum along the direction of constant specific power, while the correlation coefficient pushes the optimum along the direction of changing specific power. Hence, for a region with a high anti-correlation between wind speeds and spot prices (due to a high wind penetration), a lower specific power turbine performs better. However, the gains are minimal.

Lastly, a large portion of offshore wind might be required for dedicated hydrogen production to replace the existing gray and black hydrogen production that uses fossil fuels. A hydrogen production module that includes the electrolyzer along with the auxillary equipment is coupled to the existing framework. The optimization problem is formulated to minimize the Levelized Cost of Hydrogen (LCoH). As most of the costs are for electricity production, the response surface for LCoH is similar to that of LCoE. The cost of the hydrogen production system is significant and is proportional to the rated power of the turbine. Hence, the total cost does not change with the turbine size as the farm power is constant. The high costs of the hydrogen production system push the optimum toward low specific power turbines compared to the LCoE optimum, since the relative weightage of

every kWh produced is increased.

In general, this research presents a methodology for analyzing the drivers of turbine sizing and demonstrates how different assumptions and constraints affect the optimal size. Furthermore, the thesis highlights that the benefits of continuous turbine upscaling are marginal, reinforcing the preference for standardization over further scaling.

Samenvatting

Offshore windenergie staat op het punt een belangrijke bron van elektriciteit te worden in een koolstofarme toekomst. Een van de grootste uitdagingen om de doelstellingen voor offshore wind te realiseren zijn echter de hoge kosten van energie. Dankzij opschaling van turbines, technologische innovaties en schaalvoordelen zijn de kosten aanzienlijk gedaald. Bovendien is de focus van ontwerpoptimalisatie verschoven van uitsluitend het verfijnen van het rotorontwerp naar het minimaliseren van de genivelleerde electriciteitskosten (Levelized Cost of Electricity, LCoE) op windparkniveau. Om te beoordelen of verdere opschaling van turbines voordelig is, is het essentieel om eerst de belangrijkste drijfveren voor hun dimensionering te begrijpen en hun impact op de LCoE van het windpark te evalueren. In een subsidie-vrije markt varieert de waarde van elke kilowattuur, waardoor ontwikkelaars turbines en windparken moeten ontwerpen die de opbrengsten maximaliseren. Voor windparken die volledig gericht zijn op waterstofproductie verschuift het doel naar het minimaliseren van de genivelleerde kosten van waterstof (Levelized Cost of Hydrogen, LCoH). Dit onderzoek identificeert eerst de factoren die de grootte van turbines beïnvloeden vanuit een LCoE-perspectief en stelt een methodologie op om de impact op windparken te beoordelen. Vervolgens wordt onderzocht hoe de optimale grootte van turbines verandert wanneer er wordt geoptimaliseerd voor opbrengsten en waterstofproductie, vergeleken met de grootte van een turbine die is geoptimaliseerd voor LCoE. De centrale onderzoeksvraag van dit proefschrift luidt:

‘Wat bepaalt de optimale grootte van windturbines voor toekomstige offshore windparken?’

Om deze vraag te beantwoorden wordt een raamwerk voor multidisciplinaire ontwerwerpanalysis en optimalisatie (Multi-disciplinary Design Analysis and Optimization, MDAO) framework toegepast waarin verschillende disciplines van het windpark worden gemodelleerd en gekoppeld. Een verandering in de grootte van de turbine heeft grote implicaties op parkniveau, omdat dit de kosten van de turbines en ondersteuningsconstructies, exploitatie- en onderhoudskosten, bruto-opbrengst, zogverliezen, enz. beïnvloedt. Het raamwerk legt de variaties in kosten en productie of opbrengst vast als functie van de ontwerpvariabelen, waarbij ook alle interacties tussen de disciplines in rekening worden gebracht. De twee primaire ontwerpvariabelen voor dimensionering van een turbine zijn het nominaal vermogen en

de rotordiameter. Het raamwerk wordt uitgevoerd als een analyseblok over een discrete set rotordiameters en vermogens. Als casestudy wordt een hypothetisch windpark in de Noordzee geanalyseerd, waarbij zowel het parkoppervlak als het nominale parkvermogen als randvoorwaarden worden opgelegd. Daarnaast wordt een gevoeligheidsanalyse uitgevoerd om de impact van verschillende modelaannames, randvoorwaarden en formuleringen te beoordelen.

Het raamwerk wordt eerst toegepast om de grootte van de turbine te optimaliseren met als doel de LCoE van het windpark te minimaliseren. De resultaten laten zien dat turbines met een hoger vermogen en een kleinere rotor (hoge vermogensdichtheid) de totale kosten verlagen door minder turbines te vereisen (wegens de tijdens bedrijf op deelvermogen op het parkvermogen) en lagere kosten per turbine te realiseren. Daarentegen verhogen turbines met een lager vermogen en een grotere rotor (lage vermogensdichtheid) de jaarlijkse energieproductie (Annual Energy Production, AEP) doordat ze meer opwekken tijdens bedrijf op deelvermogen. LCoE varieert sterk in de richting van veranderende vermogensdichtheid, terwijl de variatie minimaal is langs de richting van constante vermogensdichtheid. Voor de uitgangsaannames blijkt de optimale turbinegrootte voor LCoE rond 15–16 MW te liggen, met een rotordiameter van circa 230 m. De gevoeligheidsanalyse laat zien dat LCoE en de optimale turbinemaat het meest gevoelig zijn voor windsnelheden, terwijl modelaannames de optimale oplossing vaak verschuiven langs de richting van constante vermogensdichtheid, waar de LCoE-variatie verwaarloosbaar is.

Om een subsidie-vrij scenario te simuleren waarin de waarde van elke geproduceerde kWh varieert, wordt een vereenvoudigd marktmodel gekoppeld aan het raamwerk. Dit model gebruikt als input: gemiddelde stroomprijs, standaardafwijking, en de verwachte correlatie tussen windsnelheden en stroomprijzen. Voor een set windsnelheden genereert het model stroomprijzen uit een normale verdeling, met de opgegeven parameters en de gewenste correlatie. De optimalisatie wordt vervolgens uitgevoerd voor opbrengstgerichte doelstellingen zoals aangepaste interne rentevoet (Modified Internal Rate of Return, MIRR), einstgevendheidindex (Profitability Index, PI) en netto contante waarde (Net Present Value, NPV), met dezelfde ontwerpvariabelen en randvoorwaarden als de LCoE-optimalisatie. De resultaten tonen dat het profiel van MIRR en PI sterk lijkt op dat van LCoE. Variaties in de gemiddelde stroomprijs verschuiven het optimum in de richting van constante vermogensdichtheid, terwijl de correlatiecoëfficiënt het optimum verschuift langs de richting van veranderende specifieke vermogensdichtheid. In regio's met een sterke anti-correlatie tussen windsnelheden en stroomprijzen (bijvoorbeeld door hoge windpenetratie) presteren turbines met lage vermogensdichtheid beter, al is de toename marginaal.

Tot slot zal een groot deel van de offshore windproductie mogelijk nodig zijn voor waterstofproductie ter vervanging van de huidige grijze en zwarte water-

stofproductie uit fossiele brandstoffen. Hiervoor wordt een waterstofproductiemodule, bestaande uit een elektrolyse apparaat en hulpsystemen, gekoppeld aan het raamwerk. Het optimalisatieprobleem wordt hierbij opgesteld om de LCoH te minimaliseren. Omdat de meeste kosten samenhangen met elektriciteitsproductie, vertoont het profiel voor LCoH veel gelijkenis met die van LCoE. De kosten van het waterstofsysteem zijn aanzienlijk en evenredig met het nominaal vermogen van de turbine. Hierdoor verandert de totale kostprijs niet met de grootte van de turbine, omdat het totale parkvermogen constant blijft. De hoge kosten van het waterstofsysteem verschuiven het optimum naar turbines met een lage vermogensdichtheid in vergelijking met het LCoE-optimum, aangezien elke geproduceerde kWh zwaarder meeweegt.

Samenvattend presenteert dit onderzoek een methodologie om de drijfveren van de dimensionering van turbines te analyseren en toont het hoe verschillende aannames en randvoorwaarden de optimale grootte beïnvloeden. Daarnaast benadrukt dit proefschrift dat de voordelen van voortdurende opschaling van turbines marginaal zijn, en onderstreept het de voorkeur voor standaardisatie boven verdere opschaling.

Nomenclature

Acronyms

AEP	Annual Energy Production
BEM	Blade Element Momentum
BoP	Balance of Plant
BoS	Balance of System
CoVE	Cost of Valued Energy
CV	Coefficient of variation
HHV	Higher heating value of hydrogen
IEA	International Energy Agency
LCoE	Levelized Cost of Electricity
LCoH	Levelized Cost of Hydrogen
LUT	Lookup table
MDAO	Multi-disciplinary Design Analysis and Optimization
MIRR	Modified Internal Rate of Return
NPV	Net Present Value
O&M	Operations & Maintenance
PI	Profitability Index
PPA	Power Purchase Agreements
VF	Value factor
XDSM	eXtended Design Structure Matrix

Greek symbols

α	Scaling factor for non-material blade costs
$\eta_{\text{electrolyzer}}$	Electrolyzer efficiency
γ_{mass}	Weightage of blade material costs
λ_{spot}	Spot price time series
λ_{wake}	Wake losses
μ_{spot}	Mean spot price
$\rho_{\text{correlation}}$	Correlation between wind speeds and spot prices
σ_{spot}	Standard deviation of the spot prices
τ_{rated}	Rated torque of the turbine
θ_{d}	Wind direction time series
θ_{L}	Orientation of the layout
ξ_{site}	Various site parameters
$\zeta_{\text{electrolyzer}}$	Electrolyzer to turbine sizing ratio

Other symbols

CF_{cable}	Cost per unit length for cables
$\text{CF}_{\text{pipeline}}$	Cost per unit length for hydrogen pipelines
A_{farm}	Farm area
A_{nacelle}	Nacelle frontal area
C_{cable}	Cost of the cable
C_{CAPEX}	Total capital expenditure
$c_{\text{D,nacelle}}$	Drag coefficient of the nacelle
C_{day}	Vessel day-rate
C_{DECOM}	Decommisioning costs
C_{dev}	Total project development and management costs

C_{gen}	Cost of the generator
$C_{\text{installation}}$	Total costs of installation
$C_{\text{mobilization}}$	Cost of mobilizing the vessels
C_{OPEX}	Total operations & maintenance costs
C_{other}	Other costs during turbine procurement, installation, and commissioning
$C_{\text{preventive}}$	Cost of preventive maintenance
$C_{\text{replacement}}$	Cost of component replacement
C_{rotor}	Cost of the rotor
$C_{\text{substation}}$	Total substation costs
c_P	Power coefficient
c_T	Thrust coefficient
D	Rotor diameter
d_{grid}	Distance to the onshore grid connection point
d_{harbor}	Distance to the harbor
D_{monopile}	Monopile diameter
D_{pipeline}	Diameter of the pipeline
D_{tower}	Tower base diameter
D_{yaw}	Yaw bearing diameter
F	Failure rates per turbine
H_{hub}	Hub height, measured relative to the mean sea level
I_{rated}	Rated current of the turbine
L	Wind farm operational lifetime
L_{cable}	Length of the infield cable
L_{monopile}	Length of the monopile
L_{tower}	Length of the tower

L_{tp}	Length of the transition piece
M_{gen}	Mass of the generator
m_{H_2}	Annual hydrogen production
M_{RNA}	Mass of the rotor nacelle assembly
M_{rotor}	Mass of the rotor
M_{support}	Mass of the support structure
N_{trips}	Total number of trips to the site made by the vessel during installation
N_{T}	Number of turbines
P	Rated power
$P_{\text{compressor}}$	Compressor rated power
P_{farm}	Farm rated power
Q	Hydrogen flow rate
R	Rotor radius
r	Real discount rate
R_{spot}	Total revenues earned in the spot market
$t_{\text{installation}}$	Total installation time
$t_{\text{replacement}}$	Time taken for component replacements
T_{rotor}	Rotor thrust
t_{travel}	Time taken by the vessel to travel to the site
U_{rated}	Rated wind speed of the turbine
u_{w}	Wind speed time series
$x_{\text{i}}, y_{\text{i}}$	Turbine coordinates
y_{tip}	Tip clearance
z_{platform}	Height of the platform, measured relative to the seabed
$z_{\text{tp,base}}$	Height of the transition piece base, measured relative to the seabed
z_{water}	Water depth

1

Introduction

We are the first generation to feel the effect of climate change and the last generation who can do something about it.

Barack Obama

This research involves the exploration of wind turbine design for various scenarios, ultimately resulting in several meaningful and relevant conclusions that could be beneficial for all stakeholders of offshore wind.

This chapter first highlights the importance of offshore wind. Then, it discusses how the size of wind turbines has increased significantly over the years, resulting in several cost reductions. The chapter continues by reviewing the optimization objectives and constraints used in the past and at present, and how those will change in the future.

This leads to the formulation of the key research questions that are answered in this research. The methodology that will be used to answer these questions is also briefly discussed.

Finally, the outline of the thesis is presented where the contribution of each chapter is listed.

1

1.1 Importance of offshore wind

The electrification of sectors is crucial for tackling climate change, requiring most electricity to come from low-cost renewables, mainly wind and solar. The potential of near-shore offshore wind alone is higher than the current total global electricity demand [1]. Wind energy is expected to provide a third of the expected electricity needs by 2050 with an installed capacity of about 6000 GW [2]. The expected share of wind can only be achieved by exploiting the ocean area offshore with relatively steady and high wind speeds. Limited land availability and fewer social acceptance issues further make the case for offshore wind. The massive targets for offshore wind also demand continuous innovation and cost-reduction. In recent years, the cost of energy for offshore wind has already observed a significant reduction. Figure 1.1, adapted from the International Energy Agency (IEA), shows the drop in the strike price over the years for Europe, including recently tendered projects. The strike price refers to the price paid to the wind developer, which can be used as an indication of the Levelized Cost of Electricity (LCoE) of the respective wind farms.

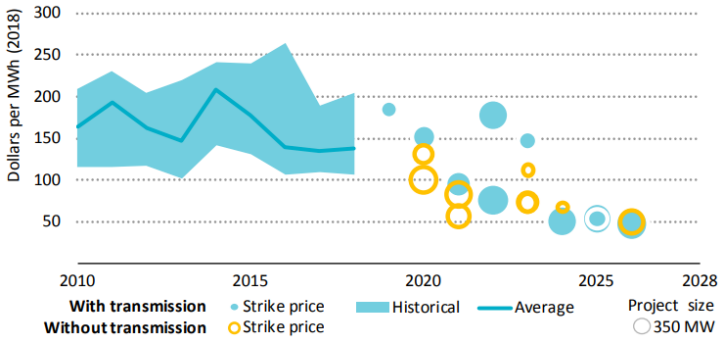

Figure 1.1: Decreasing trend of strike price in Europe (Figure from IEA [1])

The LCoE of offshore wind for some upcoming farms in the Dutch waters, without the grid connection, is already close to 50 €/MWh [3, 4]. These cost reductions in offshore wind can be largely attributed to upscaling of turbines, and declining Operations and Maintenance (O&M) costs [2, 5, 6]. Advancements in turbine technology over time have improved both costs and performance. However, turbine power coefficients are approaching the Betz limit, which may constrain further optimization opportunities in rotor design. Therefore, system-level optimization of turbines and wind farms is essential to drive further cost reductions and support the intended scale of deployment.

1.2 Growth in wind turbine sizes

The cost reductions in offshore wind can be largely attributed to upscaling of turbines [1, 2, 5, 6]. The upscaling process has increased the capital costs of the turbines with an upside of lower O&M and installation costs, ultimately reducing the LCoE [1]. The increased hub height with the upscaling of turbines allows the turbines to capture higher average wind speeds, increasing the overall Annual Energy Production (AEP), which contributes to the reduction of LCoE. Other factors like technology improvements, better maintenance strategies, etc. also contribute towards the reduction of LCoE. The increase in turbine sizes over the years, illustrated by IEA, is shown in Figure 1.2[1], where the asterisks in the image represent the turbine sizes announced and expected in the future.

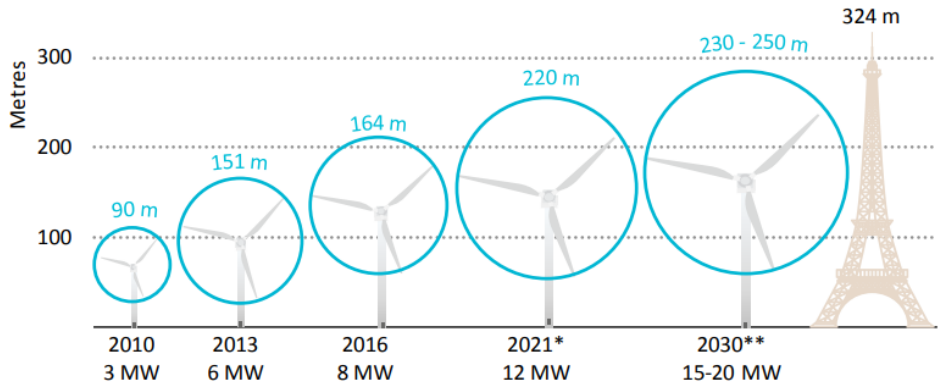

Figure 1.2: Evolution of turbine sizes over the years (Figure from [1])

The largest turbines currently in the prototype phase from manufacturers in China already exceed the expected values presented in the illustration. Some newer turbines also offer higher capacity factors compared to some old designs, which can be attributed to a lower specific power of the new designs. This could be better for the overall electricity system as a higher capacity factor wind farm could potentially serve as a baseload. For the same rated power, designs with a higher capacity factor result in a higher AEP but also result in higher costs.

However, growing turbine sizes come with challenges in rotor design, turbine installation, supply chain, etc. On the flip side, it could be more beneficial to standardize components instead of the continuous upscaling of turbines [7]. It is, therefore, important to understand if further upscaling of turbines would yield significant benefits to the energy system or to a wind farm developer.

[1]Image Source: IEA 2019; Offshore Wind Outlook, Link, License: CC BY 4.0

1

1.3 Change in design objectives and constraints

Over the years, optimization methods and metrics have changed and improved. At first, turbines were new elements in the grid system and needed to be demonstrated and developed on many fronts. They were valued for their score on primary performance indicators, such as reliability and energy yield. One of the consequences of this was a focus on the aerodynamic performance of the turbine, executed via maximizing the power coefficient (c_p) of the rotor. However, this metric would ignore the mass (and costs) of the rotor, resulting in relatively heavy structures. This was solved by minimizing the ratio of mass to the AEP. Although promising, this metric would not take into account the costs of various components. Andrew Ning et al. [8] and Chehouri et al. [9] discuss how various objective functions and constraints lead to different rotor designs. Then, turbines and farms were commercialized, but with support schemes that effectively resulted in an (almost) constant value of produced electricity. This led to a focus on the minimization of LCoE. Also, LCoE is a metric that is easy to calculate, covers all the aspects of a wind farm, and is hence universal in nature. It became the most widely adopted metric for optimization studies [10]. Various wind farms across different sites or even different technologies could be compared simply by looking at the LCoE values. Also, in subsidy-based auctions or Power Purchase Agreements (PPA) where nearly a fixed electricity price is ensured, minimizing the LCoE would effectively correspond with maximizing profit. In this era, turbines were often optimized for the support scheme, such as yielding exactly the amount of full-load hours that were subsidized in a year. However, the world is already moving towards a subsidy-free era with Hollandse Kust Noord being the first subsidy-free wind farm which will be start operating from 2025 onwards [11]. In a subsidy-free environment, the developer is exposed to the volatility of market prices. This goes away from the traditional subsidy-based approach where the wind farm developer would be ensured a fixed premium or price. The market prices, in fact, are observed to be negatively correlated with the country-wide wind generation, also known as the cannibalization effect. This is attributed to the merit order effect, where the low-cost renewables displace the expensive fossil-powered generators during instances of high renewable penetration. This price drop varies for different locations depending on the renewable penetration [12]. Also, it is expected that, in the future, revenues from capacity provision and ancillary services might be significant for wind farm developers [10]. Even though LCoE, as a metric, is useful and relevant, it fails to capture these price fluctuations and revenues. Another issue arises with the variability of wind power. Every unit of electricity produced by wind is not of the same value for the grid. For instance, an excess supply of wind during periods of low demand is not as valuable. Similarly, a low supply of wind during periods of high demand results in a high residual load. Hence, the contribution of every kWh toward the grid is not equally

valuable and this issue is not captured by LCoE [13]. The existing metrics also do not consider ecological issues or the overall lifecycle emissions, which are of great societal importance [14].

Electricity is just a part of the future energy system. To deal with energy-dense sectors where electrification may not be possible, a lot of research focuses on hydrogen as an energy carrier. Conventional hydrogen, known as gray or black hydrogen, is produced from fossil fuels, while green hydrogen is generated through electrolysis using electricity from renewable energy sources. Hydrogen finds its direct use in industries like steel, chemicals, transport, agriculture etc., and their demand is predicted to grow significantly [15]. It may also enable cost-efficient bulk transport of energy over large distances [16]. In any case, the existing gray and black hydrogen demand, of about 100 million tonnes per year [17], is significant, and that production needs to be replaced with green hydrogen. This makes it essential to produce low-cost emission-free green hydrogen. The technology for green hydrogen production via electrolysis is already in use. The key obstacle in producing green hydrogen at large scale lies in its production costs [18]. The Levelized Cost of Hydrogen (LCoH) for green hydrogen is still higher than the conventional hydrogen production costs, which can be mainly attributed to the high cost of renewable electricity required to produce hydrogen via electrolysis [18, 19]. However, with the declining costs of offshore wind and electrolyzers, green hydrogen is expected to be competitive with blue hydrogen, i.e. production from natural gas with carbon capture, by 2030 [20]. As the LCoH of green hydrogen production from wind is highly sensitive to the cost of electricity [21], it is crucial to reduce the costs of the wind farm. Designing turbines for dedicated hydrogen production may result in a lower LCoH than conventional turbines designed for electricity production. Hence, future turbines and farms should not only be designed to reduce costs but also to increase the overall economic and societal value. With this paradigm shift, it becomes crucial to revisit the design philosophy used for turbine and farm optimization.

1.4 Existing studies on turbine sizing

Most studies related to turbine optimization in a farm setting keep the rated power fixed and/or rotor diameter fixed, and the effect of upscaling the turbine itself is often not the focus. Ashuri et al. [22] optimized a 5 MW reference turbine and scaled it up to 10 MW and 20 MW to evaluate the effect on LCoE and find an increasing LCoE trend with upscaling. However, the costs for Balance of System (BoS) and O&M are assumed to simply scale with the rated power using a power function with a fixed value for the exponent. In reality, the interactions of the turbine with the other elements of the farm are much more complex and require modeling of all the elements of the wind farm. Sieros et al. [23] performed an

upscaling study for turbines in the range of 5-20 MW, with constant specific power, using classical similarity rules. The results showed an increase in the levelized production cost with turbine scale, if the same technology is used at all scales. However, the focus of the study was on a simplified upscaling method, especially for the turbine, while the models for the rest of the wind farm were expressed simply as a percentage of turbine costs. Shields et al. [24] studied the impact of turbine upscaling and plant upsizing on various farm-level parameters providing several valuable insights. They find a reduction in LCoE by up to 20% when upscaling turbines from 6 to 20 MW and upsizing the farm from a 500 MW capacity to a 2500 MW capacity. However, the study assumes a fixed cost per kW for the turbines and also limits the specific power of the turbines when upscaling. There is limited literature on turbine sizing for objectives beyond LCoE. Loth et al. [13] discuss the importance of designing for metrics beyond LCoE that account for time-varying electricity prices and propose newer metrics like Cost of Valued Energy (CoVE), for instance. Swisher et al. [25] show the benefits of very low-specific power turbines to the electricity system while Canet et al. [14] include life-cycle emissions into the design and shows the trade-offs w.r.t. the LCoE. However, a study explicitly focusing on turbine sizing for revenue-based metrics, that accounts for the effects of time-varying market prices, is missing. Thomas et al. [26] model a decentralized onshore wind-hydrogen system to optimize the turbine design for LCoH. The authors demonstrate that hydrogen-optimized turbines tend to have larger rotor diameters, with the optimal electrolyzer size closely matching the turbine's rated power. While the study offers valuable insights into wind-hydrogen systems, the scope is limited to a single onshore turbine and does not fully explore the reasons behind the design differences w.r.t. an LCoE-optimized design.

1.5 Research questions

It is clear that with these changing design objectives and constraints, turbine sizing needs to be revisited. The first step towards understanding that would be to take a deep look at the drivers for turbine sizing. The insights from that can then be used to understand how turbine sizing would change for other metrics or applications like hydrogen production. The main research question that this thesis tries to answer is,

'What drives the optimal size of wind turbines for future offshore wind farms?'

The future energy system constitutes a vast scope but this study focuses only on a few aspects. From a turbine perspective, the scope is limited to the sizing of an offshore fixed-bottom horizontal axis wind turbine, where sizing refers to the two defining parameters of the turbine, the rated power and the rotor diameter.

To answer the main research question, within the scope of this study, three sub-questions are formulated as listed below:

1. What drives the sizing of wind turbines for minimum LCoE of offshore wind farms?
2. What drives the sizing of wind turbines for economic objectives beyond LCoE?
3. What drives the sizing of wind turbines for minimum LCoH of offshore wind farms?

The first question is formulated to identify the drivers for turbine design using the widely used metric, LCoE. Secondly, turbine design for the economic objectives that include the market value of wind is explored. While the first two questions deal with electricity production, the third question is formulated to understand whether wind turbines should be designed differently for hydrogen production.

1.6 Thesis outline

Each chapter of this thesis serves as a building block toward answering the main research question. *Chapter 2* explains the modeling framework in detail, where all the dependencies and interactions between the models are discussed. *Chapter 3* applies this framework to understand and identify the key drivers of turbine design for the conventional metric, LCoE. This chapter is crucial in understanding how various factors and uncertainties affect turbine sizing. The insights are relevant to and are extended in the following chapters. *Chapter 4* extends the study to economic metrics beyond LCoE and answers the second sub-question. It discusses the dependency of the optimal turbine size on market scenarios and the metric used. *Chapter 5* answers the third sub-question by exploring the added benefit of designing turbines specifically for hydrogen production. Lastly, *Chapter 6* concludes the discussion by listing key insights of this research that are relevant to multiple stakeholders and are generic enough to be widely applicable. A visual representation of the thesis outline is shown below.

1

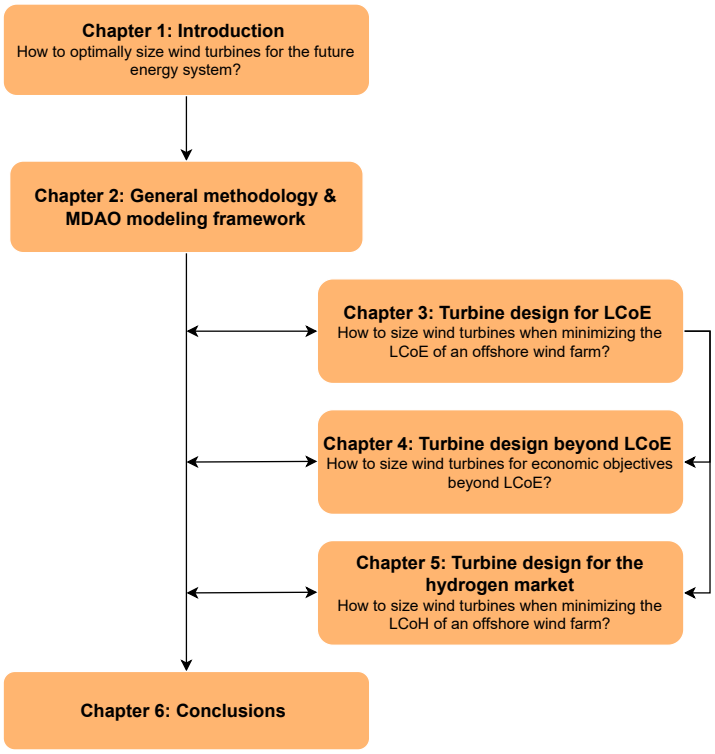

Figure 1.3: Thesis outline highlighting the common framework used to explore turbine sizing for LCoE, which serves as the baseline for objectives beyond LCoE.

2

Methodology and setup

Optimization is not just finding the best solution
it's about balancing trade-offs to meet real-world constraints

Dimitri P. Bertsekas

Designing a turbine for an offshore wind farm is a complex problem that involves the interaction of various sub-systems in a wind farm. A systems-engineering-based framework is required that can capture the trade-offs between different parts of the objective function. The framework essentially consists of models for every discipline, usually coupled with an optimizer. Depending on the use case, the user can decide the fidelity level of the models, and run the framework either as an analysis block or in an optimization loop.

This chapter first discusses the generic modeling approach along with the optimization problem formulation. A general description of the framework along with a visual representation in the form of an XDSM is shown in Section 2.4. For the purpose of this research, the focus is on the preliminary turbine design and hence, the framework consists of low-fidelity models for each discipline, explained in Section 2.5. The inputs of the models in the framework are discussed in Section 2.6. A description of the case study setup that will be used for the rest of the thesis is given in Section 2.7. Lastly, Section 2.8 shows the working of the different models by applying the input assumptions and case study description to the formulated problem.

2.1 Turbine sizing using Multi-disciplinary Design Analysis & Optimization

2

The problem of optimizing the turbine size for an offshore wind farm is complex, as changing the key specifications of the turbine impacts all elements in the farm. For instance, a change in the rated power of the turbine changes the current in the infield cables, and hence, cabling costs. If the farm power is given, changing the turbine rated power changes the number of turbines in the farm having a significant impact on O&M costs, installation costs, wake losses, etc. Similarly, any change in the rotor diameter affects the power and thrust curve of the turbine, impacting the support structure design, wake losses, etc. Hence, both key parameters of the turbine significantly affect both costs and AEP of the wind farm.

To understand the key drivers of turbine sizing, it is essential to develop and employ a systems engineering based multi-disciplinary framework that can capture farm-level effects. Such an approach is called Multi-disciplinary Design Analysis and Optimization (MDAO) where models of various disciplines, with possibly varying fidelities, are coupled with each other such that the interactions between the models are captured. The MDAO-based framework can function as an analysis tool or be integrated with an optimizer. An MDAO-based approach, initially developed for the aerospace industry, captures the trade-offs between various disciplines of a system and results in a better design, compared to traditional sequential optimization. The benefits of systems engineering towards reducing the cost of wind energy by using MDAO have been explored by various studies [22, 27–29]. An eXtended Design Structure Matrix (XDSM) of such a wind-farm level framework is shown in Figure 2.1.

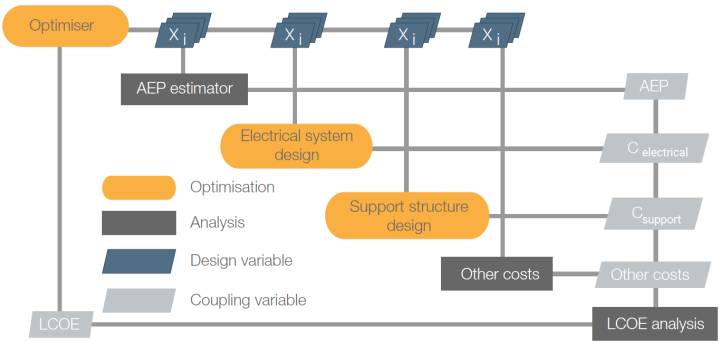

Figure 2.1: XDSM of a wind-farm level framework (Figure from Sanchez Perez Moreno [30])

To capture all the trade-offs at the farm level, especially due to a change in turbine design, an MDAO-based framework is crucial. The effect of changing turbine design on various farm-level elements like wake losses, electrical design,

support structure design, etc., can then be captured. Bortolotti et al. [31] developed reference wind turbines for onshore and offshore applications using such an MDAO-based framework. Dykes et al. [28] and Serafeim et al. [32] explored the optimization of the rotor for a turbine with a fixed rated power using the LCoE of the farm as the objective function.

2.2 Overview and rationale of the approach

For a turbine-sizing problem, capturing the essential trade-offs at a wind farm level is paramount, making the use of an MDAO-based approach that includes all disciplines in the wind farm inevitable. In an MDAO framework, coupled modules form an analysis block, which can be executed for a given set of inputs to evaluate a specific objective. This analysis block can be coupled with an optimization driver to explore the design space concerning a particular design variable. However, in this study, turbine-sizing is explored without coupling the analysis block to an optimization algorithm. Instead, the analysis block is executed for a set of design variable values using a brute-force approach.

The study also does not focus on the development of an MDAO-based framework per se but rather uses the framework as an analysis block to evaluate the LCoE of the farm for a given turbine configuration. The framework will be used to perform analyses that provide insights into the fundamentals of optimal turbine sizing. Some studies that applied MDAO to a turbine-optimization problem for a wind farm, along with the missing dependencies, are discussed in Chapter 1. The requirements of the model-fidelity for each discipline of the wind farm depend on the purpose of the study. For a turbine-sizing study with turbine rated power (P) and rotor diameter (D) as the design variables, it is key that the models for any given discipline respond correctly to the change in the design variables, directly or indirectly. For instance, an increase in the rated power results in a decrease in the number of turbines (if the farm power is kept constant), and as a consequence, results in lower O&M and installation costs. It is essential for the O&M and BoS models to capture these trends reasonably well. However, a model that assumes O&M costs to be a function of the farm rated power or a function of the turbine rated power like in Ashuri et al. [22], fails to capture the necessary trade-offs. Similarly, the turbine costs (including the support structure) change non-linearly w.r.t. changes in both the rotor diameter and rated power of the turbine. However, a model that scales the turbine costs linearly with the rated power, like in Shields et al. [24], does not capture the variations in turbine costs because of changes in the rotor diameter. This would significantly impact the findings and conclusions. Hence, it is crucial that the models for all the disciplines in the wind farm capture the dependencies on the design variables. Having low-fidelity models that can capture the essential trade-offs allows the user to quickly evaluate hundreds of

turbine designs. The purpose of the MDAO framework, in the context of this research, is not the accurate estimation of LCoE or the optimum design. The main purpose of the framework is to serve as an analysis block that captures the dependencies of various wind farm elements on the design variables and, hence, can be used in identifying the key drivers of turbine sizing. The drivers could be in the form of technology changes, farm conditions, or even policy-level changes, all of which could be identified and quantified with such a comprehensive framework. A summary of the key elements of the approach is given below.

- Model lowest necessary fidelity required for all wind farm disciplines
- Capture direct and indirect dependencies of each discipline on the design variables
- Capture interactions between different wind farm disciplines
- Analyze and visualize the response surface of the outputs
- Identify key drivers of turbine sizing by analyzing the sensitivity of the outputs to various inputs

In line with these considerations, the next sections first describe the optimization problem and the MDAO framework. The subsequent descriptions of the models focus on the dependencies that are identified to be relevant for this study, rather than on comprehensive mathematical descriptions.

2.3 General problem formulation

This section discusses the formulation of the optimization problem for a baseline case that represents constraint formulations and values, typical for an offshore wind farm in the North Sea. A sensitivity study to both the constraint formulation and the constraint values is also carried out and is presented in Chapter 3. The baseline problem is formulated as given in Equation (2.1) where the objective function is the LCoE of the offshore wind farm which is to be minimized w.r.t the rated power (P) and the rotor diameter (D) of the turbine. P_{farm} represents the rated power of the farm whereas A_{farm} represents the area of the farm.

$$\begin{aligned} \min \quad & \text{LCoE}(P, D) \\ \text{s.t.} \quad & P_{\text{farm}} = 1\,\text{GW} \\ \text{s.t.} \quad & A_{\text{farm}} = 150\,\text{km}^2 \end{aligned} \tag{2.1}$$

An equality constraint is implemented which keeps the farm rated power constant. This is usually the case for a tendered wind farm, where the grid connection

is a given. The constraint implies that with an increase in the rated power of the turbine, the number of turbines reduces to keep the farm power constant. An area equality constraint is also implemented, which represents a fixed plot of ocean area allocated to the developer to build the wind farm. As a result, the absolute spacing between the turbines depends on the number of turbines that are placed within the given area. These constraints are used for the baseline case as it is assumed to be the most representative of how current commercial wind farms in recent years have been tendered [33].

The design space w.r.t. the two design variables, rated power (P) and rotor diameter (D), is discretized due to the integer nature of the number of turbines. The step sizes, approximately 1 MW for rated power and 10 m for rotor diameter, are selected to match with typical changes in turbine platform specifications observed in the industry while also managing computational effort. The set of discrete points at which the full wind farm-level framework will be executed is shown in Figure 2.2. The selected rated power is approximately aligned with the 1 MW step size, ensuring an integer number of turbines that satisfies the 1 GW farm power constraint. On the secondary y-axis, it can be seen that to keep the farm power constant, the number of turbines reduces as the rated power of the turbine increases.

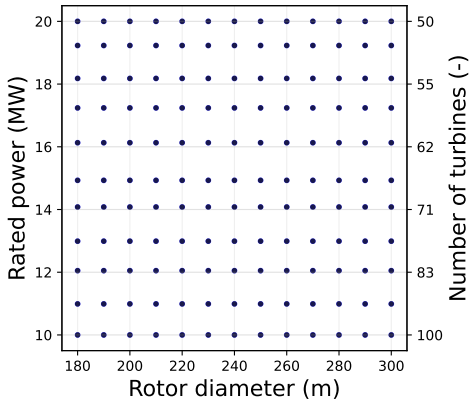

Figure 2.2: Complete design space showing all the combinations of rated power and rotor diameter

The objective is expected to have a smooth response surface, making such low-resolution sampling indicative enough. Also, the resolution of the brute-force optimisation is high enough to assess the effect of the design variables on the response surface and to identify the region where the optimum design can be found. Additionally, the number of discrete points for rated power is doubled near the apparent optimum to improve accuracy in capturing it. To evaluate a property of

interest for any given combination of rated power and rotor diameter, a polynomial surface is then fitted to the data at these discrete points. A finer step-size is then used to get an estimate of the optimum by identifying the minimum of a curve fit of the discretized surface.

2.4 General description of the framework

For this research, the MDAO-based framework developed by Tanmay [34] and Sanchez Perez Moreno [30] is expanded and updated. This framework is shown in Figure 2.3, where all the disciplines of a wind farm are modeled and coupled via coupling variables. The software is open source and can be accessed via the repository of Mehta [35]. The framework uses certain user inputs, highlighted by the white blocks. In this approach, the framework is used solely as an analysis block to explore the design space. The design variables, highlighted in the green blocks, are assigned specific discrete values during each function evaluation, which are then used to analyze the objective function and constraints.

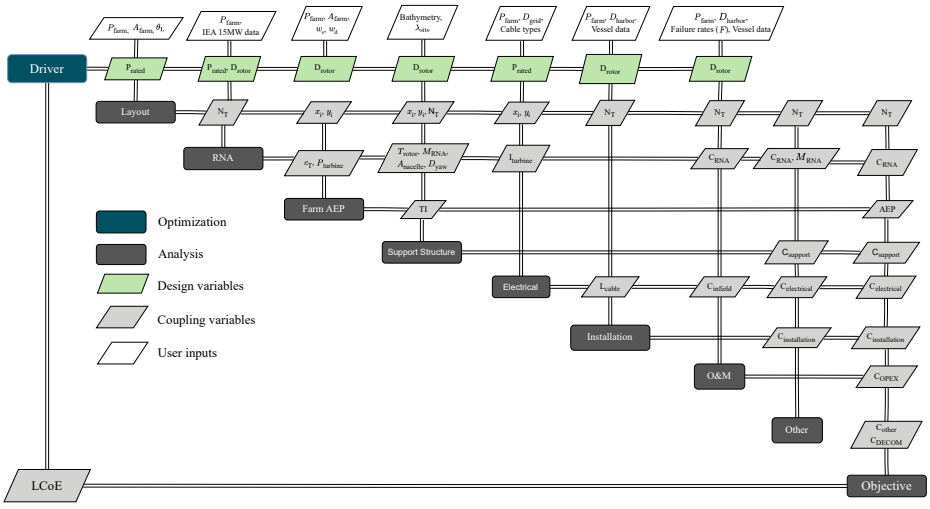

Figure 2.3: eXtended Design Structure Matrix (XDSM) of the MDAO framework.

2.5 Model description

This section provides a brief overview of all the models in the framework, highlighting the independent input parameters for each model. While this section focuses on a general description of the models, Section 2.8 demonstrates the behavior of the models for a given set of assumptions.

2.5.1 Layout

The layout module generates the wind farm layout by arranging the individual turbines based on a pre-defined arrangement. The dependencies of the layout are shown in Equation (2.2), where the turbine coordinates (x_i, y_i) are determined by the farm area constraint (A_{farm}), number of turbines in the farm (N_T), and the orientation of the entire layout (θ_L) governed by the dominant wind directions.

$$x_i, y_i = f(A_{farm},\ N_T,\ \theta_L) \tag{2.2}$$

In this study, for a given number of turbines, a layout closest to the nearest possible square arrangement is used, with residual turbines added in an incomplete row. Such a setup avoids boundary effects due to irregular layouts and ensures a fair evaluation of wake losses when comparing different turbine designs.

2.5.2 Rotor Nacelle Assembly (RNA)

The rotor aerodynamic performance is evaluated using the classic Blade Element Momentum (BEM) theory. The properties of a reference turbine are used as an input to determine the aerodynamic and structural performance and other RNA properties. The values of power coefficient (c_P) and thrust coefficient (c_T) in the partial load region are evaluated using the airfoil distribution, the normalized chord and twist profiles, and the tip speed ratio from the reference turbine. It should be noted that since the aerodynamic properties are the same as those of the reference, the resulting peak power and thrust coefficient are the same for all the designs. The rated wind speed of the turbine can then be determined followed by the evaluation of the power curve. The values used for the cut-in wind speed, cut-out wind speed, and the drivetrain efficiency (3 m/s, 25 m/s, and 94.5%, respectively) are the same for all turbine designs.

The rotor mass scaling model follows classical geometric scaling, where the reference turbine's mass scales with the cube of the rotor diameter, as both the cross section of the blade and the length scale up with the radius. This includes linear scaling of the internal layup of the blade with radius. This ensures that the tip deflection scales proportionally to the radius, which is the design driving criterion for large blades. This type of scaling is reasonable provided the specific power, and thus the rated wind speed remains constant. If the rated wind speed changes, the tip deflection, normalized with the rotor radius, would differ w.r.t. that of the reference design. The static tip deflection is primarily driven by the thrust loading at rated wind speed and stiffness of the blade. Since the thrust coefficient is the same for all the designs, the maximum static thrust is proportional to the square of the rated wind speed. The internal layup of the blade can be adjusted with the ratio of the rated wind speeds to compensate for the associated increase/decrease in the thrust, resulting in the same normalized tip deflection as that of the reference. The

model includes an additional factor to compensate for such differences in thrust loading as shown in Equation (2.3), where U_{rated} is the rated wind speed.

$$M_{\text{rotor}} = M_{\text{rotor,ref}} \cdot \left(\frac{D}{D_{\text{ref}}}\right)^3 \cdot \left(\frac{U_{\text{rated}}}{U_{\text{rated,ref}}}\right)^2 \tag{2.3}$$

The geometric scaling approach provides a comparison of designs that are conceptually equal. When using scaling coefficients derived from empirical relations, effects from changes in technology, materials, specific power, etc. would be included. This is considered undesirable for this study since it is unknown whether these effects may be extrapolated to a larger scale and what the underlying conceptual changes would be. The downside of geometric scaling is that it typically leads to sub-optimal designs.

To determine the cost of the scaled rotor (C_{rotor}), a simplified approach as shown in Equation (2.4) is used. A weight is given to the scaling of costs with blade mass (γ_{mass}) and to the non-mass related costs (1 - γ_{mass}), where the non-mass component includes tooling, labor, equipment, etc.

$$C_{\text{rotor}} = \gamma_{\text{mass}} \cdot C_{\text{rotor,ref}} \cdot \left(\frac{M_{\text{rotor}}}{M_{\text{rotor,ref}}}\right) + (1 - \gamma_{\text{mass}}) \cdot C_{\text{rotor,ref}} \cdot \left(\frac{D}{D_{\text{ref}}}\right)^{\alpha} \tag{2.4}$$

For the baseline case, a γ_{mass} of 0.6 is used, while a scaling exponent, α, of 2 is used for non-mass related aspects. These numbers are partially derived from the studies performed by NREL and Sandia National Laboratories [36–38].

The components of the nacelle include the bedplate, shafts, yaw system, electrical system, generator, etc. The cost of most components scales with mass, where the component mass is derived using the DrivetrainSE model [39]. The cost of the generator (C_{gen}) also scales up with the mass (M_{gen}), where the mass is proportional to the rated torque of the turbine (τ_{rated}), as shown in Equation (2.5).

$$C_{\text{gen}} \propto M_{\text{gen}} \propto \tau_{\text{rated}} \tag{2.5}$$

2.5.3 Annual Energy Production

The overall AEP of the farm depends on several factors, as shown in Equation (2.6). The Bastankhah Gaussian model [40] along with the squared sum model is used to estimate wind speed deficits and the wake superposition, respectively. The implementation from the PyWake library of Pedersen et al. [41] is used in the framework.

$$\text{AEP} = f(x_{\text{i}},\ y_{\text{i}},\ u_{\text{w}},\ \theta_{\text{w}},\ H_{\text{hub}},\ D,\ c_{\text{T}}\ \text{LUT},\ P_{\text{turbine}}\ \text{LUT}) \tag{2.6}$$

The wind speed and wind direction time series are represented as u_w and θ_w, respectively. The wind speed dataset used is at 100 m and is always projected, using the power law, to the hub height of the turbine design being analyzed. The thrust table of the turbine (c_T LUT) along with the wind speed, wind direction, and turbine coordinates is used to determine the wind speed deficit at each turbine. An illustration of the profile of the wind speed deficit behind a turbine, using the Bastankhah Gaussian model, is shown in Figure 2.4. As seen, for a freestream wind speed of 10 m/s, the wind speed deficit is the highest in the near wake region. The region around a normalized distance of 5D to 6D experiences some wake recovery and hence, the wind speed deficit is relatively lower.

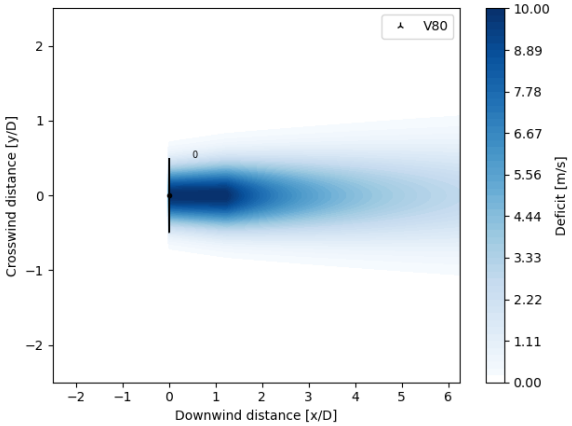

Figure 2.4: Wind speed deficit profile for the Bastankhah Gaussian model using a Vestas V80 turbine in the PyWake library [41]

To determine the overall wake losses, the 'Propagate Downwind' wind farm model in the PyWake library is used. In every iteration, the total wind speed deficit on a given turbine due to all upstream turbines is calculated using their effective wind speeds. This is quick to simulate, and for a given freestream wind speed, the effective wind speed for all the turbines in the farm can then be determined.

The power table ($P_{turbine}$ LUT) is then used to calculate the power at each turbine, summing up to give the instantaneous farm power. The sum of these instantaneous hourly farm power values over one year results in the overall AEP of the farm.

2.5.4 Support structure

The sizing module used for the design of support structures is based on the work of Zaaijer [42]. The cost model uses empirical cost factors, along with the obtained volume and mass values of the structure. Some of the dependencies of the model

are shown in Equation (2.7), followed by a detailed description of the model. The mass of the tower and foundation of a given turbine ($M_{\text{support,i}}$) depends on the local turbulence intensity (TI_i), the rotor diameter (D), hub height (H_{hub}), the maximum thrust on the rotor (T_{rotor}), the mass of the RNA (M_{RNA}), yaw bearing diameter (D_{yaw}), nacelle frontal area (A_{nacelle}) and its coefficient of drag ($c_{\text{D,nacelle}}$) to calculate the drag forces, and various site parameters (ξ_{site}). The site parameters include 50-year and 1-year extreme significant wave heights, storm surge, soil sieve size, soil friction angle, etc.

$$M_{\text{support,i}} = f(\text{TI}_\text{i},\ D,\ H_{\text{hub}},\ T_{\text{rotor}},\ M_{\text{RNA}},\ D_{\text{yaw}},\ c_{\text{D,nacelle}},\ A_{\text{nacelle}},\ \xi_{\text{site}}) \tag{2.7}$$

The tower length depends on the hub height (H_{hub}), which is defined relative to the mean sea level. It is determined by the rotor radius and the blade clearance w.r.t. the mean sea level, as shown in Equation (2.8).

$$H_{\text{hub}} = R_{\text{rotor}} + y_{\text{tip,water}} \tag{2.8}$$

To determine the tower length, the hub height must be expressed relative to the seabed. This can be done by adding the water depth (z_{water}) to the hub height. Since the platform height (z_{platform}) is defined relative to the seabed, the tower length follows from Equation (2.9).

$$L_{\text{tower}} = H_{\text{hub}} + z_{\text{water}} - z_{\text{platform}} \tag{2.9}$$

There is also a safety requirement in the form of a minimum clearance between the platform and the blade ($y_{\text{tip,platform}}$). However, the clearance of the blade from the water surface is set to be high enough to ensure the minimum clearance from the platform.

The length of the transition piece (L_{tp}) depends on the platform height (z_{platform}), which is set based on the maximum wave height with a clearance of 20%, and the base of the transition piece ($z_{\text{tp,base}}$), which is set to be slightly below the water line. Both are measured from the seabed. The monopile penetration depth ($L_{\text{monopile,penetration}}$) is set to be 10% larger than the clamping depth obtained using Blum's model for piles that undergo lateral loading. The total monopile length can be determined using Equation (2.10), as the sum of the monopile penetration depth, the length until the base of the transition piece ($z_{\text{tp,base}}$), and the overlap between the monopile and the transition piece ($L_{\text{monopile,overlap}}$).

$$L_{\text{monopile}} = L_{\text{monopile,penetration}} + z_{\text{tp,base}} + L_{\text{monopile,overlap}} \tag{2.10}$$

The aerodynamic and hydrodynamic loads and moments are calculated using the site characteristics and turbine data. The wind and wave loading is calculated

for normal operation and also for extreme conditions with a 1-year and 50-year occurrence period. Additional safety factors are introduced for ultimate loads and to compensate for fatigue. The combined wind-wave load cases include a regular operation of the turbine at rated wind speed with a maximum wave in a one-year extreme sea state, a parked turbine with reduced gust under a 50-year return period wind speed and maximum wave in a 50-year extreme sea state, and a parked turbine with a maximum gust under a 50-year return period wind speed and reduced wave in 50-year extreme sea state. The diameter of the monopile (D_{monopile}) is evaluated such that the maximum stress due to the combined wind-wave load cases is equal to the yield stress of steel. The diameter of the transition piece (D_{tp}) is set to be 300 mm larger than the diameter of the monopile. The thickness of the monopile is set to be around 1/100 times D_{monopile}. The tower top diameter is determined by the yaw bearing diameter (D_{yaw}) while the diameter of the tower base ($D_{\text{tower,base}}$) is set equal to the transition piece diameter. The thickness of the transition piece and the thickness of the tower segments are obtained using Brent's algorithm such that the maximum stresses due to the load are equal to the permissible values.

Once the geometric properties of the tower, transition piece, and monopile are known, the mass and costs are calculated using calibrated cost factors. The module also calculates the properties and costs of scour protection.

2.5.5 Electrical system

The model for the electrical system returns the cost of cabling and substations. A summary of the cost dependencies of the different components is shown in Equation (2.11).

$$C_{\text{cable,export}} = f(P_{\text{farm}},\ d_{\text{grid}}) \tag{2.11a}$$

$$C_{\text{cable,infield}} = f(L_{\text{cable}},\ I_{\text{turbine}}) \tag{2.11b}$$

$$C_{\text{substation}} = f(P_{\text{farm}}) \tag{2.11c}$$

The export cable costs are a function of the rated farm power (P_{farm}) and the distance to the onshore grid connection point (d_{grid}), as shown in Equation (2.12). The infield cable costs are determined using the infield cable length (L_{cable}) and the rated current of the turbine (I_{turbine}). The substation costs are a function of the rated farm power.

The length of the export cable is given by the distance between the offshore substation and the onshore grid connection point, taken as an input from the user (d_{grid}). For the cost of the export cable, a reference value for the cost per unit length ($C_{\text{cable,ref}}$) is scaled with the farm power and the distance to the grid.

$$C_{\text{cable,export}} = C_{\text{cable,ref}} \cdot P_{\text{farm}} \cdot d_{\text{grid}} \tag{2.12}$$

2

The infield cable length is calculated using the Esau-Williams heuristic module, which results in a branched topology, as implemented by Sanchez Perez Moreno [30]. For the infield cable, the rated current of the turbine (I_{turbine}) and the number of turbines in a string determine the total current in the string (I_{string}). The unit cost of the cable is driven by this total current. Turbines with higher power ratings have a higher rated current, resulting in a higher string current. This requires cables with larger cross-sectional areas and higher current-carrying capacities. The unit cost or cost factor (CF_{cable}) of various cable types as a function of the total string current is shown in Equation (2.13), where the costs are based on the work of Dicorato et al. [43]. The current is expressed in amperes (A), and the cost factor is in euros per meter (€/m). The variation of the cost factor is shown in Figure 2.5. The total infield cable costs can then be determined using Equation (2.14).

$$\text{CF}_{\text{cable}} = 0.0008 \cdot I_{\text{string}}^2 - 0.21 \cdot I_{\text{string}} + 198.5 \tag{2.13}$$

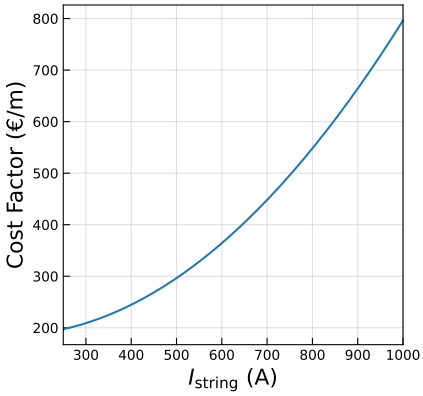

Figure 2.5: Cost of the infield cable as a function of string current

$$C_{\text{cable,infield}} = \text{CF}_{\text{cable}} \cdot L_{\text{cable}} \tag{2.14}$$

The substation costs ($C_{\text{substation}}$), as shown in Equation (2.15), have a fixed cost component (C_{fixed}) and a variable cost component (C_{variable}) that scales with the farm power.

$$C_{\text{substation}} = C_{\text{fixed}} + C_{\text{variable}} \cdot P_{\text{farm}} \tag{2.15}$$

$$\tag{2.16}$$

The total costs for the export cable and substation are fixed for any given turbine design in case of a farm power constraint. However, when there is no farm power constraint, these values scale with the farm power.

2.5.6 Installation

The installation cost model takes the vessel data as input to calculate the installation costs of the foundations, turbines, and electrical system. The dependencies are shown in Equation (2.17). The turbine installation cost ($C_{\text{installation,turbine}}$) also covers the tower installation, while the foundation installation costs ($C_{\text{installation,foundation}}$) include the installation of the monopiles and transition piece. The electrical equipment installation cost ($C_{\text{installation,electrical}}$) includes the installation of cables and the substation.

$$C_{\text{installation,foundation}} = f(D,\ N_{\text{T}}) \tag{2.17a}$$

$$C_{\text{installation,turbine}} = f(D,\ H_{\text{hub}},\ N_{\text{T}},\ d_{\text{harbor}}) \tag{2.17b}$$

$$C_{\text{installation,electrical}} = f(L_{\text{cable}},\ d_{\text{grid}},\ P_{\text{farm}}) \tag{2.17c}$$

The cost of installation for the foundation ($C_{\text{installation,foundation}}$) and the turbine ($C_{\text{installation,turbine}}$) are functions of the rotor diameter, as the vessel day rates are assumed to scale linearly with the diameter. This is an approximation made to account for the growing vessel sizes with larger turbines and foundations. The costs largely depend on the number of turbines (N_{T}) or, equivalently, the number of foundations to be installed. The installation time for the foundation is assumed to be constant whereas, for the turbine, it depends on the installation strategy used. The turbine installation strategy modeled is the one in which the tower is installed first. This is followed by the nacelle, in a bunny-ear configuration of two blades before installing the third blade [44]. Although this method is not used for current-day turbine sizes, the model for this method captures the main dependencies of installation costs on turbine scale parameters. The absolute values of the model should be interpreted with care. The hub height, along with the number of lifts, decides the total lifting time, which is then added to a fixed installation time for each turbine. The distance of the site from the nearest harbor (d_{harbor}) determines the travel time for the installation vessel. The time taken to install the cables depends on the laying and burial rate and the length of the cables (L_{cable} for the

array cables and d_{grid} for the export cable). The time taken to install one substation is fixed, while the number of substations depends on the rated farm power P_{farm}.

The summation of the installation costs for the turbine, foundation, and electricals gives the total installation costs. The reference day rate of the Wind Turbine Installation Vessel (WTIV) is scaled with the rotor diameter of the turbine.

The time for one vessel trip to the site includes the time taken to load the RNA (t_{loading}), the time taken to travel to the site (t_{travel}), and the time taken to install the RNA ($t_{\text{install,RNA}}$). The total turbine installation time ($t_{\text{installation,turbine}}$), shown in Equation (2.18), simply depends on the time taken per trip and the total number of trips made by the vessel (N_{trips}). The total time is multiplied by a factor of 1.5 to account for weather delays.

$$t_{\text{installation,turbine}} = N_{\text{trips}} \cdot (t_{\text{loading}} + t_{\text{travel}} + t_{\text{install,RNA}}) \cdot 1.5 \tag{2.18}$$

The number of trips depends on the total number of turbines (N_T) and the vessel capacity (assumed to be five in this study). The total cost for turbine installation, shown in Equation (2.19) is then given by the total vessel costs to install the RNA and the costs to mobilize and demobilize the vessel.

$$C_{\text{installation,turbine}} = C_{\text{day,WTIV}} \cdot t_{\text{installation,turbine}} + C_{\text{mobilization,WTIV}} \tag{2.19}$$

The cost of installation for the foundation ($C_{\text{installation,foundation}}$) is derived in the exact same way, where the total time taken to install the foundation ($t_{\text{installation,foundation}}$) is used.

For the cable installation, the time taken by the Cable Laying Vessel (CLV) and the Cable Burial Vessel (CBV) depends on the installation rate of the vessels. The total time taken to install the infield and export cable, as shown in Equation (2.20) and Equation (2.21) depends on the length of the cable and their installation rates ($r_{\text{installation,infield}}$ and $r_{\text{installation,export}}$, respectively) along with the safety factor for weather delays.

$$t_{\text{installation,infield}} = \frac{L_{\text{cable}}}{r_{\text{installation,infield}}} \cdot 1.5 \tag{2.20}$$

$$t_{\text{installation,export}} = \frac{d_{\text{grid}}}{r_{\text{installation,export}}} \cdot 1.5 \tag{2.21}$$

The cable installation costs can then be calculated by multiplying the time taken with the day rate for the vessels, as shown in Equation (2.22) and Equation (2.23).

$$C_{\text{installation,infield}} = t_{\text{installation,infield}} \cdot (C_{\text{day,CLV}} + C_{\text{day,CBV}}) \tag{2.22}$$

$$C_{\text{installation,export}} = t_{\text{installation,export}} \cdot (C_{\text{day,CLV}} + C_{\text{day,CBV}}) \tag{2.23}$$

The total cable installation costs are then calculated by adding the vessel mobilization costs, and some extra costs (C_{extra}) for cable pull-in, testing, etc., to the cable installation costs, as shown in Equation (2.24).

$$\begin{aligned} C_{\text{installation,cables}} = C_{\text{installation,infield}} + C_{\text{installation,export}} + C_{\text{mobilization,CLV}} \\ + C_{\text{mobilization,CBV}} + C_{\text{extra}} \end{aligned} \tag{2.24}$$

As shown in Equation (2.25), the cost to install the substations is given by the cost of installing the onshore substation ($C_{\text{installation,onshore-substation}}$), time taken to install the offshore substation ($t_{\text{installation,offshore-substation}}$), the day rates of the heavy lift vessel ($C_{\text{day,HLV}}$) and the cost to mobilize them ($C_{\text{mobilization,HLV}}$).

$$\begin{aligned} C_{\text{installation,substation}} = t_{\text{installation,offshore-substation}} \cdot C_{\text{day,HLV}} \\ + C_{\text{mobilization,HLV}} + C_{\text{installation,onshore-substation}} \end{aligned} \tag{2.25}$$

The total installation costs for the electrical system, shown in Equation (2.26), ($C_{\text{installation,electrical}}$) is simply a summation of the installation costs for the cables and the substations.

$$C_{\text{installation,electrical}} = C_{\text{installation,cables}} + C_{\text{installation,substation}} \tag{2.26}$$

2.5.7 Operations & Maintenance

The operational costs include insurance, logistics, training, etc., and maintenance costs include preventive and corrective maintenance for the turbine and BoS. The overall O&M costs are a function of several variables, as shown in Equation (2.27). The vessel day-rates are scaled linearly with D. The failure rates per turbine (F) and the number of turbines (N_{T}) determine the number of maintenance trips (N_{trips}) to be made, while the cost of the infield cables ($C_{\text{cable,infield}}$) and RNA (C_{RNA}) are used to determine the costs of major replacements. The distance to the nearest port (d_{harbor}) is used to calculate the travel time of the vessels.

$$C_{\text{OPEX}} = f(D,\ C_{\text{RNA}},\ C_{\text{cable,infield}},\ d_{\text{harbor}},\ N_{\text{T}},\ F) \tag{2.27}$$

The total Operations and Maintenance (O&M) costs consist of the fixed operational costs ($C_{\text{operational}}$), the costs for preventive maintenance and corrective maintenance (for both turbines and balance of plant). This constitutes costs of the vessel, costs of spare parts, and technician costs.

The costs for preventive maintenance, as shown in Equation (2.28), include the costs to inspect the turbine, the support structure, and the substations. This is done via Crew Transfer Vessels (CTVs).

$$C_{\text{preventive}} = t_{\text{service}} \cdot N_{\text{CTV}} \cdot C_{\text{day,CTV}} \tag{2.28}$$

Corrective maintenance constitutes minor repairs, major repairs, or major replacements. The majority of the costs are due to major replacement since that requires the use of a WTIV. The number of vessel trips is equal to the number of instances of failure ($N_{\text{instances}}$), which, in turn, depends on the failure rate (F) and the number of turbines (N_{T}). The time taken for any replacement or repair depends on the time taken by the vessel to travel to the site and make the replacement, and the total number of such failure instances in a year. For instance, the total time taken for major replacement ($t_{\text{replacement,major}}$), as shown in Equation (2.29), depends on the vessel travel time ($t_{\text{travel,WTIV}}$), component replacement time ($t_{\text{replacement,component}}$), and the number of instances ($N_{\text{instances}}$).

$$t_{\text{replacement,major}} = N_{\text{instances}} \cdot (t_{\text{replacecment,component}} + t_{\text{travel,WTIV}}) \tag{2.29}$$

As an example, the total costs for major replacement for the RNA in a given year constitute the vessel costs and the spare part costs, expressed as a fraction of the RNA costs (C_{RNA}), as shown in Equation (2.30).

$$C_{\text{replacement,major}} = t_{\text{replacement,major}} \cdot C_{\text{day,WTIV}} + 0.1 \cdot C_{\text{RNA}} \cdot N_{\text{instances}} \tag{2.30}$$

Similarly, the costs of minor repairs, major repairs, and cable replacements can be determined using the respective failure rates, repair times, and spare part costs. The spare part cost for various failure types are given in Table 2.1. The spare part costs are derived from Dinwoodie et al. [45], Shields et al. [24], Smart et al. [46] and Mangat et al. [7], as shown in Table 2.1, where C_{RNA} represents the cost of a single RNA, $N_{\text{instances}}$ represents the total number of failure events in a year, and $C_{\text{cable,infield}}$ represents the total cost of infield cables. The total failure instances in a year depend on the failure rate per turbine (F) and the number of turbines (N_{T}).

Table 2.1: Failure types and their respective spare part costs.

Failure type	Spare part cost
Minor repair	$0.001 \cdot C_{\text{RNA}} \cdot N_{\text{instances}}$
Major repair	$0.005 \cdot C_{\text{RNA}} \cdot N_{\text{instances}}$
Major replacement	$0.1 \cdot C_{\text{RNA}} \cdot N_{\text{instances}}$
Cable replacement	$0.0025 \cdot C_{\text{cable,infield}}$

Lastly, the cost of the technicians ($C_{\text{technicians}}$) depends on the number of technicians, that are scaled with the number of turbines in the farm, and a fixed annual salary. The total O&M costs can then be evaluated as shown in Equation (2.31).

$$C_{\text{OPEX}} = C_{\text{operations}} + C_{\text{preventive}} + C_{\text{repair,minor}} + C_{\text{repair,major}} + C_{\text{replacement,major}} + C_{\text{technicians}} \tag{2.31}$$

The type of maintenance (preventive or corrective), the failure rates and the number of turbines decide the type of vessel to be deployed, the number of maintenance trips per vessel type, and spare part costs. The total time spent by the vessel for performing repairs (including the transit time), multiplied by the day-rate of the respective vessel type, determines the total vessel costs. The spare part cost for RNA-related repairs is expressed as a fraction of the RNA costs while the infield cable replacement costs are expressed as a fraction of the total infield cable costs.

2.5.8 Other costs

Other costs include 'other turbine costs', 'other costs for installation and commissioning', 'project development and management costs', and 'decommissioning costs'. A summary of all the 'other costs' is shown in Equation (2.32).

$$C_{\text{other,turbine}} = 0.3 \cdot C_{\text{CAPEX,turbine}} \tag{2.32a}$$

$$C_{\text{other,farm}} = 0.1 \cdot C_{\text{CAPEX,farm}} \tag{2.32b}$$

$$C_{\text{dev}} = 0.05 \cdot C_{\text{CAPEX,farm}} \tag{2.32c}$$

$$C_{\text{DECOM}} = f(L_{\text{cable}},\, N_{\text{T}},\, M_{\text{RNA}},\, H_{\text{hub}}) \tag{2.32d}$$

The other costs related to the turbine ($C_{\text{other,turbine}}$) include, among others, turbine profit margins and warranty, and represent roughly 30% of the overall turbine capital expenditure (CAPEX). The other costs related to the farm installation and commissioning ($C_{\text{other,farm}}$) include insurance, contingency, etc., and represent approximately 10% of the overall farm CAPEX. Costs related to project development and management (C_{dev}) include various surveys, resource assessments, and engineering consultancy, to name a few, and represent 5% of the overall farm CAPEX [47]. The decommissioning costs (C_{DECOM}) involve the removal and disposal of the turbines, foundations, cables, etc.

2.6 Model input parameters

To run the MDAO framework as an analysis block, several input parameters are required, as listed below.

1. **Turbine parameters:** The International Energy Agency (IEA) 15 MW turbine [48] is used as a reference for scaling various properties of the turbine being designed. To scale the aerodynamic properties and scale the structural properties of a given turbine design, the airfoil properties, tip speed ratio (λ), chord (c_{r}), twist (θ_{r}), and mass distribution (m_{r}) of the reference turbine are used. Also, the mass of several components in the nacelle, like bedplate (M_{bedplate}) and generator (M_{gen}), are scaled from the reference-turbine values, when designing the new turbine.

2. **Electrical system:** For the infield cables, the study assumes a constant of five turbines in a string. This results in a total power in the string ranging from 50 MW to 100 MW based on the turbine rated power range. As a result, for turbines with lower rated power, the cross section of the infield cable is much lower than that of a turbine with a high rated power. For the export cable, the reference value of €150 million is used for scaling, based on a 220 kV cable delivering 1 GW [47]. For the substation cost scaling, a fixed cost component of €94 million and a variable cost component of €53 million are used, also based on a reference 1 GW offshore wind farm [47].

3. **Vessel data:** The vessel data[1], as shown in Table 2.2, are used to calculate the installation and O&M costs of the wind farm. The cost data used are based on the work of Dinwoodie et al. [45], Smart et al. [46], BVG Associates [47], Shields et al. [24], and Mangat et al. [7]. The cable laying rate of the CLV and the burial rate of CBV are also used as inputs.

4. **Failure rates:** The O&M cost model uses the expected number of minor and major failures for the turbine and BoS as inputs to determine the number of trips required by the respective vessel. The failure rates and spare part costs are derived from Dinwoodie et al. [45], Shields et al. [24], Smart et al. [46] and Mangat et al. [7], as shown in Table 2.3.

[1] WTIV - Wind Turbine Installation Vessel, HLV - Heavy Lift Vessel, CLV - Cable Laying vessel, CBV - Cable Burial Vessel, CTV - Crew Transfer Vessel, DSV - Diving Support Vessel

Table 2.2: Vessel data used for installation and O&M cost modelling.

Vessel type	Purpose	Day-rate (€)	Transit speed (km/h)	Mobilization costs (€)
WTIV	Installation: Foundation, turbine, O&M	200000	10	500000
HLV	Installation: Substation	500000	7	500000
CLV	Installation: Cable lay	110000	6	550000
CBV	Installation: Cable burrial	140000	6	550000
CTV	Crew transfer	3000	40	-
DSV	O&M: Scour repair	75000	6	225000

Table 2.3: Failure types and their respective failure rates (occurences per turbine), repair times, and vessel type required.

Failure type	F	Repair time (h)	Vessel type
Minor repair	3	7.5	CTV
Major repair	0.3	22	CTV
Major replacement	0.08	34	WTIV
Scour repair	0.023	8	DSV
Cable replacement	0.0004	32	CLV

2.7 General case study elements

This section discusses the case study analyzed for the formulated problem. A hypothetical site and wind farm in the North Sea are considered. The site parameters and the farm orientation define the case study. The wind rose for the hypothetical site, shown in Figure 2.6 (a), uses ERA5 hourly reanalysis data for a location near the Borssele wind farm in the North Sea [49]. The sample layout in Figure 2.6 (b) illustrates the wind speed deficits for the 15 MW reference turbine with 67 turbines and an approximate farm power of 1 GW.

It can be seen how the turbines are first arranged in a square grid of 64 turbines and the remaining three turbines are added along a new column. It can be seen from the wind rose that the South-West direction has the highest probability of all wind speed occurrences. This is the reason why the diagonal of the layout is oriented towards the South-West direction. Since there is a farm-power and a farm-area constraint, the number of turbines in the farm depends on the rated power of the turbine, and the normalized spacing depends on the rotor diameter. Some other case-defining parameters, like the distance to grid, water depth, etc., representative of tendered wind farms in the North Sea [50], are listed in Table 2.4.

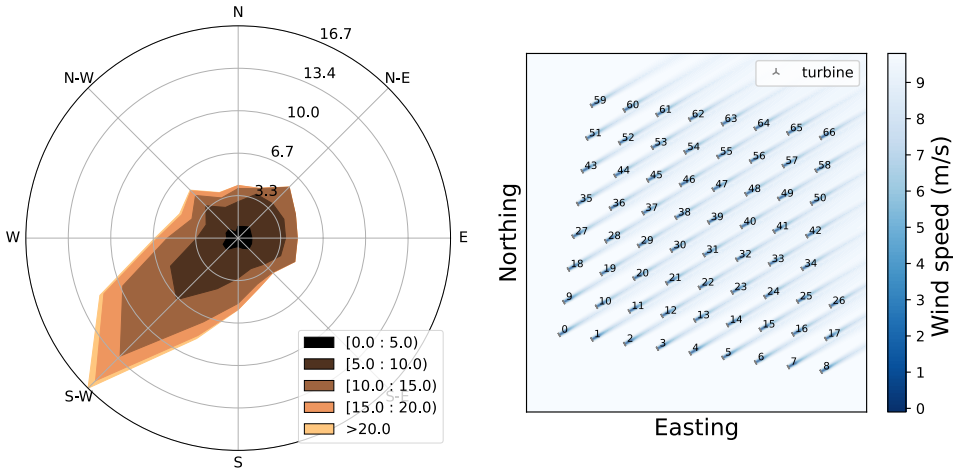

Figure 2.6: (a) Directional wind speeds (in m/s) and probabilities for the hypothetical site. (b) Farm layout for a 15 MW turbine and 1 GW of farm power.

Table 2.4: Case study parameters

Parameter	Value	Unit
Distance to grid	60	km
Distance to harbor	40	km
Water depth	30	m
Mean wind speed at 100 m	9.4	m/s
Maximum wave height (50 year)	5	m
Wind farm lifetime	25	years
Wind shear	0.11	-
Real discount rate	5	%

2.8 Model demonstration

This section demonstrates the outputs of each submodule in the framework using the inputs and case study parameters described in the previous sections. The focus is on illustrating the variation in different cost components and production levels w.r.t. turbine rated power and rotor diameter. Consequently, the trends are more significant than the absolute values.

Figure 2.7 shows how the blade mass (M_{blade}) scales across the entire design space. The blade mass of the IEA 15 MW reference turbine ($M_{\text{blade,ref}}$), used as the reference for scaling, is 65 tonnes [48] as shown in the figure.

The increase in blade mass with rotor diameter is dominated by the increase of chord length and internal layup thickness, which is initially proportional to rotor

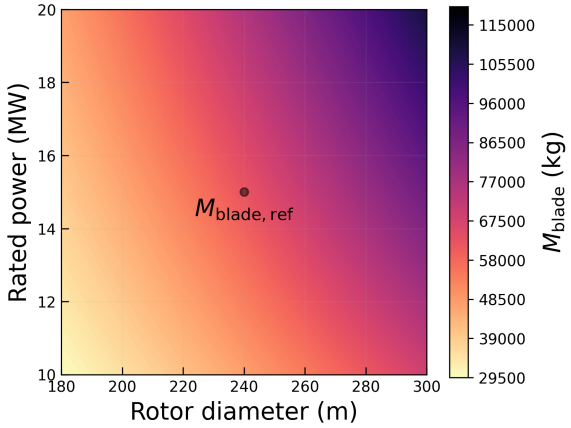

Figure 2.7: Scaling of the blade mass w.r.t. rated power and rotor diameter

diameter. With increasing rotor diameter, at constant rated power, the rated wind speed goes down. This leads to a slight reduction in layup thickness, but less than the increase due to geometric scaling. The increase in blade mass for increasing rated power can be explained likewise by an increase in rated wind speed, without any geometric scaling effect.

The farm power curve is a result of the turbine power curve and the wake losses that depend on the wind speed and wind direction. The differences in the power curves of some turbine designs are shown in Figure 2.8. The spread for each wind speed can be attributed to the direction-specific wake losses. Based on the problem formulation explained before, a change in the turbine rated power alone alters the number of turbines in the farm (fixed farm power constraint) and a change in the rotor diameter alone alters the normalized spacing (fixed farm area constraint).

Only altering the rotor diameter (keeping the rated power of the turbine constant) changes the farm power curve drastically, mainly because of a change in the partial load region of the turbine power curve itself, as shown in Figure 2.8 (a). On the other hand, changing the turbine's rated power (for the same rotor diameter) mainly alters the number of turbines in the farm while extending the partial load region of the turbine. This extension of the partial load region to higher wind speeds is also visible in the farm power curve, as seen in Figure 2.8 (b).

A lower farm power for the 20 MW turbine (with the same rotor diameter as the 10 MW turbine) can be attributed to the reduced number of turbines due to the farm power constraint. Both wind farm power curves also include the effect of a change in the magnitude of the wake losses, but those are secondary to the fundamental changes described above.

The variation of wake losses across the entire design space, for a fixed farm

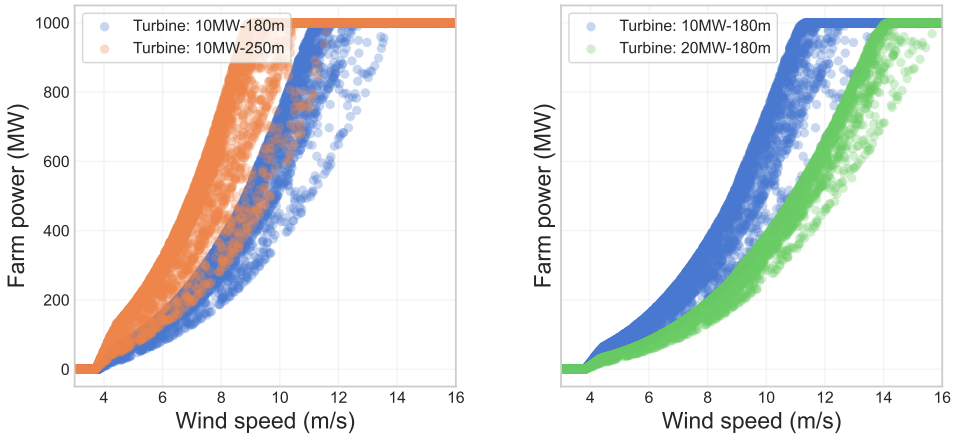

Figure 2.8: (a) Farm power curve variation due to a change in the turbine rotor diameter (b) Farm power curve variation due to a change in the turbine rated power

power and area, is shown in Figure 2.9. It can be seen that the wake losses are maximum for the lowest specific power turbine (smallest rating and largest rotor diameter) and minimum for the highest specific power turbine (largest rating and smallest rotor diameter). The rated power of the turbine determines the number of turbines in the farm (farm power constraint). For a given number of turbines in the farm, the absolute spacing between the turbines is set by the farm area constraint. For a given rating, the larger the rotor diameter, the lower the normalized spacing, resulting in higher wake losses. Also, for the same rotor diameter, the larger the rating, the lower the number of turbines in the farm, resulting in a lower wake loss due to fewer turbines and a larger normalized spacing.

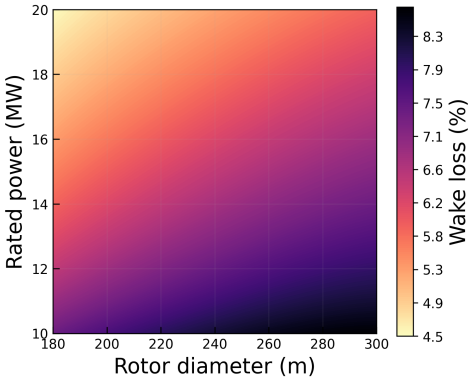

Figure 2.9: Wake loss variation across the entire design space

The variation of total support structure costs (farm-level) across the turbine design space is shown in Figure 2.10. The support structure costs are driven by the bending moment and the hub height of the structure, which scales non-linearly with the rotor diameter and also scale with the rated wind speed, which in turn depends on both the rotor diameter and the rated power. The bending moment would be the highest for a 300 m rotor with a slight difference as a function of rated power due to a difference in the rated wind speed. However, the absolute costs for the 10 MW turbine with a 300 m rotor are the highest as the number of turbines are maximum.

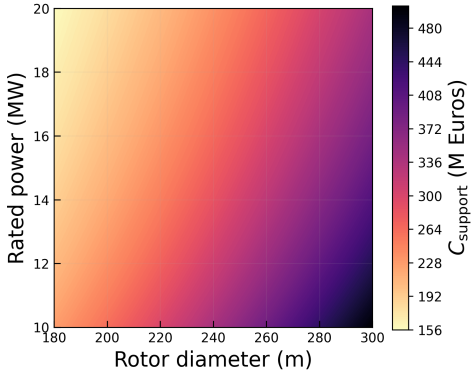

Figure 2.10: Scaling of the support structure costs across the entire design space

The variation of the total electrical costs across the design space is shown in Figure 2.11. The substation and the export cable costs, that are fixed across the entire design space, make up most of the electrical costs. The variation seen in the figure can be attributed to the infield cable costs. The infield cable costs are driven by the cable length and the current across the cables, both of which are not impacted by the rotor diameter. An increase in the rated power reduces the number of turbines in the farm (farm power equality constraint) but the turbines are also placed farther apart (farm area equality constraint). Hence, the cable length does not see a major change but the current flowing through a string increases with an increase in the rated power of the turbine, resulting in higher costs.

The variation of the total installation costs across the entire design space is shown in Figure 2.12. The installation costs for the substation and the export cable do not vary with the size of the turbine. The variation is therefore mainly dominated by the installation costs of the turbine itself and the foundation. Since costs are largely determined by the number of turbines, a turbine with a rating of 10 MW has the highest costs. Also, since the vessel costs are assumed to scale with the rotor diameter, a slight increase in costs with an increase in the rotor diameter

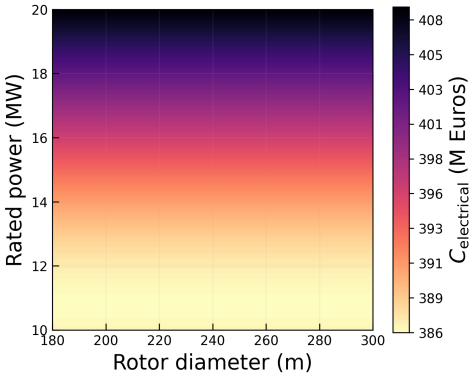

Figure 2.11: Scaling of the electrical infrastructure costs across the entire design space

(for the same rating) can be seen. In reality, the behavior of the vessel costs w.r.t. the rotor diameter is expected to be more discrete due to step changes in the vessel size.

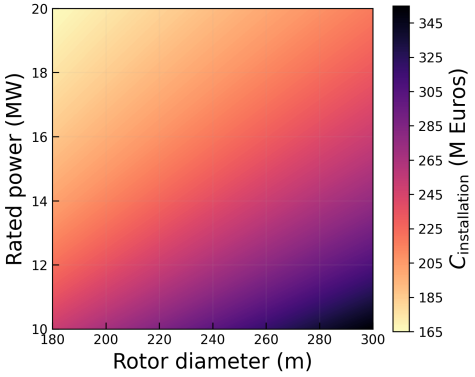

Figure 2.12: Scaling of the total installation costs across the entire design space

The variation in the O&M costs across the entire design space is similar to the installation costs, as shown in Figure 2.13. The variable component of the O&M costs are largely driven by the vessel trips for major replacements and hence, are lower for a 20 MW turbine which would result in the lowest number of turbines in the farm (farm power equality constraint). The increase in cost with an increase in the rotor diameter can be attributed to the higher spare part cost, that scales with the cost of the actual component, and the slight increase in vessel costs with an increase in the rotor diameter.

Figure 2.14 shows the scaling of all the 'other' costs across the entire design

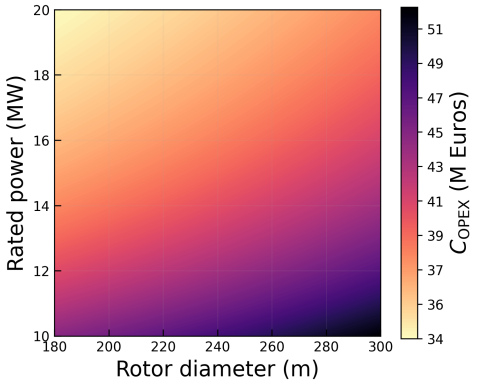

Figure 2.13: Scaling of the operations and maintenance costs across the entire design space

space. Since the costs are a multiple of total farm CAPEX, the variation of 'other costs' also represents the variation of the total farm CAPEX across the design space. As seen previously, the costs of the turbines, support structures, and installation are the highest for the lowest specific turbine (10 MW rating with a 300 m rotor) since that would result in the maximum number of turbines in the farm with the largest possible rotor.

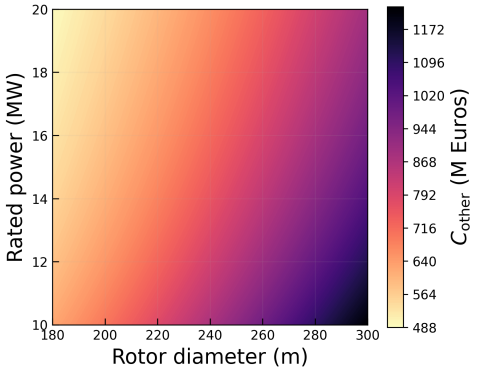

Figure 2.14: Scaling of the other costs w.r.t. rated power and rotor diameter

2.9 Significance threshold for turbine optimization

The optimization of turbine sizes does not always result in a substantial change in the objective function. To interpret the results meaningfully and assess the impact of turbine scaling, it is important to define a threshold for what constitutes

a significant improvement. In this study, a change greater than 5% in the objective function is considered significant.

For typical offshore wind projects, LCoE values range between 50–100 €/MWh, and the internal rate of return (IRR) can be assumed to be around 5-10%, broadly in line with the weighted average cost of capital [47]. Under these conditions, a 5% improvement corresponds to a reduction of 2.5–5 €/MWh in LCoE or an approximate 0.25-0.5 percentage point increase in IRR. From a wind farm developer's perspective, such improvements are not only valuable but also likely to influence investment decisions.

In contrast, smaller improvements, such as a 1% reduction in LCoE (0.5–1 €/MWh) or a 0.1 percentage point increase in IRR, while potentially beneficial, are unlikely to impact major investment decisions. These marginal gains may still be of interest but are not considered significant in the context of turbine sizing optimization.

3

Turbine sizing for Levelized Cost of Electricity

The true cost of energy isn't measured just in dollars and cents
it's calculated in the toll on our environment, our health, and our future.

Al Gore

The MDAO framework developed is a useful tool that can help in answering several questions related to wind turbine and farm design. With continuous upscaling of turbines and changing objectives and constraints, determining the future directions w.r.t. turbine design is more relevant than ever. However, it is, first, crucial to understand the drivers behind the traditional turbine design process that has led to this continuous upscaling of turbines in order to reduce the cost of energy.

This chapter focuses on turbine design from an energy cost reduction perspective. Section 3.1 discusses LCoE as the key metric in turbine and farm design. The optimization problem and case study setup are covered in Chapter 2. The formulation of LCoE, the objective function relevant to this chapter, is shown in Section 3.3, followed by an analysis of the design sensitivity to uncertainties and inputs in Section 3.4.

This chapter is based on the publication in **Wind Energy Science, 141-163, 9 (1) [51]**. In this chapter and in the paper, the tower length scaling in the AEP module and the support structure module used differs slightly from the model presented in Chapter 2. As a result, larger rotors (with larger towers) were preferred because their effect on tower costs was underestimated. After fixing this, the LCoE baseline optimum shifted from 16 MW-236 m in this chapter to 15.5 MW-230 m in Chapter 4 and further. Chapter 4 and Chapter 5 will use the model from Chapter 2 to redetermine the LCoE optimum, which will therefore differ from the one in this chapter. The optimums may differ, but the trends and discussions from this chapter are still valid.

3.1 Introduction

LCoE is a metric that is easy to calculate, covers all aspects of a wind farm, and is therefore universal in nature. Various wind farms across different sites or even different technologies could be compared simply by looking at the LCoE values. To achieve further cost reductions, the benefits of systems engineering by using Multi-disciplinary Design Analysis and Optimization (MDAO) have also been explored by Ashuri et al. [22], Sanchez Perez Moreno et al. [27], Dykes et al. [28], and Bortolotti et al. [29]. An MDAO-based approach captures the trade-offs between various disciplines of a system and results in a better design, compared to traditional sequential optimization. The studies also point out the importance of using the overall LCoE of the wind farm as the global objective function. Bortolotti et al. [31] developed reference wind turbines for onshore and offshore applications using such an MDAO-based framework. Dykes et al. [28] and Serafeim et al. [32] explored the optimization of the rotor for a turbine with a fixed rated power using the LCoE of the farm as the objective function. Most studies related to turbine optimization in a farm setting keep the rated power fixed and/or rotor diameter fixed, and the effect of upscaling the turbine itself is often not the focus. Ashuri et al. [22] optimized a 5MW reference turbine and scaled it to 10MW and 20MW to evaluate the effect on LCoE and find an increasing trend in LCoE with up-scaling. However, the costs for Balance of System (BoS) and O&M are assumed to scale with the rated power, with a fixed value for the exponent. In reality, the interactions of the turbine with the other elements of the farm are much more complex and require modeling of all the disciplines of the wind farm. Sieros et al. [23] performed an upscaling study for turbines in the range of 5-20 MW, with constant specific power, using classical similarity rules. The results showed an increase in the levelized production cost with turbine scale, for the same technology level. However, the focus of the study was on a simplified upscaling method, especially for the turbine, while the models for the rest of the wind farm were expressed simply as a percentage of turbine costs. Shields et al. [24] studied the impact of turbine upscaling and plant upsizing on various farm-level parameters providing several valuable insights. They find a reduction in LCoE of up to 20% when upscaling turbines from 6 to 20 MW and upsizing the farm from a 500 MW capacity to a 2500 MW capacity. However, the study assumes a fixed cost per kW for the turbines and also limits the specific power of the turbines when upscaling.

The limitations in previous work w.r.t. the turbine design space and turbine costs are expected to have a significant impact on the generalization of the results and conclusions. Both the numerical findings and the insights into drivers for turbine scaling will be affected. The work presented in this chapter aims to capture, more comprehensively, the variations in the turbine design and costs when scaling turbines, while also including the interactions and trade-offs occurring at a farm

level. The main research question this study tries to answer is as follows:

What drives the sizing of wind turbines for minimum LCoE of offshore wind farms?

The question can be further broken down into four sub-questions:

1. For a typical case, how does the turbine scale drive various trade-offs at a farm level, and what is the optimum turbine size?
2. How do uncertainties, technology changes, and economic conditions drive the optimum turbine design?
3. How do various farm design conditions drive the optimum turbine design?
4. How do farm-level constraints drive the optimum turbine design?

The turbine size refers to the two main defining variables of the turbine, rated power and the rotor diameter. The two variables are optimized w.r.t. the LCoE of a hypothetical wind farm, using the MDAO framework that includes low-fidelity models for every discipline of an offshore wind farm. The findings of this work may inform policy-makers and wind farm developers with useful insights. However, the implementation is simplified and the chosen set of design variables is limited. Thus, this study aims to be exploratory work that provides the potential possibilities of application of MDAO in large-scale wind farm design problems.

3.2 Levelized cost of electricity as objective function

The LCoE of the wind farm is given by Equation (3.1) where L is the operating lifetime of the wind farm, n is the year number, and r is the real discount rate. The numerator contains the Capital Expenditures (C_{CAPEX}) that are paid off initially, the summation of all the annual actualized Operation and Maintenance Expenditures (C_{OPEX}), and the costs to decommission the entire wind farm at the end of its lifetime (C_{DECOM}). The denominator contains the summation of the actualized AEP values.

$$\text{LCoE} = \frac{C_{\text{CAPEX}} + \sum_{n=1}^{L} \frac{C_{\text{OPEX}}}{(1+r)^n} + \frac{C_{\text{DECOM}}}{(1+r)^L}}{\sum_{n=1}^{L} \frac{\text{AEP}}{(1+r)^n}} \tag{3.1}$$

3.3 Results for the baseline case

This section discusses the results for the defined baseline case and shows the effect of the two design variables on various farm-level parameters. First, the results

with similar specific power designs are presented for a better understanding of general upscaling trends often observed in the industry, followed by the results for the entire design space. The latter gives an overall idea about the changes in turbine design and the specific power of the optimum designs and also discusses the possibility of a global optimum.

3.3.1 Similar specific power designs

The LCoE cost breakdown for a 10 MW turbine and a 20 MW turbine with a similar specific power is shown in Figure 3.1. In both cases, the farm power and area are kept constant. It can be seen how the share of turbine costs (rotor, nacelle, tower) goes up as the turbine is upscaled. However, the O&M costs drop, mainly because of a lower number of turbines (for a larger turbine rating). The same reason also accounts for the reduction in turbine and foundation installation cost share. The absolute costs of most of the electrical system (export cable and substation) are constant, as the farm power is unchanged. However, the cable costs go up for the upscaled turbine, due to an increase in the array cable cost. This can be attributed to a higher current flowing through each string of five turbines.

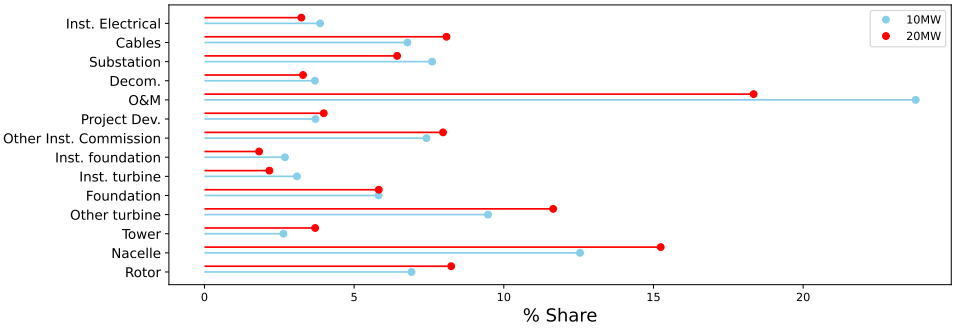

Figure 3.1: LCoE cost breakdown of a 10 MW turbine and a 20 MW turbine, both with a specific power of 350 Wm^{-2}.

The effect of upscaling turbines (with the same specific power) on various farm-level parameters is shown in Figure 3.2 (a) and Figure 3.2 (b). It can be seen that the overall costs of the turbine and the support structure increase with upscaling. This indicates a non-linear increase in the absolute costs per support structure. The cost of the RNA is dominated by the increase in rotor and generator costs, while the increase in support structure (tower and foundation) costs can be mainly attributed to higher hub heights, higher mass of the RNA, and the increase in thrust. As the export cable and substation costs are fixed due to a fixed farm power, the increase in infield cable costs (due to a higher current carried through the cable) results in an increasing trend of electrical costs. It can also be seen how upscaling decreases

the installation and O&M costs. This can be largely attributed to the decrease in the number of turbines, as the rated power of the turbine increases (for the same farm power). This decrease in the number of turbines results in a lower number of failure events, reduced vessel time required offshore, and hence, lower vessel costs. The increase in AEP can be attributed to two main reasons. First, upscaling the rated power results in a lower number of turbines in the farm (for the same farm power), resulting in lower wake losses. Second, upscaling the rotor diameter leads to a linear increase in the hub height, resulting in higher wind speeds.

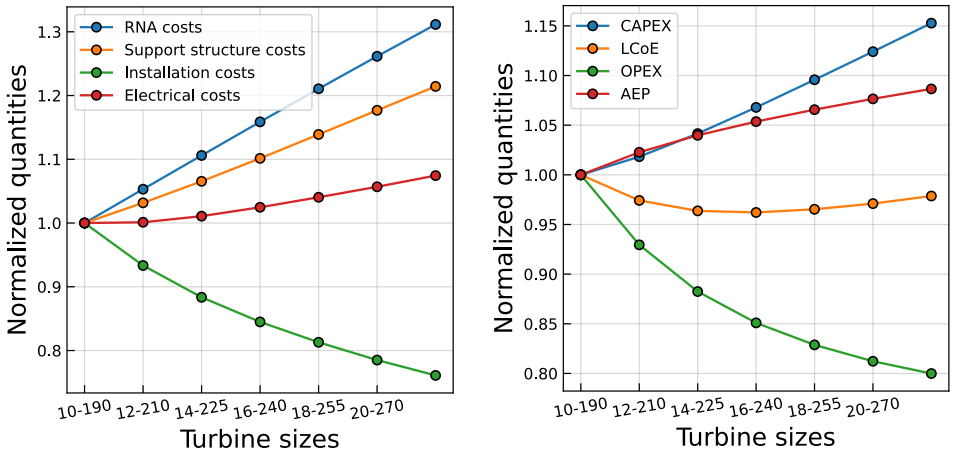

Figure 3.2: (a) Change in components of capital expenditures (normalized) w.r.t. upscaling of turbines with the same specific power. (b) Change in crucial farm-level quantities (normalized) w.r.t. upscaling of turbines with the same specific power.

It can be seen, in general, how upscaling results in a decrease in the O&M costs, an increase in the overall capital expenditures, and an increase in AEP, all of which significantly contribute to the LCoE. However, the trade-offs result in the possibility of an optimum w.r.t. LCoE, as shown in Figure 3.2 (b).

3.3.2 Complete design space

The results for the entire design space explored are presented in this section. As all possible combinations of power and diameter are considered, the effect on various farm-level parameters can also be observed for designs with different specific powers. The magnitude and direction of the gradients of the elements in LCoE (Equation (3.1)) at each design point can offer some interesting insights. The cost (capital expenditures, O&M, and decommissioning), AEP, and the LCoE gradients at each evaluation point are shown in Figure 3.3 for the baseline case.

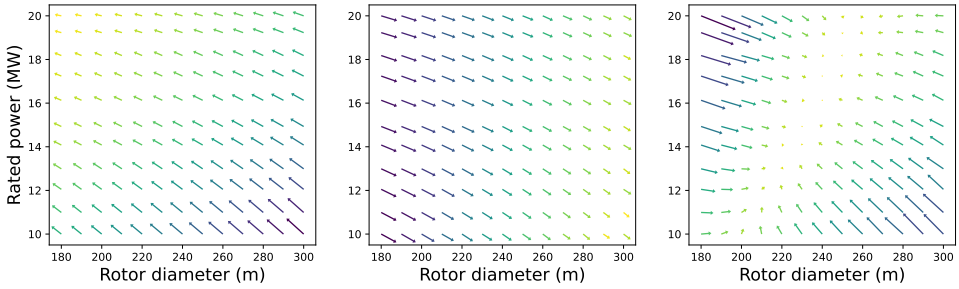

Figure 3.3: Cost, AEP, and LCoE gradients for the baseline problem formulation (from left to right).

It can be seen how the cost gradients always point toward a higher rating and lower diameter as the direction for the steepest descent, while all AEP gradients point towards lower ratings and larger diameters as the direction for the steepest ascent. The magnitude of the cost gradients changes rapidly with a rated power change, while the magnitude of the AEP gradients changes rapidly with a rotor diameter change. From the LCoE gradients, which are a result of the cost and AEP gradients, it is evident that there exists a region where the gradient magnitudes are close to zero. This is indicative of a global optimum. The global optimum for the formulated problem and the defined case is marked in Figure 3.4. In the colormap, each contour line represents a 0.5% change in the LCoE. This information is useful for a designer, as it indicates the increase in LCoE for a design that deviates from the optimum. It can be seen that a 1% change in the LCoE encompasses a large range of turbine designs, indicating that a deviation in the optimum does not necessarily correspond to a large deviation in the LCoE. This, however, is subject to uncertainties in the models. The plot also includes the largest turbines announced by some turbine manufacturers around the world, where most are already within a range of 1% LCoE from the baseline optimum obtained in this study. The equal specific power lines show that the baseline optimum and the commercial turbines have a specific power range of 300-400 Wm^{-2}. Section 2.9 defines a change of 5% or more in the objective as significant. It can be seen that within the analysed domain of the design variables, the change in LCoE is significant in the direction of changing specific power, while it is insignificant in the direction of constant specific power.

At times, the industry has been constrained by the blade length and it can be useful to know the optimum generator rating for that given rotor diameter. Figure 3.5 (a) shows the optimum rated power for a given rotor diameter and the optimum diameter for a given rating. While the 'optimum rated power' line follows a near-constant specific power trend, the specific power of the 'optimum rotor diameter' follows an increasing trend (300 Wm^{-2} for the 10 MW turbine to

425 Wm^{-2} for the 20 MW turbine). For a farm with a higher-rated-power turbine and fewer turbines, the share of O&M and installation is already relatively low, making the optimum more sensitive to turbine costs. As a result, the specific power increases with an increase in the rated power of the turbine. The cross-over point corresponds with the global optimum. Figure 3.5 (b) shows the variation of LCoE as a function of the specific power where the LCoE changes rapidly beyond a certain range of specific powers.

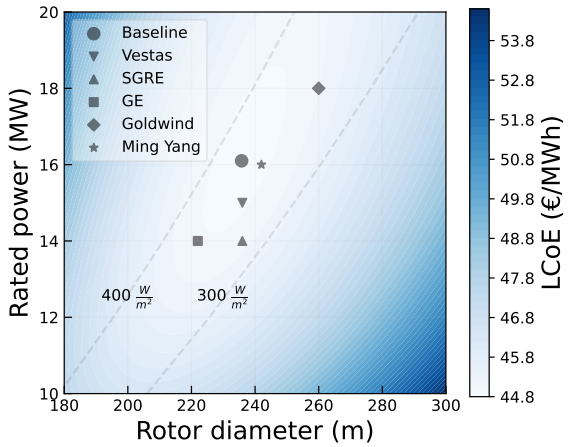

Figure 3.4: Response map of LCoE w.r.t. the two design variables.

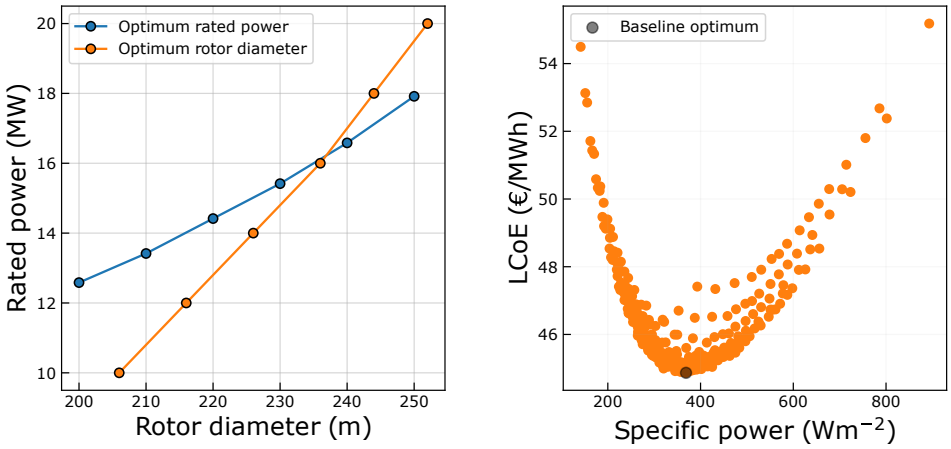

Figure 3.5: (a) Optimum rated power and rotor diameter per constrained diameter and rated power, respectively. (b) LCoE plotted against the specific power

To understand several trade-offs that occur at a wind farm level and how they are affected by turbine design, it is useful to see the gradients of various cost and AEP components at the optimum. The gradient of LCoE w.r.t. the rotor diameter and rated power is shown in Equation (3.2) and Equation (3.3), respectively. It is expressed in the form of cost and AEP gradients along with their weights.

$$\frac{\partial \mathrm{LCoE}}{\partial D} = \frac{1}{\mathrm{AEP}^2}\left(\mathrm{AEP}\cdot\frac{\partial C}{\partial D} - C\cdot\frac{\partial \mathrm{AEP}}{\partial D}\right) = A\cdot\frac{\partial C}{\partial D} - B\cdot\frac{\partial \mathrm{AEP}}{\partial D} \tag{3.2}$$

$$\frac{\partial \mathrm{LCoE}}{\partial P} = \frac{1}{\mathrm{AEP}^2}\left(\mathrm{AEP}\cdot\frac{\partial C}{\partial P} - C\cdot\frac{\partial \mathrm{AEP}}{\partial P}\right) = A\cdot\frac{\partial C}{\partial P} - B\cdot\frac{\partial \mathrm{AEP}}{\partial P} \tag{3.3}$$

The weights A and B are shown in Equation (3.4).

$$A = \frac{1}{\mathrm{AEP}} \quad \text{and} \quad B = \frac{C}{\mathrm{AEP}^2} \tag{3.4}$$

The overall cost gradient is simply a summation of the gradients of various costs like turbine, O&M, installation, and other farm costs, as shown, only w.r.t. the rotor diameter, in Equation (3.5). The gradients w.r.t. the rated power can be similarly obtained.

$$\frac{\partial C}{\partial D} = \frac{\partial}{\partial D}(C_{\mathrm{turbine}} + C_{\mathrm{other}} + C_{\mathrm{support}} + C_{\mathrm{installation}} + C_{\mathrm{OPEX}} + C_{\mathrm{electrical}}) \tag{3.5}$$

The net AEP is a function of the wake losses (λ_{wake}) and the gross AEP (without wake losses). The gradient of net AEP, hence, can be expressed as the summation of gradients for gross AEP and wake losses, as shown, only w.r.t. the rotor diameter, in Equation (3.6). The gradients w.r.t. the rated power can be similarly obtained.

$$\frac{\partial \mathrm{AEP}}{\partial D} = \frac{\partial}{\partial D}\left(\mathrm{AEP}_{\mathrm{gross}}\cdot(1-\lambda_{\mathrm{wake}})\right) = (1-\lambda_{\mathrm{wake}})\cdot\frac{\partial \mathrm{AEP}_{\mathrm{gross}}}{\partial D} - \mathrm{AEP}_{\mathrm{gross}}\cdot\frac{\partial \lambda_{\mathrm{wake}}}{\partial D} \tag{3.6}$$

Gradients of costs and AEP components that include the weights A and B are indicated with an accent. The gradients at the LCoE optimum are shown in Figure 3.6, where the cost gradients are negative and point in the direction of decreasing costs. For the cost gradients, it can be seen how RNA and 'other' costs have the highest magnitudes and have a higher dependence on the rotor diameter. The RNA costs decrease mainly with a decrease in the rotor diameter due to the lower blade mass. Its gradient points towards increasing the rating, as a higher rated power would result in a lower number of turbines in the farm (due to the farm power constraint), decreasing the overall cost of the turbines without a significant increase in the cost per turbine. The support structure costs show a

similar behaviour but have a lower magnitude. The O&M and installation costs exhibit a higher dependence on the rated power of the turbine compared to the rotor diameter. This can be attributed to the reduced number of turbines with upscaling, leading to fewer installation trips or a low number of major replacements. This results in low vessel costs. Their gradients also point towards a lower diameter, because a reduction in the rotor diameter reduces the required vessel size and hence, the vessel costs. The costs of the export cable and substation are held constant due to the equality constraint on the farm power. However, the array cable costs change and the infield cable topology depends on the number of turbines in the farm. Owing to the farm area equality constraint, a low number of turbines results in turbines being spread apart. The absolute distance between the turbines is only a function of the number of turbines in the farm and does not depend on the rotor diameter. It can be seen that the electrical-cost gradient points toward lower rated power. This is because a lower rated power results in lower current flowing through a string of 5 turbines, hence reducing array cable costs.

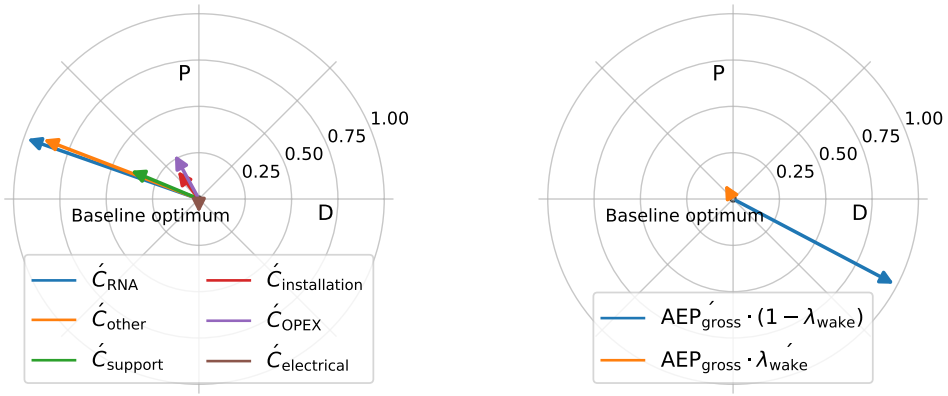

Figure 3.6: Cost and AEP gradient components at the optimum for the baseline case.

The gross AEP increases with an increase in rotor diameter and a decrease in the rated power. A higher rotor diameter gives a larger swept area and higher power (and hence AEP) for the same wind speed. Similarly, a decrease in the rated power, for the same rotor diameter, results in high-capacity-factor (or low-specific-power) turbines. Turbines with a higher capacity factor result in a higher gross AEP than lower capacity factor designs, irrespective of the rated power of the turbine, as the total farm power is constant in both cases. The wake loss gradient points in the direction of decreasing wake losses. A higher rating results in a lower number of turbines resulting in a lower overall wind speed deficit. A lower number of turbines also increases the absolute distance between the turbines as they are

placed further apart due to the equality constraint on farm area. As the absolute distance is a function of the number of turbines and is fixed for a given turbine rated power, reducing the rotor diameter results in a higher normalized spacing, again contributing to lower wind speed deficits. It should be noted that turbines with a higher rating and smaller rotors (high specific power) have high wake losses. This is because they have a larger partial load region, where the wake losses are the largest. In this region, the turbine operates at high c_T and a reduction in wind speed leads to a decrease in power, unlike in the full load region. However, this effect is overpowered by the reduction in the overall wind speed deficit caused by a lower number of turbines and larger normalized spacings.

The possibility of a global optimum indicates that the existing trend of continuous upscaling needs to be closely examined. However, it should be noted that the absolute value of the optimum depends on the current assumptions and future developments w.r.t. technology and costs.

3.3.3 Significance of gradient components

The behaviour of individual contributions to the gradients at the optimum, in a typical wind farm, in terms of both magnitude and direction, is discussed in Section 3.3.2. The understanding of this behaviour is key in identifying drivers for turbine sizing in a typical wind farm. To understand how certain changes in technology, farm conditions, or specific tendering requirements affect the optimum, one could simply look at how the changes impact the individual gradients and their weight.

For instance, a change in the fixed costs, like the costs of export cables or substation, changes only the weighting of the AEP gradient (see Equation (5.12)). This implies that if cables get more expensive, the optimum turbine shifts towards lower specific power turbines due to the stretching of the AEP gradient. Similarly, the removal of the export cable costs reduces the weighting of the AEP gradient, shifting the optimum towards higher specific power turbines. This situation applies, for instance, to the Netherlands, where the transmission system operator provides an offshore electrical connection. Sometimes, the effect on the gradient is more complex, such as for instance a change in blade material. Such a change alters both the magnitude and direction of the RNA cost gradient, resulting in a shift in the optimum along the direction of constant specific power.

Such an approach is useful since it shows how drivers that alter mainly the weight of the gradients (like changes in fixed costs, wind resource, etc.) shift the optimum in the direction of changing specific power, where the impact on LCoE is also significant (see Figure 3.4). On the other hand, drivers that alter both the direction and magnitude of the gradients (like some technological changes) shift the optimum in the direction of constant specific power, where the impact on LCoE is insignificant

(see Figure 3.4). Since the framework uses low-fidelity models, the absolute values of LCoE and optimum designs should not be taken at face value. However, the values match reasonably well with those observed for recently announced turbines and wind farms, adding confidence in the reliability of the results. The analysis of gradient components shows how the framework captures the essential dependencies and how it can be useful in identifying key drivers.
Models that do not include these dependencies might lead to misleading conclusions. This can also be explained by analyzing the gradients. For instance, a model wherein the turbine costs are expressed purely as a function of rated power would assume that the costs increase linearly with the rating. In that case, an increase in the turbine rating from 10 MW to 20 MW would double the costs of an individual turbine while the number of turbines in the farm is reduced to half (due to the farm power constraint). Hence, the total costs of the turbines in the farm remain constant across the entire design space, resulting in the gradients for the RNA costs being zero. As a consequence of this model assumption, the total cost gradient would significantly decrease in magnitude and would now be skewed more in the direction of the rated power. The net resultant of the total cost gradient and the AEP gradient would then significantly push the optimum toward larger ratings and rotors. Practitioners and scientists who focus on LCoE accuracy and fidelity of specific models may overlook the effect that misrepresentation of dependencies may have on gradients in an optimization problem. The insights from this chapter may help them make model developments that best match the needs for usage in an MDAO framework.

3.4 Sensitivity analysis of the optimum design

The results presented so far represent the baseline case for a chosen value for each user input and model parameter. However, to identify the design driving parameters and address the uncertainty in these parameters, a sensitivity study is performed. The parameters chosen are directly influenced by the design variables and are seen to have a significant impact on either the costs or the AEP. Different types of sensitivities are carried out in this study, which can be broadly categorized into the sensitivity w.r.t. the model parameters, design inputs, and problem formulation.

3.4.1 Sensitivity to model parameters

The parameters used in the model are subject to variations either due to uncertainties in estimation or due to differences in future technologies or different economic conditions. The sensitivity w.r.t. the model parameters take into account the variations in the optimum design due to these parameter variations. The choice of rotor diameter and the rated power of the turbine have a large influence on the rotor costs and the O&M costs. Hence, the sensitivity study w.r.t. these two models is

performed.

Rotor mass and costs model

As the rotor diameter has a direct influence on the rotor costs, and rotor costs take up a noticeable share of the LCoE, a sensitivity is performed w.r.t. the parameters used in rotor mass and cost scaling. The parameters considered for the sensitivity analysis w.r.t. the rotor and their range of values are listed in Table 3.1. All the parameters can be found in Equation (2.4). The mass scaling coefficient is used to scale the rotor mass with the rotor diameter and can differ depending on technological developments. The baseline value used for the reference blade cost is originally scaled from existing data on costs of 90-100 m blades [47]. However, the reference cost per se has uncertainties, and hence, a range of 60% about this value is used. These parameters vary depending on a change in the material, technological/cost developments, design environment, etc. On the other hand, the variations in the reference cost of the blade can be attributed to uncertainties in quantifying the same.

Table 3.1: Parameters used for quantifying the sensitivity of the optimum designs w.r.t. the rotor.

Parameter	Baseline value	Range
Mass scaling coefficient (Diameter exponent)	3	(2,3.5)
Mass weightage (γ_{mass})	0.6	(0.4,1)
Non-mass scaling coefficient (α)	2	(1.5,4)
Normalized cost of reference blade ($C_{\text{rotor,ref}}$)	1	(0.7,1.3)

The spread of global optimum designs for random combinations of the parameters within the ranges given in Table 3.1 can be seen in Figure 3.7 (a). The individual effect of the cost-model parameters (where one parameter is varied keeping all other parameters at their baseline values) can be seen in Figure 3.7 (b). For better readability, the optimum designs corresponding to the lower end of the parameter variation range are plotted with a larger marker size.

A higher value of each of these parameters pushes the global optimum to the left and below the baseline optimum (and vice versa). A decrease in the mass scaling coefficient results in less than cubic scaling of the mass w.r.t. the diameter, also resulting in lower rotor costs than the baseline case (for the same diameter value). As a result, the optimum shifts towards larger rotors. An increase in the mass weighting coefficient results in a higher contribution of the material costs to the overall rotor costs. This again pushes the optimum towards smaller rotors. Similarly, an increase in the non-mass scaling coefficient increases the rate at which non-mass-related costs scale w.r.t. the diameter. The result is a shift in optimum towards smaller rotors. The reference cost of the blade, however, does not have a

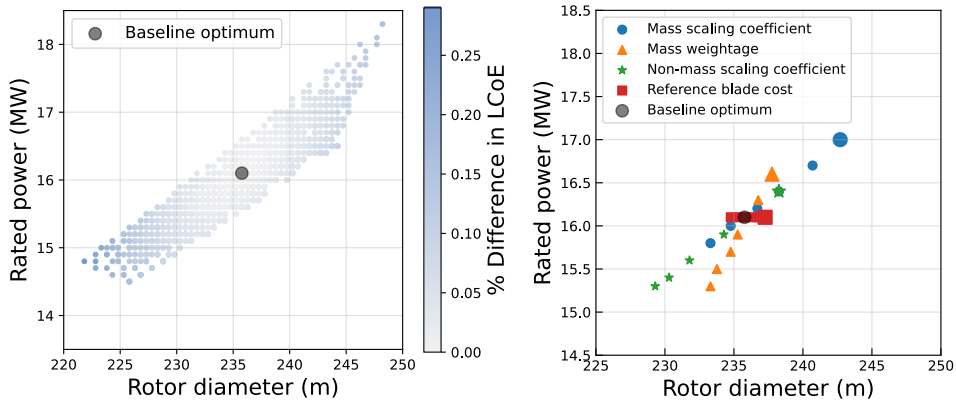

Figure 3.7: (a) Sensitivity of the optimum design to rotor model parameters for random combinations of parameter values. (b) One-at-the-time variation per parameter (the larger markers correspond to the lower end of the parameter variation range).

significant impact on the optimum designs. While the other parameters directly influence how the costs scale with the rotor diameter, the reference cost of the blade, as seen in Equation (2.4), does not directly influence the cost scaling w.r.t. the diameter. Instead, it only sets the weight of rotor costs, relative to other cost components.

Hence, the optimum designs are observed to be quite sensitive to the mass scaling coefficient, mass weighting, and the non-mass scaling coefficient. It should be noted that although the sensitivity leads to a large variation in the global optimum, a minimal difference in LCoE is observed between the new optimum designs and the baseline optimum.

O&M costs model

The O&M costs have the largest share in the LCoE of the farm and the cost model is also quite sensitive to its input parameters. Hence, a sensitivity study is performed w.r.t the parameters shown in Table 3.2. The fixed costs related to the operations vary depending on the project and location. The failure rate refers to the major replacements in the RNA and is turbine technology dependent, but it also has uncertainties in its estimation. The vessel day rates also depend on the location and are quite volatile. Also, the scaling of vessel day rates with turbine sizes is uncertain. The vessel mentioned here refers to the WTIV, which is also used for major replacements.

Figure 3.8 (a) shows the global spread of the optimum designs w.r.t. the variations in the O&M model parameters and inputs. The individual effect of the cost-model parameters (where one parameter is varied keeping all other parame-

Table 3.2: Parameters used for quantifying the sensitivity of optimum w.r.t. O&M.

Parameter	Baseline value	Range
Fixed costs (M€)	22.5	(10,30)
Failure rate (%)	8	(4,12)
Vessel day-rate (M€)	0.2	(0.1,0.3)
Vessel day-rate scaling coefficient	1	(0,3)

ters at their baseline values) can be seen in Figure 3.8 (b). For better readability, the optimum designs corresponding to the lower end of the parameter variation range are plotted with a larger marker size.

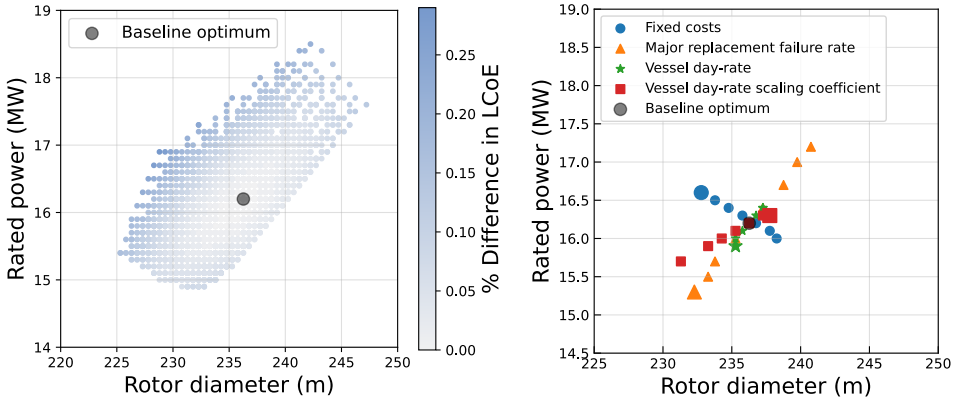

Figure 3.8: (a) Sensitivity of the optimum design to O&M model parameters for random combinations of parameter values. (b) One-at-the-time variation per parameter (the larger markers correspond to the lower end of the parameter variation range).

The fixed costs have an indirect effect on the optimum. A change in the fixed costs affects the weight of the AEP gradient (Equation (5.12)). A lower fixed cost reduces the weight of the AEP gradient, pushing the optimum toward the direction of the cost gradient (smaller rotors and larger ratings). The fixed costs do not alter the cost gradients but only the weight of the AEP gradient, increasing/ decreasing its magnitude. Hence, the optimum moves along the direction of the cost/AEP gradient. Except for the fixed costs, changes in any other parameter alter the O&M gradient magnitude and hence, change both the magnitude and direction of the total cost gradient. The overall vector sum of the changes in the direction of the cost gradient along with the changes in the magnitude of the cost and AEP gradient causes a shift along the constant specific power line. For a low failure rate, the number of trips for major replacements is reduced, resulting in lower vessel and spare part costs. This pushes the optimum designs towards a lower rated power

(and higher number of turbines) than that of the baseline one. The vessel day rates affect the overall vessel costs. Like the failure rate, this affects the total repair costs and it thus affects the optimum in the same direction. However, since the vessel costs are only a part of the total repair costs, the difference in the optimum designs is not as significant for the given range of day rates. The vessel day rate scaling coefficient, on the other hand, affects how the day rates scale w.r.t. the rotor diameter. A coefficient of zero results in the same day rate, no matter what the turbine size is, incentivizing upscaling. A high coefficient quickly scales up the day rates with rotor size, resulting in smaller rotors.

The fixed cost component of O&M costs, the turbine failure rates, and the scaling of vessel rates with the rotor size are the biggest design drivers, while the uncertainties in the day rate itself do not have a significant impact on the optimum designs. It should be noted that, although the sensitivity leads to a large variation in the global optimum, a minimal difference in LCoE is observed between the new optimum designs and the baseline optimum.

3.4.2 Sensitivity to farm design conditions

The farm design conditions depend on the design environment and are bound to be different for every project. Hence, a sensitivity study is performed w.r.t. several important design conditions like the wind speeds at the site, available farm area, distance to grid, and the total farm power (or grid connection available). The variability range of design conditions is shown in Table 3.3.

Table 3.3: Parameters used for quantifying the sensitivity of optimum w.r.t. design conditions, where u_w refers to the wind speeds used in the baseline case.

Parameter	Values
Wind speed	$(0.85{\cdot}u_w, 0.9{\cdot}u_w, 1.1{\cdot}u_w)$
Farm area (km^2)	(100, 200)
Distance to grid (km)	(30, 90)
Farm power (MW)	(600, 800, 1200, 1400)

The effect of the design conditions on the LCoE of these optimums is shown in Figure 3.9 (a), while the variation in the global optimum design w.r.t. the variations in the design conditions can be seen in Figure 3.9 (b). To show the correspondence between Figure 3.9 (a) and Figure 3.9 (b), the optimum rotor diameter and rated power values for the lower end of the design input range are mentioned next to their corresponding LCoE values. Compared to the baseline case, it can be seen that a change in the wind speed at the site has the maximum effect on both the LCoE and the optimum design. A low wind speed site pushes for low specific power turbines with larger rotor diameters and lower ratings than the baseline,

also resulting in higher LCoE values. This trend is in line with what is seen for turbines in the market and corresponds with typical OEM portfolios. A change in the farm power also has a significant effect on both the LCoE and the optimum designs. Obtaining a larger farm power by increasing the number of turbines (for the same turbine rated power), would increase wake losses, O&M costs, installation costs, electrical system costs, etc. Designs with a higher rated power avoid these effects, and therefore, provide the optimum way to achieve higher farm powers. The available farm area and the distance to grid have a lower impact on the LCoE and, hence, on the optimum design. A low farm area increases the wake losses resulting in a higher LCoE of the farm. To compensate for the high wake losses, the optimum shifts towards higher turbine ratings to reduce the number of turbines in the farm. The distance to the grid only changes the costs of the export cable. Consequently, the effect on the LCoE and the optimum design is minimal. The greatest benefit of tailoring designs to site conditions, in terms of LCoE, is observed for changing wind conditions. In the low wind scenario, opting for low specific power designs, compared to the baseline optimum, resulted in an LCoE reduction of 1.25%.

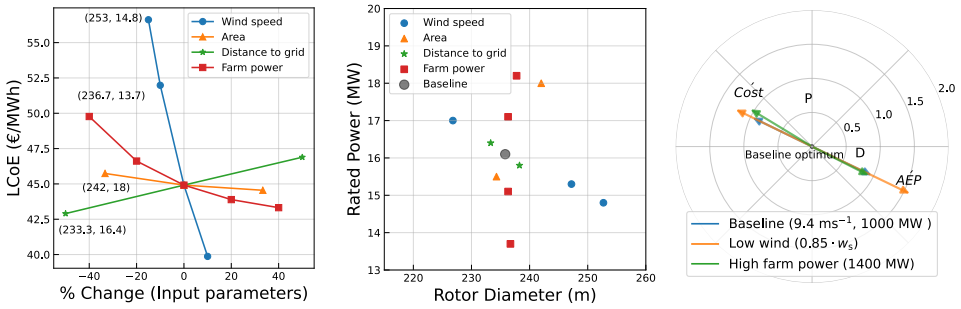

Figure 3.9: (a) Change in LCoE w.r.t. change in design conditions. (b) Change in the optimum w.r.t. change in design conditions. (c) Change in gradients at the baseline optimum for different design conditions.

As the wind regime and the farm power cause the optimum design to shift the most, and along different dimensions, the driving forces behind these shifts are analysed. At the baseline optimum, the gradient of the LCoE is zero, with respect to both changes in diameter and rated power. When the wind regime or farm power changes, the gradient of LCoE at the baseline optimum is no longer zero, and the optimum shifts towards the direction of steepest descent. To identify the contributions of the changes in costs, gross AEP, and wake losses to the direction of the new gradient, the separation of terms according to Equations (3.2) to (3.6) is shown in Figure 3.9 (c). The weighted cost and AEP gradients for the baseline are equal in size and in opposite directions, in accordance with their vector sum being

zero.

For the low wind case, both weighted gradients increase. Although the cost and thus the cost gradient themselves are not affected by the changed wind climate, the weighted cost gradient increases due to the division by the lowered AEP. The AEP gradient is weighted with the square of the AEP, so the effect of the lower AEP on the weighted AEP gradient is much larger. In addition, the AEP gradient itself will have changed. The sensitivity of AEP to changes in rated power and rotor diameter has changed, since the new probability distribution of wind speeds changes the importance of different parts of the power curve. However, this effect is much smaller. Since the changes in the weighted gradients are dominated by the changes in the weights (shown in Equation (5.12)), the two gradient vectors are exactly or mostly aligned with the original vectors. The bigger increase in the weighted AEP gradient pushes the optimum in that direction. Figure 3.3 shows that moving in that direction decreases the AEP gradient and increases the cost gradient. The new optimum will be found where this effect compensates for the imbalance that was identified at the baseline point.

A change in farm power (1400 MW) has a more complex effect on the weighted gradients. At the baseline point, the increase in farm power is achieved only by increasing the number of turbines. If AEP and all costs would increase linearly with the number of turbines, the weighted gradients would be the same as for the baseline. The unweighted gradients of costs and AEP would then also increase linearly with the number of turbines, and that would exactly compensate for the linear change in the magnitude of the weights. Therefore, the deviations observed in Figure 3.9 (c) are caused by non-linear dependencies. The increase of the number of turbines in the same constraint area leads to a lower average spacing, which in turn leads to two primary non-linear effects: One, the costs increase less than linear, because the total infield cable length grows less than linearly. Two, due to an increase in wake losses, the AEP increases less than linearly. Both have a direct effect on the weights and order of magnitude of the unweighted gradients, which both stretch or compress the baseline weighted gradients along their original orientation. Which non-linearity dominates can only be identified by quantifying them, but according to the graph the differences are small. Both non-linear effects also influence the direction of the unweighted gradients and with that the direction of the weighted gradients. Apparently, for the larger farm, it is a little more favorable to increase the rated power to reduce costs, while the AEP has a similar dependency on the design variables, as that of the baseline. The overall effect of the change in magnitude and direction of the weighted gradients leads to a vector sum that points slightly towards higher rated powers. This residual gradient for LCoE is far smaller than was the case for the lower wind climate. However, it is now caused partly by differences in the angle between the weighted cost and AEP gradients

and not only by a difference in size. This means that at the new optimum point, this difference in angle must be compensated. Figure 3.3 reveals that the angles of the gradients change far less rapidly over the domain than their magnitude. This explains why the optimum design for the larger wind farm is at a similar distance from the baseline as the optimum design for lower wind speeds.

Figure 3.9 (b) shows that the sensitivity to area is largely aligned with that of the sensitivity to farm power. Likewise, the sensitivity to the distance to grid aligns with that of wind speed. The rationale for each of them resembles the discussion of each of their respective counterparts given above, but for a reversed effect. For changes in the distance to grid, the AEP remains the same and the total costs change. This mainly affects the weight 'B' of the gradients (Equation (5.12)) resulting in a slight pull or compression of the weighted AEP gradient. For changes in the area, the AEP and costs both remain nearly the same, with again some effects on wake losses and infield-cable costs. The final effect is due to a combination of small changes in the weights, as well as small changes in the direction of the gradients.

3.4.3 Sensitivity to farm-level constraints

The optimum designs are highly subject to the farm-level constraints themselves. In the baseline case, a fixed farm power and fixed farm area scenario are considered. However, in some cases, there might be a constraint only on the grid connection or only on the available area. Hence, a sensitivity w.r.t. these different constraints is also performed. The problem formulation is varied by removing one of the equality constraints from the baseline case. So other than the baseline case, a problem with a power-only constraint and a problem with an area-only constraint are considered.

Fixed farm power

In many scenarios, developers are provided with just a fixed grid connection with no strict limitations on the ocean area. The 'fixed-farm-power-only' constraint represents this scenario where a fixed grid connection of 1 GW is used and a fixed normalized spacing (downwind and crosswind) of 5D is assumed. The overall shift in the optimum is shown in Figure 3.10 (a), while the change in the weighted cost and AEP gradients, plotted at the baseline optimum, is shown in Figure 3.10 (b).

In this constraint formulation, a major change in the behaviour of wake losses and infield cable costs is observed. The change in the magnitude and direction of the cost gradient can be attributed to the differences in the infield cable cost gradient. Unlike the baseline case, the infield-cable costs do not show a significant dependence on the rated power anymore. For a given rotor diameter, the absolute distance between the turbines is fixed. Hence, an increase in rated power reduces the number of turbines, thus decreasing the overall cable length and costs. However, this will also increase the power flowing through a single cable, which increases

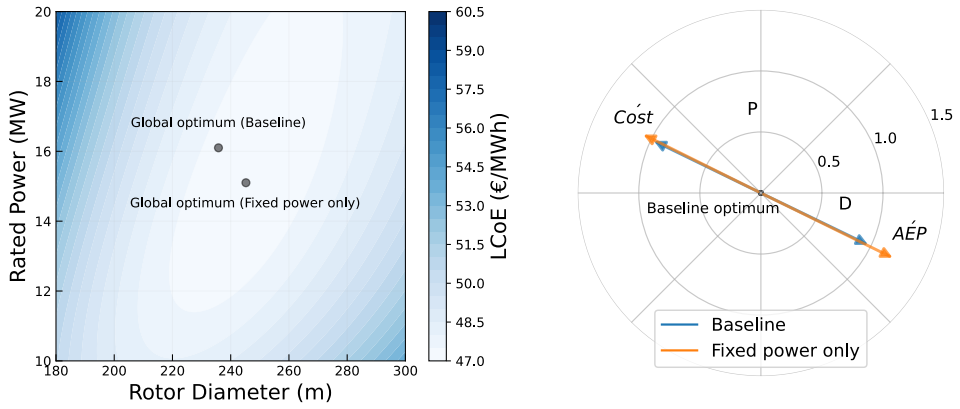

Figure 3.10: (a) Shift in the optimum design for the 'fixed-farm-power-only' case. (b) Differences in gradients for 'fixed-farm-power-only' case plotted at the baseline optimum.

the costs. These two opposing effects reduce the dependence of infield-cable costs on the rated power. On the other hand, the rotor diameter of the turbine influences the absolute distance between the turbines and hence, the infield cable length. As a result, the infield cost gradient depends more on the rotor diameter than on the rated power, resulting in the overall change in both the direction and magnitude of the net cost gradient, compared to that of the baseline.

The behavior of wake losses also changes significantly with the change in the constraint formulation. The wind speed deficits depend on the normalized spacing between turbines and the operating thrust coefficient of the upstream turbine. In the baseline case, a change in the turbine power or diameter changed both the normalized spacing and the power/thrust curve of the turbine. However, the wake losses were mainly dominated by the normalized spacing (around 7.5D for the baseline optimum). In the 'fixed-farm-power-only' case, the normalized spacing is fixed (at 5D) and does not depend on the number of turbines. So a change in the turbine design only changes the power/thrust curve. The wind speed deficit experienced by downstream turbines is highest when the upstream turbines operate in their partial load region, because that is where the thrust coefficient and power gradient are highest. As a result, the net AEP gradient pushes the optimum towards larger rotors and lower ratings (low specific power turbines), which have a steeper power curve and a reduced partial load region. This results in lower wake losses.

Since the change in the wake loss gradient dominates the change in the infield cable cost gradient, the net effect is a push in the resulting optimum towards lower ratings and larger rotors.

Fixed farm area

This constraint formulation represents a scenario where the ocean area is limited and developers are mostly area constrained. This applies, for instance, to coastal regions, close to a strong grid connection. The farm area available is considered to be fixed in this case. For a given rotor diameter and normalized spacing, the area constraint determines the maximum allowable number of turbines, since the farm area will always be used to its full capacity. Also, the turbine rated power has no impact on the number of turbines in the farm. In this analysis, a normalized spacing (downwind and crosswind) of 5D is assumed. The optimum rated power is observed to be much higher than that in the baseline case (Figure 3.11 (a)). The change in the weighted cost and AEP gradients, plotted at the baseline optimum, is shown in Figure 3.11 (b). It should be noted that Figure 3.11 (b) shows the direction of the steepest descent/ascent at the baseline optimum, and moving along that direction will lead to another point where the gradient direction will differ, ultimately leading to the global optimum.

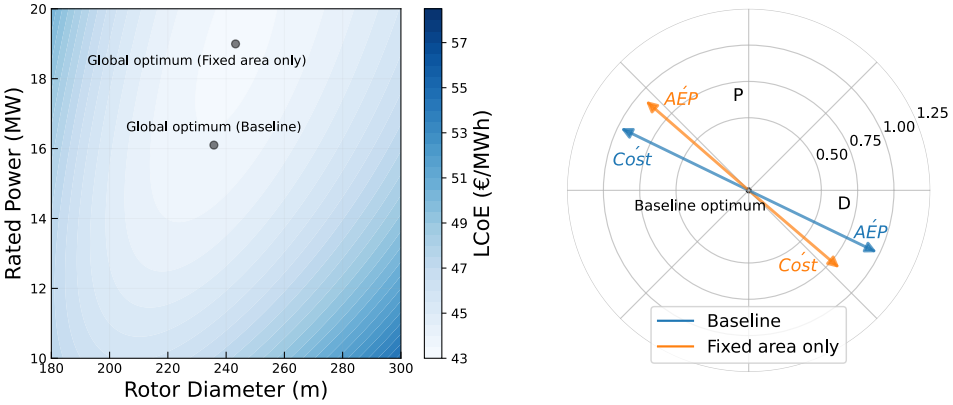

Figure 3.11: (a) Shift in the optimum design for the 'fixed-farm-area-only' case. (b) Differences in gradients for 'fixed-farm-area-only' case plotted at the baseline optimum.

Compared to the baseline (Figure 3.6), a completely opposite behavior of both the costs and AEP gradients can be clearly observed. This can be attributed to the net change in the direction and magnitude of the individual cost and AEP components, as explained below:

- A decrease in the rotor diameter decreases the costs of a single turbine but results in more turbines in the farm. These opposing effects reduce the dependence of the total turbine costs for the farm on the rotor diameter. On the other hand, increasing the turbine-rated power increases the RNA costs,

and has no impact on the number of turbines. As a result, the RNA cost gradient points toward lower rated powers.

- As the farm power is now variable and depends on the number of turbines in the farm and the rated power of each turbine, the costs of the export cable and substations also vary. The infield costs now go down with an increase in the rotor diameter (less turbines in the farm) and lower ratings (less current flowing through the cables). As a result, the overall electrical cost gradient points towards lower rated powers and larger rotors.

- As the number of turbines is now a function of the rotor diameter, the O&M and installation cost gradients point towards larger rotors. This is because, for the 'fixed-farm-area-only' case, where the area constraint and normalized spacing are defined, a larger rotor diameter results in a lower number of turbines in the defined area, resulting in lower vessel costs.

- The gross AEP (without wake losses) of the farm goes up with an increase in the rated power and a decrease in the rotor diameter. This is because a decrease in the rotor diameter allows more turbines in the farm and an increase in the rated power allows for more power to be produced at higher wind speeds without having any impact on the overall number of turbines in the farm. As a consequence, the gross AEP vector points towards larger rated powers and smaller rotor diameters.

- Similar to the 'fixed-farm-power-only' case, since the normalized spacing is fixed, the wake losses are minimized by reducing the partial load region of the turbine. This is achieved by moving to larger rotors and a lower rated power. Also, larger rotors reduce the number of turbines in the farm, further reducing wake losses.

The effects discussed above explain the difference in the behavior of the cost and AEP gradients. It can be seen that the AEP gradient is larger in magnitude and is also not in line with the cost gradient. This creates a push towards larger ratings and at the new optimum the differences in the directions and magnitude of the weighted cost and AEP gradients are compensated.

3.5 Discussion

This work explored how turbine scaling affects various farm-level quantities and also identified the design driving parameters. Key insights gained from this research are presented below.

- The optimum size of 16 MW – 236 m for a typical case is already close to the state-of-the-art observed in the industry. For a farm with a fixed area and a fixed power for the grid connection, reduction of farm costs is attained via high specific power turbines. This is achieved mainly via reducing the rotor diameter. On the other hand, an increase in the AEP is attained via low specific power turbines achieved mainly via increasing the rotor diameter. The apparent trade-off results in an optimum turbine design w.r.t. LCoE. Also, a large change in the turbine design along a constant specific power line results in a small LCoE change. On the other hand, a small change in the turbine design, but in the direction of changing specific power, results in a large LCoE change.

- Uncertainties in modeling or future technology/cost developments drive the optimum along a fixed specific power line. However, the optimum for the typical case mentioned above is robust to these differences in the model behavior, w.r.t. LCoE. For instance, the variations in the scaling of rotor mass, estimation of failure rates, vessel cost scaling, etc. resulted in an uncertainty range of 10% for the optimum diameter and 20% for the optimum rated power evaluation. However, this uncertainty in the optimum led to a difference of less than 0.5% in the LCoE.

- Project-specific parameters drive a change mainly in the specific power of the design. The variations in wind conditions and farm power density values were seen to have the largest impact on both the optimum turbine size and the specific power of the design. As an example, for the case presented here, changing the wind regime by 15% mainly affects the rotor diameter of the optimum resulting in a specific power shift from 390 Wm^{-2} to 310 Wm^{-2}. On the other hand, varying the farm power density constraint by 40% mainly affects the rated power of the optimum resulting in a specific power shift from 390 Wm^{-2} to 430 Wm^{-2}. However, redesigning the turbine for these changes resulted in a maximum benefit of the order of 1-2% w.r.t. LCoE.

- Relative to a typical case, a scenario with only area constraints pushes the optimum towards high specific power designs extracting the maximum energy out of a turbine. A scenario with only farm power constraints pushes the optimum towards low specific power designs reducing the wake losses in the partial load region. Turbine designers can adapt to these changing problem formulations either by downrating the turbine for a 'farm power constrained' scenario or by uprating the turbine for an 'area constrained' scenario.

These findings agree with how technological advancements led to the continued shift of the turbine scale observed in the past decades. Technology and cost developments drive a shift in the optimum scale with limited effect on specific power (second bullet point). The sensitivity of LCoE along lines of equal specific power is low around the optimum, allowing a large range of scales to co-exist during a certain era (first bullet point). The findings also agree with the fairly stable range of specific powers offered in the past at different scales. These portfolios are driven by variations in project-specific conditions (third bullet point). However, while the optimum specific power is fairly sensitive to particular project conditions, turbines of a fairly wide range of scales can perform equally well (first bullet point). The findings of bullet point 4 are less visible in practice and in the literature, but they reveal the effects of farm-level constraints on the optimum specific power and scale that are similar to those of project conditions. Besides the more obvious consequence for farm developers to pick the most suitable turbine for their case, this finding also means that the policies around spatial planning and tender formulation have an impact on the optimum turbine design and performance. An approach as shown in this chapter can help quantify those impacts. The findings in this research are obtained using low-fidelity cost models and the IEA 15 MW turbine as the reference design. However, the absolute values of the optimum will likely differ for a different reference turbine as the starting point for scaling, and a future study exploring the sensitivity to different reference designs with higher fidelity cost models is recommended. Nevertheless, the confidence in the use of scaling laws is largest when the scale of the reference turbine and of the global optimum are similar, as is the case here.

The study provides a simplified approach that can be applied to a complex turbine sizing problem in order to generate meaningful insights. The findings of this study help the scientific community to focus future research on the most important aspects and goals. They provide insight into how various model improvements impact both the performance and the optimum turbine size. For instance, consider an improvement in the RNA model leading to an increase in the magnitude of its gradient and a higher dependency on rated power. The consequence of this improvement would be a large shift in the optimum along the constant specific power line, towards larger ratings and rotor diameters, without a significant change in the LCoE for the new optimum. Similar insights can be drawn w.r.t. other model improvements, based on the gradients presented in this study. The findings also show how constraints influence turbine sizing, guiding future studies w.r.t. the optimization problem formulation. The research serves as a stepping stone for the sizing of future reference turbines. However, the marginal change in LCoE across a wide range of designs shows the limited benefit of continuous upscaling, which must be balanced against the technical challenges and risks it poses.

4

Turbine sizing for profitability

The shift to cleaner energy is not a matter of ideology or morality. It is a matter of economics, technology, and inevitability.

Michael Liebreich

Knowledge about how various factors drive the global optimum of turbine design can be of significant value to the wind energy community. However, the insights gained from the previous chapter were focused solely on the cost of energy. As more and more subsidy-free tenders are rolling out, it is important to understand how these fluctuating market prices drive the global optimum design and how much it differs w.r.t. traditional LCoE-optimized designs. This chapter aims at bridging this knowledge gap by including a simplified market model into the developed framework and applying it to several metrics beyond LCoE.

The working of the day-ahead market and the classic cannibalization effect is explained in Section 4.1. The various profitability metrics and market scenarios used in this study are shown in Section 4.2. A simplified market model developed to simulate the various market price scenarios is explained in Section 4.3. Finally, Section 4.4 discusses how various market price scenarios and choice of metrics drive the optimum turbine design.

This chapter is based on the publication in **Wind Energy Science, 2283–2300, 9 (12) [52]**.

4.1 Introduction

Chapter 3 shows how LCoE is a comprehensive metric that can be used to optimize the turbine size for an offshore wind farm. LCoE is a metric that is easy to calculate, covers all the aspects of a wind farm, and is hence universal in nature. Various wind farms across different sites or even different technologies could be compared simply by looking at the LCoE values. In subsidy-based auctions or Power Purchase Agreements (PPA) where nearly a fixed electricity price is ensured, minimizing the LCoE would effectively correspond with maximizing profit. However, the system dynamics and market incentives are rapidly changing resulting in newer design objectives (beyond LCoE). This may demand a change in the turbine and farm design philosophy.

In a subsidy-free environment, the developer is exposed to the volatility of the market prices. This goes away from the traditional subsidy-based approach where the wind farm developer would be ensured a fixed premium or price. Due to the merit-order effect in the day-ahead market, regions with a high wind penetration, quite often, displace the expensive generators during times of high winds, resulting in low prices. This effect is also known as the cannibalization effect. The drop in the market value of wind with an increasing share of renewables has been shown in several studies, such as Mills and Wiser [53] and Hirth [54]. As market prices negatively correlate with grid-wide average wind speed (cannibalization), turbines should not only be designed to reduce costs but also to increase the value of the produced electricity. Shields et al. [24] performed an extensive study showing the benefits of upscaling turbines and farms to reduce the LCoE. Some of the shortcomings of the study are addressed in Mehta et al. [51]. However, both studies are focused on the LCoE and do not include market prices.

Since LCoE, as a metric, does not capture the varying electricity price per kWh, the market value of wind goes unaccounted for, and this is why there is a need to look beyond LCoE [55]. This has led to the expectation that such market-driven designs have larger rotors, to generate more electricity at high prices, during low-wind-speed periods. Some studies propose very low specific power turbines that produce high power at lower wind speeds and also cut out earlier when conventional wind turbines reach their rated power. This results in higher revenues, and is also beneficial to the electricity system as it results in better system adequacy [25, 56]. Chen and Thiringer [57] include market prices and look at leveraging overplanting and curtailment to increase wind farm profits. However, the study looks at absolute profits and does not look at all the changing cost elements in a wind farm. However, to comment on the profitability of a given turbine design, a comprehensive analysis taking into account all the cost benefits and revenue gains at a wind farm level is required. There is little consensus on whether the discussed concepts reap higher economic benefits (using profitability metrics beyond LCoE) for a wind farm

developer.

Profitability metrics like Internal Rate of Return (IRR), Net Present Value (NPV), Profitability Index (PI), etc. that include both costs and revenues are commonly used to assess the economic performance of wind farm projects [58]. Some other metrics like Value Factor (VF) and the Cost of Valued Energy (CoVE), formulated by Simpson et al. [59], also take into account the market value of wind. Since each metric has a different formulation, the economic performance of the wind farm depends on the choice of the economic metric, which poses an additional challenge w.r.t. wind turbine design optimization. This study tries to address these gaps by exploring how turbines should be sized for subsidy-free markets. The term 'markets' refers to different possible future realizations of the day-ahead market, where the bulk of the electricity is traded. The research question can hence be formulated as:

How do wind turbine size and specific power change, w.r.t. an LCoE-optimized turbine, when maximizing its economic value in the day-ahead market?

To answer the main question, two sub-questions are formulated that will be addressed in this work.

1. How do various economic metrics, that include the market value of wind energy, drive turbine design?
2. How do different day-ahead market price scenarios drive turbine design?

The turbine size and specific power refers to two main system-level parameters of a turbine, the rated power and rotor diameter. These are the two design variables that are optimized in this study. It should be noted that this study looks at the wind farm developer's perspective and only includes revenues from the day-ahead (spot) market, excluding revenues from any capacity payments and grid (or other ancillary) services. The share of revenue may shift from energy markets to capacity or ancillary services markets in a future with high penetrations of renewables [60]. We already see subsidy-free offshore wind farms coming up that will be exposed to variable market prices [61]. With this paradigm shift, it then becomes crucial to revisit the design philosophy used for turbine and farm optimization.

4.2 Economic metrics beyond levelized cost of electricity

This section lists the various economic metrics used as objective functions in the study. The different market scenarios, for which each of these metrics will be evaluated, are also discussed.

Various economic metrics exist that are often used to evaluate the profitability of a project. Metrics commonly used for financial assessment of renewable energy projects include IRR, NPV, Benefit-to-cost ratio (BCR), Return on Investment (ROI), simple or discounted Payback Period (PBP), etc. [58, 62]. González et al. [63] optimize the layout of a wind farm using NPV as the objective function. Shamshirband et al. [64] use both NPV and IRR to optimize the number of turbines to be installed in a wind farm. Ciavarra et al. [65] optimize the hub height of each turbine in the farm using both AEP and IRR as objective functions. Joshi et al. [66] normalize the NPV with the energy output when optimizing airborne wind energy systems. Pookpunt et al. [67] perform wind farm layout optimization for a variety of metrics including NPV, IRR, and PI. Habbou et al. [68] look at PI and LCoE to evaluate the profitability of hybrid power plants in European markets. Simpson et al. [59] proposed CoVE as a metric that normalizes the LCoE with the value factor, which captures the value received by the wind farm developer w.r.t. the average market clearing price.

Each metric has a different formulation and certain benefits and drawbacks. The following metrics are considered in this study:

1. **Levelized Cost of Electricity (LCoE):** This will serve as the baseline objective, which is to be minimized. The LCoE of the wind farm is already described in Equation (3.1) as a part of Chapter 3.

2. **Net Present Value (NPV):** NPV is a measure of the absolute profit where all the future revenues and costs have been discounted to represent their value in the present. A positive NPV indicates a profitable investment. Equation (4.1) shows the formulation of NPV, where Cf_n represents the cash flows over the years and C_{CAPEX} represents the initial investment, and r is the discount rate. NPV is an objective that needs to be maximized.

$$\text{NPV} = \sum_{n=1}^{L} \frac{Cf_n}{(1+r)^n} - C_{\text{CAPEX}} \tag{4.1}$$

3. **Profitability Index (PI):** PI, same as the Present Value Index (PVI) or BCR, is the ratio between the present value of future cashflows and the present value of the initial investment. It is, in essence, the same as NPV normalized with C_{CAPEX}, as shown in Equation (4.2) [69]. An index greater than 1 indicates a profitable scenario. PI is an objective that needs to be maximized.

$$\text{PI} = 1 + \frac{\text{NPV}}{C_{\text{CAPEX}}} \tag{4.2}$$

4. **Modified Internal Rate of Return (MIRR):** MIRR is a modified version of the IRR which is the rate at which the NPV of a project is zero. However, IRR assumes that the positive cashflows are reinvested at the IRR instead of the company's cost of capital. MIRR takes this into account and also eliminates the issue of having multiple IRRs. It is an objective that needs to be maximized. It is given by Equation (4.3) for a case where the cashflow (Cf) is constant throughout the lifetime, L, and r is the reinvestment rate of the revenue [69].

$$(1+\text{MIRR})^L = \frac{Cf}{C_{\text{CAPEX}}}\left[\frac{(1+r)^L-1}{r}\right] \tag{4.3}$$

5. **Cost of Valued Energy (CoVE):** CoVE, proposed by [59] covers both the costs and revenue aspects. It is a function of the LCoE of the farm and the value factor (VF), as shown in Equation (4.4). CoVE is an objective that needs to be minimized.

$$\text{CoVE} = \frac{\text{LCoE}}{\text{VF}} \tag{4.4}$$

The value factor for a specific year is given by Equation (4.5) where the average price that the wind developer receives is normalized with the mean spot price.

$$\text{VF} = \frac{\frac{\sum_t P_{\text{farm}} \cdot \lambda_{\text{spot}}}{\sum_t P_{\text{farm}}}}{\mu_{\text{spot}}} \tag{4.5}$$

NPV is a measure of the absolute profit of the project since it is a summation of the initial investment and the present value of the future revenues. Since it is not normalized, it is often used to compare the returns of different projects with a similar initial investment. For a design problem where the investment varies with a change in the design variables, the use of NPV can be problematic. For instance, consider that an investment of €10 yields €20 of discounted revenues. Even if simply doubling the investment yields twice the revenue, the NPV would also double, indicating a much better design which may clearly not be the case. This problem is solved by metrics like PI or BCR, which essentially normalize NPV with the initial investment. However, the use of NPV together with IRR is quite common in capital budgeting and in various academic studies, as exemplified above. IRR is the rate of return at which NPV is zero. Since IRR is normalized and indicates a % return, it serves better for a design problem with varying investments. However, even IRR is to be used with caution. Due to yearly revenues, the invested sum is

gradually paid off. Thus, the rate of return is not achieved over the total lifetime for the total investment. CoVE simplifies cash-flow effects with the same real-interest approach as LCoE while considering the dependency of revenues on wind speed. However, not all market price variations are captured by CoVE. For instance, simply doubling the market prices will double the revenues, giving a different PI, NPV, and IRR, but will result in the same value factor and CoVE.

The turbine optimization problem explored in this study involves a change in investment across all elements of the wind farm. Hence, using metrics like NPV might give misleading results. Metrics like PI and IRR are clearly better suited for a turbine or farm design optimization problem. However, since the other metrics listed above are commonly used in renewable energy financing and in academic studies, the consequence of using potentially inappropriate metrics will also be explored.

4.3 Market model

This section discusses the approach used to model day-ahead markets. For this study, an eXtended Design Structure Matrix (XDSM) of the framework used to evaluate all the wind-farm level parameters is shown in Figure 4.1. In addition to the framework described in Chapter 2, a market model is incorporated to generate spot prices based on user-provided inputs specifying a day-ahead market scenario, which are ultimately used to evaluate metrics based on profitability. For each set of design variables and a given market scenario, the framework is executed and the economic performance of the wind farm is evaluated.

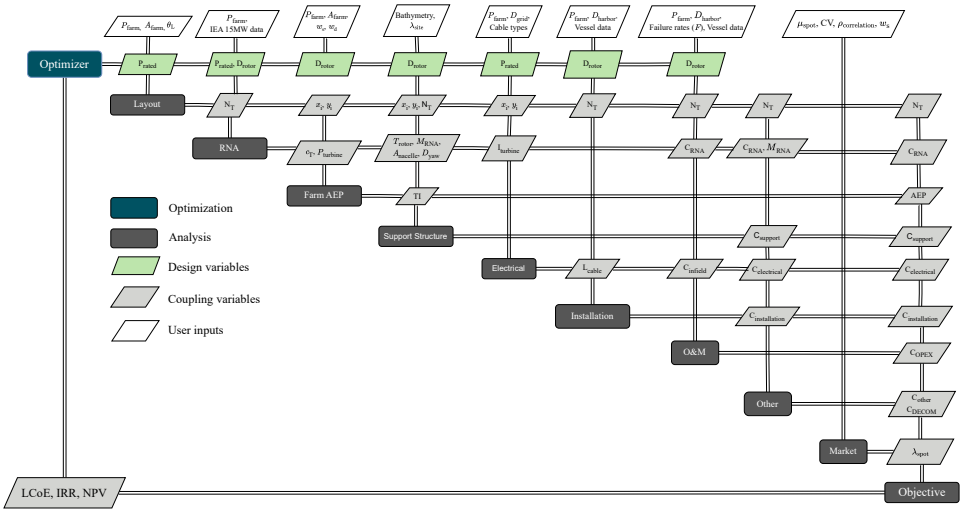

Figure 4.1: XDSM of the wind-farm level MDAO framework

The costs and farm power from the wind farm framework along with the spot prices from the market model give the cashflows of the project and hence, several economic indicators like the Internal Rate of Return (IRR), Net Present Value (NPV), etc., can be evaluated.

The hourly prices for spot markets can be simulated using complex market models like Balmorel [70] or EMMA [71]. These are energy system models that minimize the system cost required to satisfy the demand. To simulate a future scenario, various inputs like electricity demand, capacity and costs of various generation technologies, fuel costs, cross-border trade, carbon prices, etc. are required. This enables the model to capture the complex market effects. However, it also makes it difficult to use such models to quickly simulate hundreds of future price scenarios to evaluate a business case of a project. Verstraten and van der Weijde [72] argue that these complex models can be used as benchmarks while simpler models can be used to assess renewable business cases. The authors show the effect of change in the capacity of various technologies on the market clearing price using an in-house stochastic market simulator. However, the tool still requires information about the capacities of different assets, their operational strategies, and the electricity demand as inputs. For this study, it is important to capture the cannibalization effect of wind power generation. From a turbine design perspective for a given wind farm, this translates to the relationship between spot market prices and wind speeds. The purpose of the market model is not to accurately predict spot prices for a given year in the future. Instead, the purpose is to have a parameterized model to generate spot prices where the model parameters can be easily varied to simulate various future market scenarios. The generated spot price data can then be used to determine annual revenues.

The relation between spot prices and wind speed can be represented with the help of a univariate model that uses a linear or a polynomial fit. However, it is difficult to comment on how the coefficients would evolve in the future. Hence, this study uses a different approach to model the spot prices. Figure 4.2 (a) shows the distribution of the spot prices for the years 2016-2020 for Denmark while Figure 4.2 (b) shows the same for the Netherlands, taken from the European Network of Transmission System Operators for Electricity (ENTSO-E) [73]. While the Netherlands observed a higher mean value of spot prices than Denmark (due to a relatively lower renewable penetration), the standard deviation was the same. It can be seen that the spot price distribution can be approximated by a normal distribution. This approximation is later verified w.r.t. how it affects the annual revenues of a wind farm. Instead of using the absolute standard deviation, the spread around the mean can also be expressed in the form of a coefficient of variation (CV), i.e. the ratio of the standard deviation to the mean. Thus, with a constant CV, the variability in the price increases/decreases along with the mean

price.

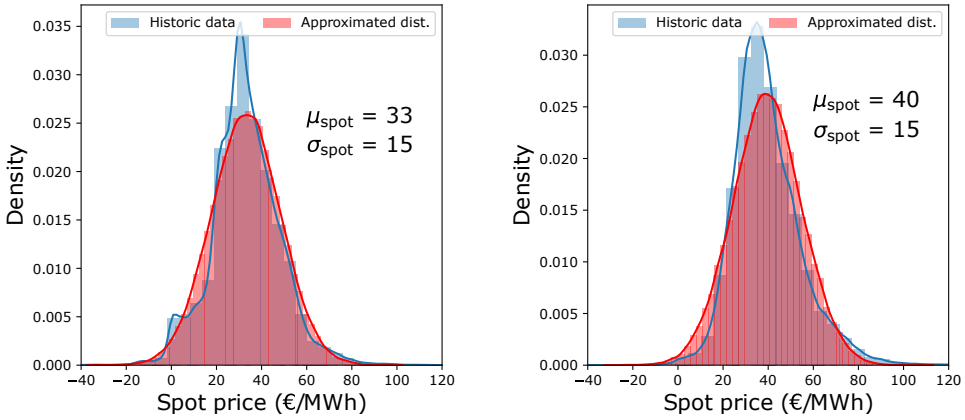

Figure 4.2: Spot price distribution and its approximation to a normal distribution for (a) Denmark (b) the Netherlands

Also, due to the cannibalization effect, spot prices have a negative correlation with wind generation. An illustration of the cannibalization effect, for Denmark and the Netherlands, is shown in Figure 4.3 (a) and Figure 4.3 (b) respectively, where the spot prices for the years 2016-2019 are plotted against the wind speed for a sample wind farm in both the Danish and Dutch regions of the North Sea. As the wind energy penetration in Denmark is higher, compared to that of the Netherlands, it experiences a higher negative correlation between spot prices and wind speeds. The spot price data (λ_{spot}) to be generated can be expressed as a function of various parameters shown in Equation (4.6), where μ_{spot} is the mean of the normal distribution for spot prices, CV is the coefficient of variation, and $\rho_{correlation}$ is the correlation coefficient between spot prices and the site-specific wind speeds.

$$\lambda_{spot} = f(u_w, \mu_{spot}, CV, \rho_{correlation}) \tag{4.6}$$

Based on the wind speed time series (u_w) and the correlation coefficient ($\rho_{correlation}$), a correlated vector can be formulated as shown in Equation (4.7).

$$\lambda'_{spot} = \rho_{correlation} \cdot \hat{u}_w + \sqrt{1 - \rho^2_{correlation}} \cdot \hat{z} \tag{4.7}$$

Here, λ'_{spot} is an intermediate vector that represents the correlation between wind speed and spot price, $\hat{u}_w$ is the unit vector obtained by normalizing a centered version of the wind speed time series u_w, $\hat{z}$ is a random noise vector with the same dimensionality as u_w.

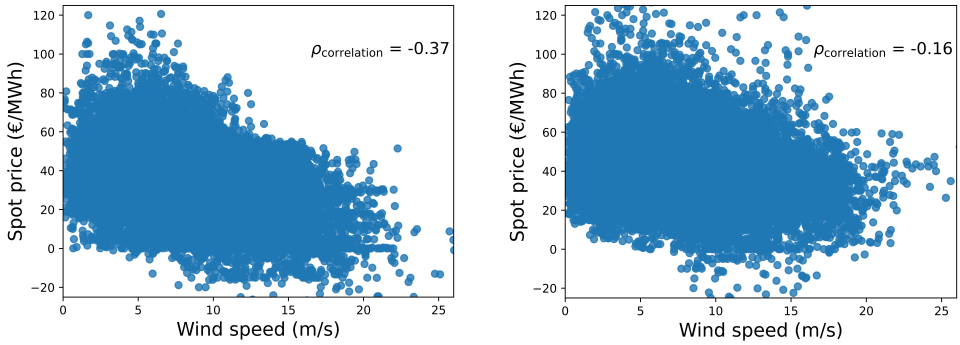

Figure 4.3: Correlation between spot prices and site-specific wind speeds for (a) Denmark (b) the Netherlands

The correlated vector can then be scaled to match the desired mean (μ_{spot}) and standard deviation (σ_{spot}) to produce the final spot price vector (λ_{spot}), given by Equation (4.8).

$$\lambda_{spot} = \mu_{spot} + \sigma_{spot} \cdot \lambda'_{spot} \tag{4.8}$$

The correlation coefficient only has an effect when the standard deviation is high enough. For low standard deviations, the correlation coefficient has no meaning. A low value of CV, which corresponds to a lower standard deviation, results in a smaller spread of data around the mean. As a consequence, for values of CV close to 0, even a high negative correlation of -1 would result in no variations of the spot prices w.r.t. the wind speed. This effect is shown in Figure 4.4 where the generated spot price data for a given mean and a high negative correlation is plotted, for two different values of CV. It can be seen that for low values of CV, the spot prices do not change much. This effect is also shown for time series data of a week where the spot prices for a lower CV (in orange) do not change much even for large fluctuations in the wind speed (in black).

In this study, the CV is kept constant for most analyses. It is known that the value for CV also differs, but it is expected to have the smallest range of variability of all the three market parameters. Keeping it constant simplifies the model, while still being able to capture the most relevant variations. However, a sensitivity of the results to CV is also carried out to evaluate the consequence of this simplification. The spot prices can be generated by sampling data from the normal distribution (defined by μ_{spot} and CV) such that the correlation between the spot price vector and the input wind speed vector is equal to the defined $\rho_{correlation}$. It should be noted that the prices are generated for a year (using hourly wind speed data) and that the corresponding revenue is considered to be the same for all years throughout the

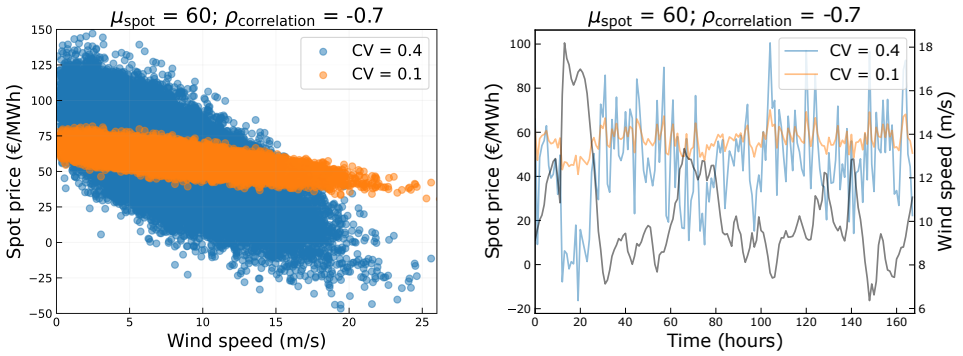

Figure 4.4: Effect of Coefficient of Variation (CV) for a given mean spot price and correlation coefficient

lifetime of the wind farm. With the approximated values of μ_{spot}, CV, and $\rho_{correlation}$ for Denmark and the Netherlands, as shown in Figure 4.2 and Figure 4.3, the spot prices can be generated, as shown in Figure 4.5.

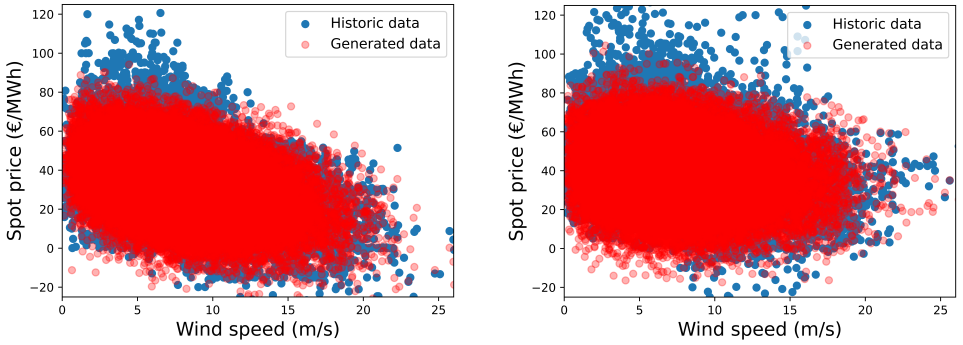

Figure 4.5: Historic spot price data and generated data for (a) Denmark (b) the Netherlands

The purpose of the simplified market model is to represent the relation between spot prices and local wind speed with the help of two defining parameters (μ_{spot} and $\rho_{correlation}$) that can be easily varied to simulate multiple realizations of the future market. For instance, a high correlation coefficient would represent a location with a high wind penetration like Denmark. A correlation of zero represents a constant average price per kWh which could be the case with a PPA or a fixed feed-in tariff.

The spot prices are used, eventually, to determine the annual revenue of the wind farm, which will further be used to evaluate the chosen economic objective function. The revenue of a hypothetical 1 GW wind farm in Denmark is calculated using the historic spot price data and the generated spot price data, shown in Figure 4.6. The hourly revenues using the historic spot price data are compared

with the revenues using the model-generated spot price data. Both follow a similar trend where the revenues increase until a certain point followed by a decrease in the revenue at high wind speeds due to relatively lower spot prices. The spot prices are higher at low wind speeds but the median revenues are relatively lower due to a lower power production. The annual revenues are obtained by summing up the hourly revenues and both values (using historic data and model-generated data) are found to be similar, with a difference of less than 1%. A similar difference is observed also for the Netherlands. This implies that although the model misses out on complex market dynamics, the variation of revenues with the wind speed and the calculated annual revenues are in the correct order, making it fit for this study.

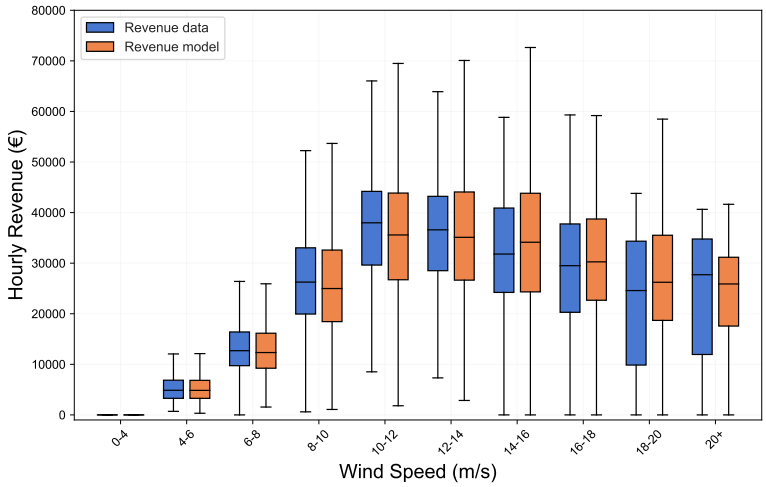

Figure 4.6: A comparison of the hourly revenue as a function of wind speed using historic data and the generated spot price data for Denmark

Market scenarios

The range of values, along with the number of discrete points used within this range, is shown in Table 4.1. The values at the bounds will result in extreme optimums and a change in these bounds will simply shift these extreme optimum designs. However, instead of the boundary points of the input, what is interesting is how the mean price and the correlation coefficient drive the optimum. Each combination of these two parameters represents a particular market scenario, with a total of 154 market scenarios being simulated. To reiterate, a value of 0.4 for the coefficient of variation is used for the baseline case to simulate all possible combinations of mean spot price and the correlation coefficient. Additionally, a sensitivity analysis is conducted to assess the impact of the coefficient of variation on the results.

Table 4.1: Market parameter variations

Parameter	Range	No. discrete points	Unit
Mean spot price (μ_{spot})	[40, 100]	14	€/MWh
Correlation coefficient ($\rho_{\text{correlation}}$)	[-1, 0]	11	–
Coefficient of variation (CV)	[0.4, 0.7]	2	–

4.4 Results & sensitivity

This section first discusses the resulting optimum for all the different scenarios. The differences in performance, for each metric, across the entire design space are then shown for a given market scenario. Finally, the overall performance of a few designs across all the market scenarios and objective functions is discussed.

4.4.1 Optimum designs for all market scenarios

For each market scenario, the optimum design may result in a positive business case or a negative business case. For instance, a positive business case has a profitability index higher than unity, a MIRR larger than the discount rate used for LCoE, and a positive NPV. A negative business case has a profitability index of less than unity, a MIRR lower than the discount rate used for LCoE, and a negative NPV. It is important to understand that the lowest specific power designs (low ratings and larger rotors) have the steepest power curve and the highest AEP and revenue, while the designs with the highest specific power (high ratings and smaller rotors) have the lowest wind farm costs. Figure 4.7 (a) shows the gradients for the total costs over the entire design space, while Figure 4.7 (b) shows the revenue gradients from selling electricity in the spot market, for a given market scenario.

The cost gradients always point towards the turbine with the highest rating and lowest rotor diameter. This is because an increase in rating decreases the number of turbines in the farm, reducing the O&M costs and installation costs, and a decrease in the rotor diameter decreases the turbine and support structure costs. Also, it can be seen how the revenue gradients point towards the turbine with the lowest rating and the largest rotor, resulting in the steepest power curve, having the highest revenue. Higher rated power in itself does not lead to higher revenues, since the total power of the farm remains constant. When changing the market scenario, the cost gradient for all the designs remains unchanged, while the revenue gradient for a design over its lifetime is altered. These gradients are shown to support later interpretations and explanations of the results.

Figure 4.8 (a) shows the LCoE of the entire design space along with the global optimum (rated power of 15.5 MW and rotor diameter of 230 m) that is already close to some of the state-of-the-art turbines, while Figure 4.8 (b) shows the optimum designs for all the market scenarios and all economic metrics. This optimum for

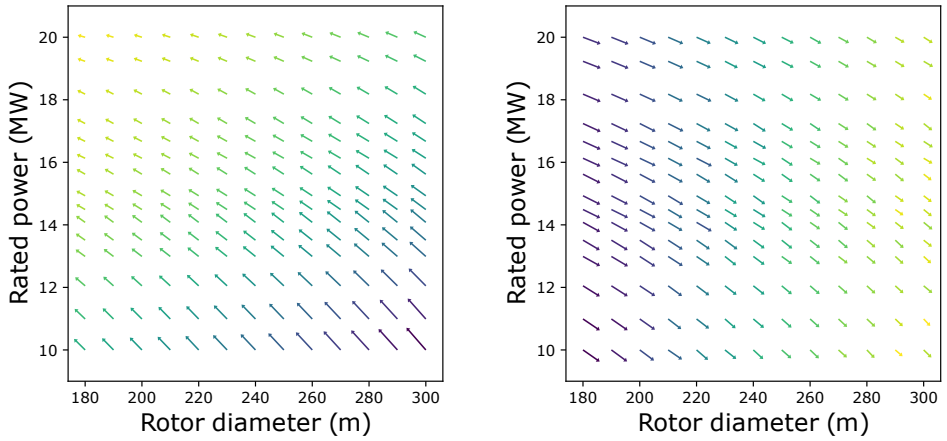

Figure 4.7: (a) Cost gradients for the entire design space (b) Revenue gradients for the entire design space

LCoE serves as the baseline for comparison against market-optimized designs. A detailed discussion about the LCoE-optimum and its sensitivity to various model parameters, design inputs, and the problem formulation can be found in Chapter 3.

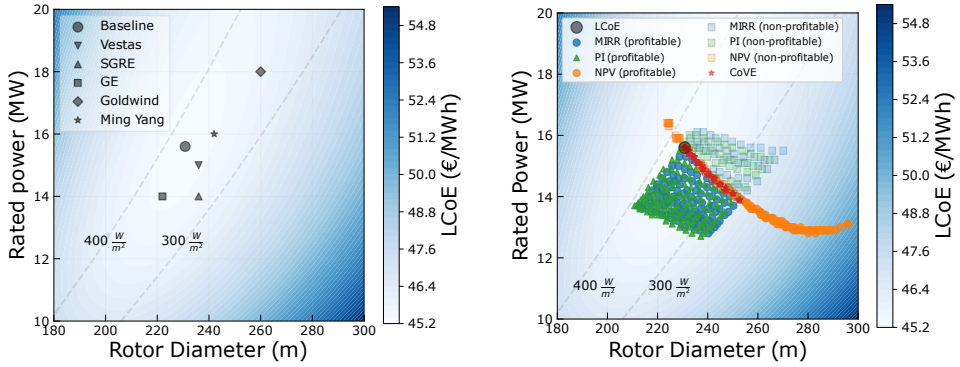

Figure 4.8: (a) Optimum turbine design for LCoE (b) Optimum turbine design for various objective functions and market scenarios

For each metric, the optimum designs for various market scenarios are different and are separately plotted. The optimum designs for market scenarios that resulted in a negative business case are plotted with a high transparency. Various market scenarios result in a spread of optimum designs for both MIRR and PI, while for NPV and CoVE, the optimums always move in the same direction. For NPV, the optimum approaches the rotor diameter limit at high mean spot prices. This can

be attributed to the behavior of the cost and revenue gradients, especially closer to the boundaries. It can be seen that depending on the choice of the economic metric and the realization of the future market, the optimum can differ significantly compared to the traditional LCoE-optimized design. Further explanations on how different market model parameters (μ_{spot} and $\rho_{\text{correlation}}$) drive the optimum for each economic metric are given below.

Effect of mean spot price

The mean spot price has a different effect on each metric. A change in the mean spot price also changes the standard deviation (as CV is constant) and hence, the distribution from which the prices are sampled. Figure 4.9 shows how, for a $\rho_{\text{correlation}}$ of zero, the mean spot price drives the optimum in different directions, depending on the metric. The arrows in the figure point in the direction of increasing mean spot prices.

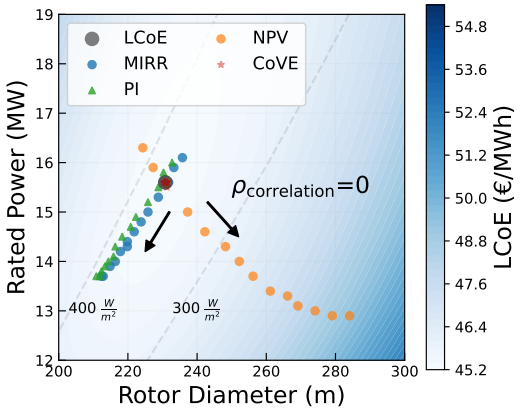

Figure 4.9: Optimum designs for different mean spot prices (for a correlation coefficient of 0)

The effect of the mean on the optimum for different metrics can be better explained by looking at the formulation of the metric itself. CoVE depends on the LCoE and the value factor (shown in Equation (4.5)). The value factor is the ratio of the price received by the developer (wind farm power-weighted average of the spot prices) and the mean spot price. An increase in the mean spot price almost equally increases the received spot price by the developer, canceling out the effect. Hence, a change in mean spot price has an insignificant effect on the value factor. As a consequence, CoVE and the optimum design w.r.t. CoVE do not change with a change in the mean spot price. MIRR and PI are metrics that are normalized with the initial investment and exhibit a similar behavior w.r.t. the shift in optimum. This is a measure of the best return (revenue) per euro invested. The behavior of

both metrics can be explained by looking at the formulation of PI, as shown in Equation (4.9), where the cashflow in each year (Cf_n) is the net revenue, which is simply the operations and maintenance costs ($C_{\mathrm{O\&M}}$) taken out from the total revenue earned from selling the electricity in the spot market (R_{spot}).

$$\begin{aligned} \mathrm{PI} &= \frac{\sum_{n=1}^{L} \frac{Cf_n}{(1+r)^n}}{C_{\mathrm{CAPEX}}} \\ &= \frac{\sum_{n=1}^{L} \frac{R_{\mathrm{spot}}}{(1+r)^n} - \sum_{n=1}^{L} \frac{C_{\mathrm{O\&M}}}{(1+r)^n}}{C_{\mathrm{CAPEX}}} \end{aligned} \tag{4.9}$$

For simplification, the summation of discounted revenues is written as R, and the summation of discounted operations and maintenance costs is written as O. The gradient of PI w.r.t. the rotor diameter (D) can be given by Equation (4.10). The gradients, along with their associated weights, for the revenue, operation and maintenance costs, and the initial investment are clearly separated. The gradient w.r.t. the rated power (P) can be similarly calculated.

$$\begin{aligned} \frac{\partial \mathrm{PI}}{\partial D} &= \frac{\partial}{\partial D}\left(\frac{\mathrm{R}-\mathrm{O}}{C_{\mathrm{CAPEX}}}\right) \\ &= \frac{1}{C_{\mathrm{CAPEX}}} \cdot \frac{\partial \mathrm{R}}{\partial D} - \frac{1}{C_{\mathrm{CAPEX}}} \cdot \frac{\partial \mathrm{O}}{\partial D} - \frac{(\mathrm{R}-\mathrm{O})}{C_{\mathrm{CAPEX}}^2} \cdot \frac{\partial C_{\mathrm{CAPEX}}}{\partial D} \end{aligned} \tag{4.10}$$

A change in the market scenario directly affects the revenue gradient but also results in a different absolute revenue. Hence, the weight of the gradient for C_{CAPEX} also changes with a change in the market scenario. The effect of the mean spot price on these gradients will determine the direction in which the optimum is driven.

Since NPV is simply a summation of the discounted revenues, initial investment, and discounted operations and maintenance costs, the gradients of NPV w.r.t. the rotor diameter are given by Equation (4.11). A change in the market scenario only alters the magnitude of the revenue gradient, while the cost gradients remain unaffected, unlike for PI or MIRR.

$$\frac{\partial \mathrm{NPV}}{\partial D} = \frac{\partial \mathrm{R}}{\partial D} - \frac{\partial \mathrm{O}}{\partial D} - \frac{\partial C_{\mathrm{CAPEX}}}{\partial D} \tag{4.11}$$

The effect of mean spot price on the gradients for NPV and PI is shown in Figure 4.10, where the gradients at the LCoE-optimized design are plotted. The

gradients for a mean spot price of 45 €/MWh and a mean spot price of 100 €/MWh, both with a correlation of 0, are shown. The gradients are normalized with the magnitude of the gradient with the maximum value.

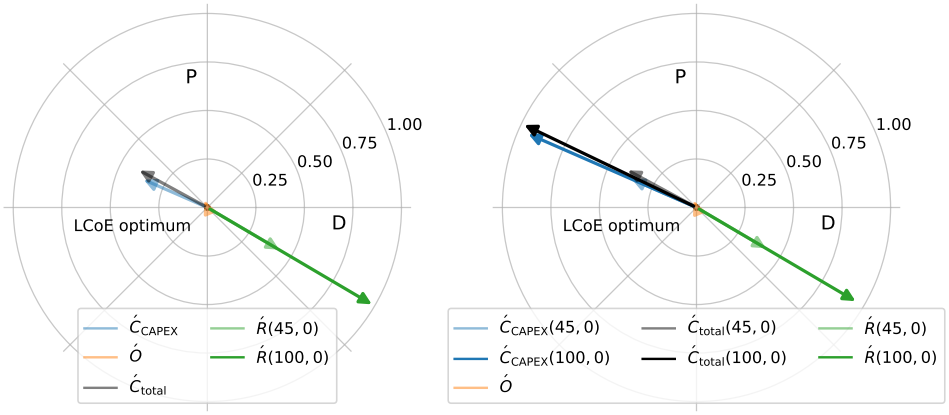

Figure 4.10: Effect of change in mean spot price on (a) NPV gradients and (b) PI gradients at the LCoE optimum.

A market scenario with a mean price of 45 €/MWh and a correlation of 0 represents a scenario where a fixed price around the minimum LCoE value is received for every unit of energy produced. The summation of the gradient (with the weights) for the initial investment (C'_{CAPEX}) and the gradient (with the weights) for the operations and maintenance costs ($\acute{O}$) result in the total cost gradient (C'_{total}). For the mean spot price of 45 €/MWh (and correlation of 0), the gradients for costs and revenue are in balance, indicating that the LCoE-optimum point is also the market-optimum design, for both metrics. This is because the LCoE at this point is approximately 45 €/MWh, representing the minimum LCoE across the design space.

An increase in the mean spot price to 100 €/MWh clearly has an impact on the revenue gradient ($\acute{R}$). This is the only change in the NPV gradients. Hence, the optimum moves along the direction of the revenue gradient. Any change in the mean spot price will always move the optimum along the direction of the revenue gradient, which was shown in Figure 4.7. For the gradients of PI, shown in Figure 4.10 (b), it can be seen that, since the absolute revenue also changes, the weight of C'_{CAPEX} also goes up (shown in Equation (4.10)). This results in an increase in C'_{CAPEX}. Since $\acute{O}$ does not change, a change in C'_{CAPEX} causes a shift in both magnitude and direction of the total cost gradient (C'_{total}). This change in direction leads to a shift in optimum along a different direction than the direction along the line of C'_{total} and $\acute{R}$. The resultant of the new cost and revenue gradients

pushes the optimum towards downsized turbines with lower ratings and smaller rotors. The same effect is also observed for MIRR. This is represented by the optimum designs along the constant specific power line, shown in Figure 4.8. From the LCoE-optimum design, the optimum designs in the direction of the constant specific power are driven by different mean spot prices. That line corresponds to a correlation of 0. Similarly, for other values of the correlation coefficient, the mean spot price also drives the optimum in the direction of constant specific power, albeit from a different starting point than the LCoE optimum.

Effect of the correlation coefficient

The correlation coefficient affects the rate of change of spot prices w.r.t. the wind speed. For the same mean and standard deviation, a correlation of zero results in no relation between the spot prices and wind speed, while a correlation of -1 results in a perfectly anti-correlated line. However, the correlation coefficient drives the optimum differently, compared to the mean spot prices. Figure 4.11 shows how, for a fixed μ_{spot} of 45 €/MWh, the correlation coefficient drives the optimums in the same direction but with differing magnitudes, depending on the metric. The arrows in the figure point in the direction of increasing (more negative) correlation coefficients.

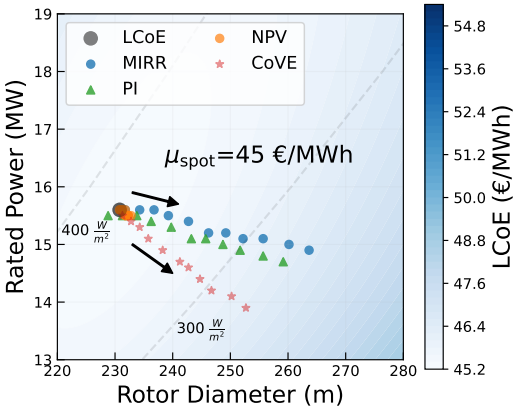

Figure 4.11: Optimum designs for different correlation coefficients (for a mean spot price of 45 €/MWh)

The effect of change in the correlation coefficient on the gradients for NPV and PI is shown in Figure 4.12. The figure shows the revenue and cost gradients for a market with a mean price of 45 €/MWh and for two different correlation values, 0 and -1, resembling no correlation and perfect anti-correlation. It can be seen that the revenue gradient ($\dot{R}$) for the high correlation case is slightly larger than the gradient with no correlation. For NPV, that is the only change in the gradients,

again driving the optimum along the direction of the revenue gradient. However, it can be seen that the change in the revenue gradient is minor compared to the change caused by the variations in the mean spot price.

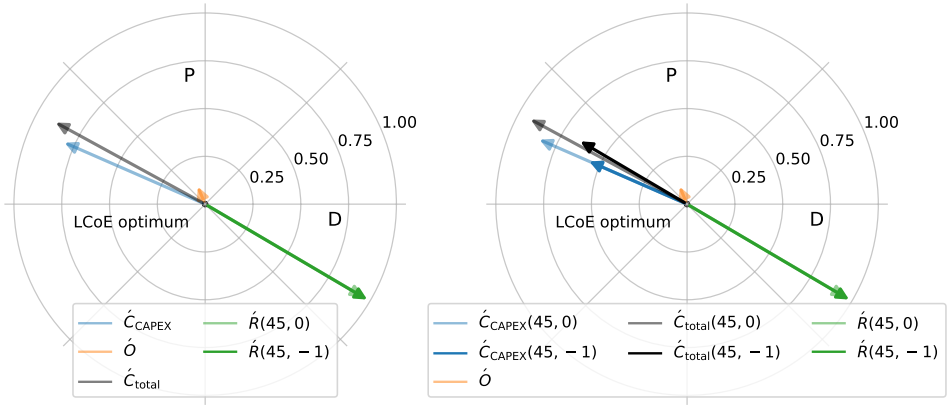

Figure 4.12: Effect of change in the correlation coefficient on (a) NPV gradients and (b) PI gradients at the LCoE optimum

For the same mean spot price, an increase in the correlation coefficient increases the value of the power produced at lower wind speeds and results in a shift in optimum towards larger rotors (lower specific powers). For PI (and MIRR), because of the change in the absolute revenue, the weight of C'_{CAPEX} decreases, as indicated by the decrease in the vector magnitude. This also causes a slight change in the direction of the total cost gradient (C'_{total}). For the scenario with a high correlation, the magnitude of $\acute{R}$ is much larger compared to the magnitude of C'_{total}. The resultant of these two vectors drives the optimum in the direction of the revenue gradient, same as for NPV. The difference in magnitude of the two vectors for PI and MIRR is much larger than the difference observed for NPV. Hence, the correlation has a relatively larger effect on the optimum design w.r.t. PI and MIRR, compared to NPV.

For higher correlation coefficients (more negative), the power produced at lower wind speeds is valued much more than at higher wind speeds. Hence, designs with a low specific power have a higher value factor for market scenarios with high (more negative) correlation coefficients. As a consequence, the correlation coefficient also drives the optimum w.r.t. CoVE towards larger rotors and lower ratings.

Summary of the effect of market parameters

This section summarizes how both the market parameters drive the optimum turbine design. The results show that the choice of metric has a crucial impact on

the magnitudes and directions of changes in the optimal designs w.r.t. changes in the mean spot price and the correlation coefficient. For NPV, only the magnitude of the revenue gradient changes when the mean spot price or the correlation coefficient changes. For PI/MIRR, along with the changes in the magnitude of the revenue gradient, both the magnitude and direction of the cost gradient also change. This is caused by the effect that normalization by mean revenues has on the weights of the CAPEX gradient.

For changes in the mean spot price, absolute profits (NPV) drive the solution in a direction perpendicular to the change for normalized profits (PI, MIRR). The magnitude of change is significant for both NPV and PI/MIRR. Normalization with the mean revenue, for CoVE, makes the design insensitive to changes in the mean spot price. For changes in the correlation coefficient, the direction of change in the optimum does not depend on the metric, and the optimum is always driven in the direction of changing specific power. A larger (more negative) correlation pushes the optimum towards larger rotors and lower power ratings (lower specific powers). However, the magnitude of change is relatively larger for PI/MIRR than that for NPV. Since only the correlation coefficient influences the value factor, the spread of optimum designs for CoVE, shown in Figure 4.8, can be attributed to changes in the correlation coefficient.

The change in the gradients of each metric explains how the optimum shifts w.r.t. changes in the mean spot price and the correlation coefficient. Section 4.4.1 shows how metrics other than MIRR or PI may lead to completely different design trends, especially w.r.t. the mean spot price. As discussed before, the difference in behavior is a result of the formulation of the metric itself. It is, now, also apparent how the results of NPV differ and might be misleading, compared to other economic metrics, for optimization problems with changing investments. Although CoVE captures the changes in the market value of wind, it does not respond to changes in the mean spot prices, and hence, may not be ideal when evaluating the business case for a developer. Therefore, in the following sections, only the analyses w.r.t. PI and MIRR are discussed in further detail.

4.4.2 Performance of all designs for a single market scenario

In the previous section, Figure 4.8 showed the LCoE across the entire design space. It also showed that the LCoE along the constant specific power line does not change significantly, compared to the LCoE at the optimum, even for large changes in the design. Similarly, even though the market scenarios result in different optimum designs, it is important to evaluate the difference in the absolute performance of PI and MIRR across the entire design space. A market scenario that results in a large change in the optimum, compared to the LCoE-optimized design, is considered. The performance across the entire design space for a market scenario with a mean

price of 100 €/MWh and a correlation coefficient of -1 is shown in Figure 4.13. For both PI and MIRR, the global optimum for the given market scenario and the LCoE optimum are also shown.

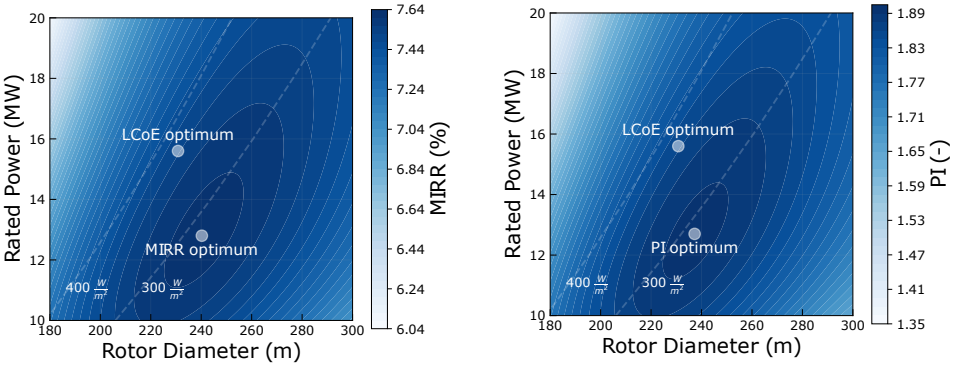

Figure 4.13: Performance of the entire design space w.r.t. (a) MIRR and (b) PI for a market scenario with μ_{spot} = 100 €/MWh and $\rho_{\text{correlation}}$ = -1

Section 2.9 defines a change of 5% or more in the objective function as significant. For both MIRR and PI, it can be seen that although the market-driven optimum is different from the LCoE optimum, the difference in the value of the metric itself is insignificant. The value of MIRR and PI for the LCoE-optimized design is about 2-3% lower than the maximum value of the design specifically optimized for MIRR and PI. It can be seen that even for an extreme market scenario, the values for MIRR and PI for a large range of designs around the optimum are similar to the value for the optimum design. Depending on the market scenario, the optimum differs and so does the difference in the absolute value of the metric. However, the difference in the absolute values of MIRR and PI between a market-optimized design and an LCoE-optimized design is less significant.

4.4.3 Performance of different designs over all market scenarios

It is clear that for any given objective, different market scenarios result in different optimum designs. The difference in the value of the metric itself for one market scenario was also discussed in Section 4.4.2. However, it is crucial to understand if there is any added value in optimizing designs specifically for a certain market scenario and to understand the risk of designing for the wrong market. Hence, the performance of some designs over the complete range of market scenarios is determined for both MIRR and PI. The designs used for comparison are the LCoE-optimized design (15.5 MW-230 m), a downsized turbine (14 MW-220 m) with similar specific power as the LCoE-optimized turbine, a low specific power turbine

(14 MW-260 m), and an upscaled turbine close to the state of the art in the industry (18 MW-260 m), but with slightly lower specific power than the LCoE-optimized turbine. Figure 4.14 shows the performance of the four sample designs plotted against μ_{spot} for the two extreme values of $\rho_{\text{correlation}}$. The dotted horizontal line in the plots separates the profitable and non-profitable values.

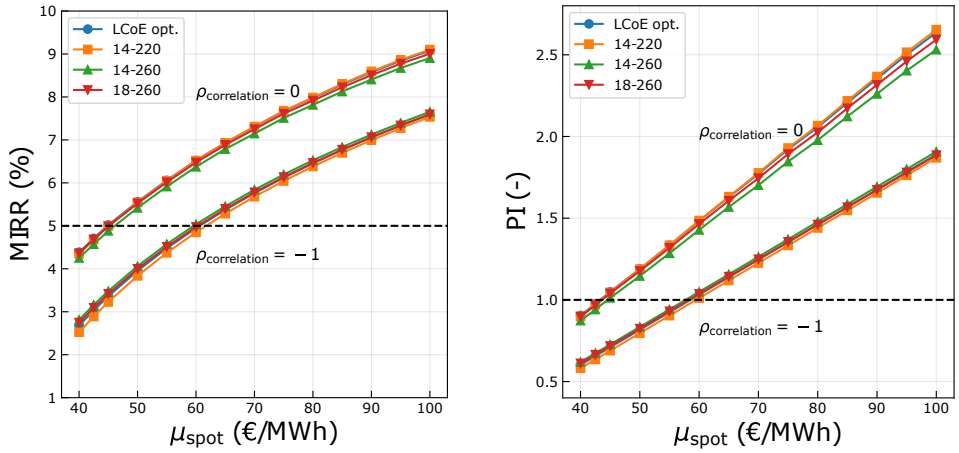

Figure 4.14: Performance of the designs w.r.t. (a) MIRR and (b) PI over the complete range of market scenarios

Clearly, both MIRR and PI increase with an increase in the mean spot price, for all the designs. Also, the values drop with an increase in the correlation coefficient (more negative). This is simply because a higher mean spot price (for the same correlation) results in higher revenues and a higher correlation (for the same mean spot price) leads to lower prices at high-yield wind speeds, resulting in lower revenues. It can also be seen that the variations in the economic value due to the design choices are insignificant compared to the variations due to the uncertainties in the market scenario. The mean spot price and the correlation will be determined by how wind generation, demand, and various other technologies develop in the future. These factors will largely determine the economic performance of the wind farm rather than the choice of turbine design. The differences in the performance are significant only when designing for certain extreme market scenarios (low mean spot price and a high negative correlation or high mean spot price and no correlation).

For most scenarios, all the designs exhibit a similar performance, for both MIRR and PI. For a correlation coefficient of zero, the LCoE-optimized design performs better than the low specific power designs, for any given mean spot price. For scenarios with a high correlation, the low specific power designs perform

marginally better than the LCoE-optimized design, for any given mean spot price. This suggests that although a design optimized for the market might have a slightly higher MIRR or PI, an LCoE-optimized design already performs quite well w.r.t. MIRR and PI.

4.4.4 Sensitivity to the coefficient of variation

With the rise in wind and solar penetration over the next few years, the price variations are expected to increase, as mentioned in Swisher et al. [25]. The effect of the correlation coefficient is amplified for a higher CV value, as shown in Figure 4.4. At some point, very large price variations might lead to some restoring measures, be it by storage or regulations. Also, if, in the future, CV increases due to other renewables like solar, then the correlation coefficient w.r.t. wind would decrease. Figure 4.15 presents results for a CV value of 0.7, higher than the baseline value of 0.4. The optimum designs for all market scenarios and two relevant objectives are shown in Figure 4.15 (a). The difference in the absolute value of MIRR between the two designs for a mean spot price of 100 and correlation of -0.5 is shown in Figure 4.15 (b).

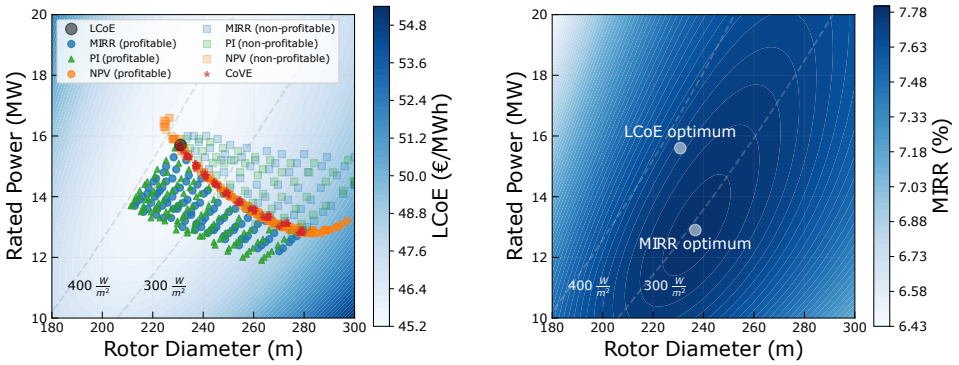

Figure 4.15: (a) Optimum designs for various objective functions and market scenarios with a high CV (b) MIRR across the entire turbine design space for an extreme market scenario with a high CV.

As seen in the figures, the differences in the design and the value of the objective are similar to those of the base case. However, the differences are significant for the highly unlikely scenarios of high CV with high levels of anti-correlation. For higher CV values, the standard deviation of the spot prices is also higher, leading to a larger spread in the prices. For high anti-correlation values, this difference in spot prices between lower and higher wind speeds is amplified, further favoring low specific power turbines. Hence, redesigning the turbine specifically for the market could be beneficial for future scenarios where the price variations are extremely high, along with high levels of anti-correlation with wind.

4.5 Discussion

This research looked at how various economic metrics (MIRR, PI, NPV, and CoVE) and different future market scenarios would drive the optimum turbine design. The research specifically considered turbines in a hypothetical offshore wind farm in the North Sea where the farm power and area were kept constant. Also, the revenues only from the day-ahead market were considered. Some general insights from this study are listed below.

- MIRR and PI exhibit a similar behavior w.r.t. both changes in the mean spot price and the drop in spot prices w.r.t. the wind speed (cannibalization effect). Compared to the LCoE-optimized turbine, an increase in the mean spot price drives the optimum towards downsized turbines with similar specific power. For regions with a high wind penetration, resulting in a larger drop in spot prices w.r.t. the wind speed, the optimum shifts towards lower specific power turbines in the direction perpendicular to the constant specific power line. The study also showed how MIRR and PI, which normalize the revenues with the initial investment, are better suited for a turbine optimization problem compared to NPV, which measures absolute profits.

- The benefits of redesigning the turbine for a specific market scenario are marginal. It is seen that even in an extreme market scenario, the values of MIRR and PI for an LCoE-optimized are 7.5% and 1.86 respectively, while the values for the market-optimized design are 7.6% and 1.89, respectively. The relative differences are insignificant for most market scenarios. However, a market-driven design could potentially be beneficial for future (less likely) scenarios with even more extreme cannibalization.

- The impact of the choice of the design itself on MIRR/PI is found to be insignificant for most market scenarios. The value of MIRR/PI for most designs in a wide range of specific powers (200-400 Wm^{-2}) is only up to 10% lower compared to the value of the market-optimized design.

To operate in future subsidy-free day-ahead markets, the optimum and economic performance will largely be governed by how market prices develop. However, for metrics like MIRR and PI that allow a fair comparison of designs, a large range of designs perform well. The results of this study indicate that there is a limited need to focus efforts on redesigning turbines that are better suited for a specific market scenario. LCoE-optimized turbines are found to perform well for most day-ahead market scenarios. Turbine optimization might still be largely driven by various other factors like wind resources, farm parameters, grid and/or area constraints, etc.

5

Turbine sizing for decentralized offshore hydrogen production

Wind energy isn't just powering the grid;
it's powering communities, industries, and a sustainable future.

Michael Skelly

To limit the consequences of climate change, generation from renewables coupled with large scale electrification is necessary. However, the deployment of renewables has its own challenges, and not all sectors can be electrified. Green hydrogen production from wind energy can alleviate some of these challenges. Also, the existing high demand for hydrogen, which is largely met by fossil fuels, needs to be transitioned to green hydrogen. The current costs of green hydrogen production are high due to the high costs of electricity used for electrolysis. This study looks into the benefits of optimizing a turbine specifically for decentralized hydrogen production and the reduction in the Levelized Cost of Hydrogen (LCoH) compared to the use of conventional Levelized Cost of Energy (LCoE) optimized turbines.

A brief introduction to the studies related to wind-produced hydrogen is given in Section 5.1 followed by the formulation of LCoH in Section 5.2. The modeling aspects related to hydrogen production and costs are explained in Section 5.3. The hydrogen-specific assumptions used in the case study are shown in Section 5.4. Finally, Section 5.5 discusses the differences between an LCoH-optimized and an LCoE-optimized design followed by a sensitivity analysis of the optimum.

5.1 Introduction

Most studies focused on green hydrogen production from wind energy assume a fixed turbine and farm configuration, originally optimized for electricity production. However, turbine design has a direct impact on the Capital Expenditure (CAPEX) and Operational Expenditure (OPEX) of a wind farm and the amount of hydrogen produced. Thomas et al. [26] explore how the design of a turbine optimized for hydrogen production changes compared to a turbine optimized for electricity production. The research presented is in the same direction as the work presented in this chapter. The research provides an optimization framework for a decentralized wind-hydrogen system and explores a single-turbine case study for a site in Texas. The findings suggest a larger rotor diameter for a hydrogen-optimized turbine and the optimum electrolyzer size to be similar to that of the turbine rating. The research provides useful insights into the modelling aspects of a wind-hydrogen system but the scope is limited to a single onshore wind turbine. Additionally, the reasoning behind the differences between the two designs is not emphasized. This study explicitly focuses on how a turbine designed specifically for hydrogen production would differ from a turbine designed for electricity production, and to know whether it further reduces the LCoH. The economics of various hydrogen production configurations has been studied before [74]. However, that study assumes both electricity and hydrogen infrastructure are present, and the production of electricity or hydrogen depends on the most economical strategy. A similar hybrid usage strategy is demonstrated by Glenk and Reichelstein [75]. Various hydrogen production configurations, such as centralized offshore production, decentralized offshore production, and onshore production, along with their respective advantages and disadvantages, have been discussed in the literature [76]. Decentralized production offers cost advantages by eliminating the need for transformers, converters, and switchgear used in the RNA. Therefore, this study focuses on decentralized hydrogen production, where the electrolyzer stacks, together with the auxiliary units and compressors, are integrated into the turbine itself. In this configuration, hydrogen is directly transported to shore via pipelines, which is considered more economical than centralized offshore production, since the latter requires an additional and costly offshore platform for hydrogen production components.

This study conducts a sizing analysis for green hydrogen production (minimizing LCoH) and electricity production (minimizing LCoE) and draws a comparison between the two. The main research question can be formulated as follows:

How does turbine sizing optimized specifically for decentralized offshore hydrogen production differ from turbine sizing optimized for electricity production?

The research activities required to answer the main question are:

1. Optimize the turbine size w.r.t. the LCoE for a typical case
2. Determine the optimum turbine size w.r.t. the LCoH and the corresponding optimum electrolyzer to turbine capacity ratio
3. Identify the drivers for the difference in turbine designs
4. Explore the sensitivity of the optimum w.r.t. the costs of the electrolyzer system

The turbine size refers to two main system-level parameters of a turbine, the rated power and rotor diameter. These are the two design variables that are optimized in this study.

5.2 Levelized cost of hydrogen as objective function

The LCoH is given by Equation (5.1) where n is a given year, L is the operating lifetime of the wind farm and r is the real discount rate. The numerator contains the capital expenditures (C_{CAPEX}) that are paid initially, the summation of all the annual actualized operation and maintenance costs (C_{OPEX}), and the decommissioning costs paid at the end of the lifetime (C_{DECOM}) while the denominator contains the summation of the actualized hydrogen production values (m_{H2}).

$$\text{LCoH} = \frac{C_{\text{CAPEX}} + \sum_{n=1}^{L} \frac{C_{\text{OPEX}}}{(1+r)^n} + \frac{C_{\text{DECOM}}}{(1+r)^L}}{\sum_{n=1}^{L} \frac{m_{\text{H2}}}{(1+r)^n}} \tag{5.1}$$

5.3 Hydrogen production and transportation module

This study focuses on a turbine-integrated hydrogen production configuration where each turbine has an integrated electrolyzer that produces hydrogen at 30 bar, which is later compressed to 80 bar and exported to shore, as shown in Figure 5.1. The next sections address the model for the hydrogen production and export system. Compared to the conventional configuration used for electricity production, the hydrogen production system has several changes:

- Removal of the DC/AC converter since the input to the electrolyzer is DC.
- Addition of the electrolyzer system and some auxiliary equipment like dryers, separators, coolers, and a deionization system.

- Addition of a compressor system to compress the hydrogen produced to 80 bar.
- Replacement of the cabling system with infield and export pipelines to transport the hydrogen produced.

The wind turbine itself supplies the electricity required to power the auxiliary equipment and the compressors.

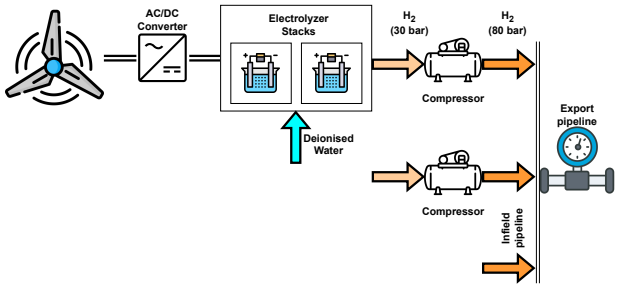

Figure 5.1: Schematic of the turbine-integrated hydrogen production configuration [77]

5.3.1 Electrolyzer system

A Polymer Exchange Membrane (PEM) electrolyzer is used inside each turbine due to its compactness, high output pressures, high efficiencies, and near-zero minimum operating load requirement [18]. The electrolyzer system consists of the stacks along with the auxiliary unit. The auxiliary unit includes equipment for deionized water circulation, hydrogen processing, and cooling. The system efficiency is based on the work of Kopp et al. [78], where the hydrogen produced using an electrolyzer with a peak power of 6 MW connected to a wind farm of 8 MW was measured. The hydrogen produced was later compressed to 225 bar. The efficiency curve includes the efficiencies of the stacks, the auxiliary unit, and the compressor. The curve is tweaked to account for the differences in their system and the system used in this study. This study does not use a rectifier since the power from the AC/DC converter in the turbine is directly fed into the stacks. Also, the compressor pressure used in this study is 80 bar, while the study by Kopp et al. [78] used an output pressure of 225 bar. The system efficiency peaks at about 30% input load followed by a slight drop in efficiency with further increase in the input load, as shown in Figure 5.2. This shape can be attributed to the nature of the DC efficiency of the stack and the efficiency of the auxiliary components like the cooling unit, compressors, pumps, etc. The DC efficiency of the stacks is the highest at low input loads and decreases with an increase in the input load while

the efficiency of the auxiliary equipment increases rapidly until about 30-40% input load and then flattens out [18][79]. This results in the resultant efficiency curve of the overall electrolyzer system. In this study, both a variable efficiency curve and a fixed efficiency curve are modeled, as shown in Figure 5.2. The fixed efficiency curve is a simplification that ignores the effects of the change in efficiency with input load. Since both models are used by other studies in literature, both curves are modeled so that they can be used to understand the differences in the turbine sizing due to the nature of the efficiency curve. The value of the fixed efficiency is calibrated such that, at the LCoE optimum, the hydrogen produced due to the variable efficiency curve is the same as the hydrogen produced with the fixed efficiency curve.

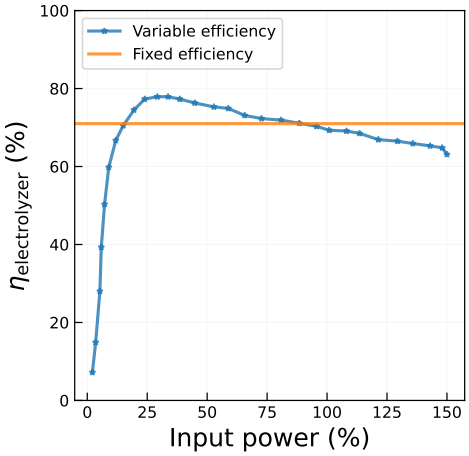

Figure 5.2: Variable and fixed efficiency curve of the electrolyzer system

For a given instantaneous turbine power (P_t), the mass flow rate of hydrogen (Q) in kg/hr is given by Equation (5.2) where HHV represents the higher heating value of hydrogen and $\eta_{electrolyzer}$ represents the instantaneous electrolyzer efficiency, which is a function of the input turbine power. The flow rate per turbine would differ since the input turbine power would mainly depend on the wind speed deficit experienced by the turbine.

$$Q = \frac{P_t \cdot \eta_{electrolyzer}(P_t)}{HHV} \tag{5.2}$$

It should be noted that no efficiency degradation over the lifetime is considered. There would be some minor differences in the voltage efficiency decrease because of different utilization of the electrolyzer for different turbine designs. However, any other degradation is not expected to favor one turbine design more than the

other. Hence, although hydrogen production would be reduced with the inclusion of degradation, the impact on the optimum is expected to be insignificant.

The costs of the electrolyzer system include the costs for the stacks and the Balance of Plant (BoP), which consists of the cooling system, hydrogen processing equipment, and the deionization system. A wide range of electrolyzer costs have been reported in literature [80]. The costs used in this study are discussed in the case study section. Groenemans et al. [81] assumes a total cost as low as $300/kW for the entire electrolyzer system. This low estimate is based on future developments and does not represent current cost estimates. However, a sensitivity to electrolyzer system costs is also carried out in the current study.

The costs and instantaneous efficiency of the electrolyzer also depend on its sizing ratio ($\zeta_{\text{electrolyzer}}$), which is a ratio of the electrolyzer rated power ($P_{\text{electrolyzer}}$) and the turbine rated power (P_{turbine}) for a decentralized hydrogen production system, as shown in Equation (5.3). Here, $P_{\text{electrolyzer}}$ refers to the rated power of the entire electrolyzer system (stacks and auxiliary equipment) and the compressor.

$$\zeta_{\text{electrolyzer}} = \frac{P_{\text{electrolyzer}}}{P_{\text{turbine}}} \tag{5.3}$$

The electrolyzer is allowed to operate at input loads greater than 100% for 15 mins, after which, any power greater than $P_{\text{electrolyzer}}$ is curtailed.

5.3.2 Compressor

The compressor is used to compress the hydrogen produced at 30 bar to around 80 bar. The system efficiency curve of the electrolyzer already includes the losses from the compressor. The costs of the compressor are expressed as a linear function of the rated power, as shown in Equation (5.4) where the rated power is given by Equation (5.5) [82]. The scaling factor is expressed in $/kW, while the rated power of the compressor is given in kW.

$$C_{\text{comp}} = 2545 \cdot P_{\text{comp}} \tag{5.4}$$

Q is the flow rate of hydrogen which depends on the hydrogen produced at turbine rated power, p_{out} and p_{in} represent the output and inlet pressures, Z is the hydrogen compressibility factor, N is the number of compressor stages assumed to be two, T is the compressor inlet temperature assumed to be 310.95 K, γ is the ratio of specific heats, M_{H2} is the molecular mass of hydrogen, η_{comp} is the compressor efficiency assumed to be 75%, and R is the universal gas constant.

$$P_{\text{comp}} = Q \cdot \frac{Z \cdot T \cdot R}{M_{\text{H2}} \cdot \eta_{\text{comp}}} \cdot \frac{N \cdot \gamma}{\gamma - 1} \left(\left(\frac{p_{\text{out}}}{p_{\text{in}}} \right)^{\frac{\gamma - 1}{N \cdot \gamma}} - 1 \right) \tag{5.5}$$

5.3.3 Pipeline

The pipeline costs depend on the diameter, which in turn depends on the flow rate, and the total length. The total pipeline costs include material costs, labor costs, miscellaneous costs like contingencies, engineering, etc., and right of way costs [83]. The total costs per unit length ($CF_{pipeline}$ in €/m) is expressed as a function of the pipeline diameter ($D_{pipeline}$ in mm), based on the model described in Reuß et al. [84], as shown in Equation (5.6).

$$CF_{pipeline} = 1.05 \cdot \left(0.0006 \cdot D_{pipeline}^2 + 0.418 \cdot D_{pipeline} + 295\right) \tag{5.6}$$

The cost factor for a given range of values for the pipeline diameter is shown in Figure 5.3. The costs are in a similar range as that in Néstor González Díez et al. [85] and Parker [83]. The cost factor is then multiplied by the infield pipeline and export pipeline length to get their respective costs.

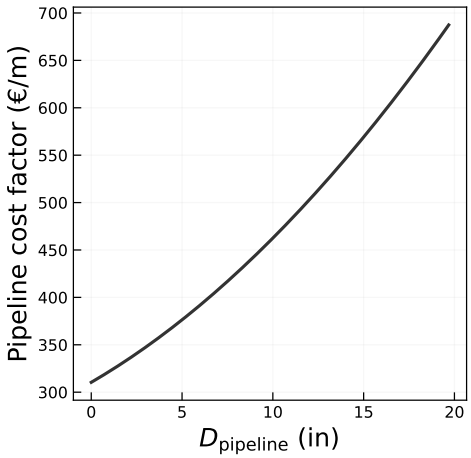

Figure 5.3: Pipeline cost factor as a function of pipeline diameter (based on [84])

For the export pipeline, the flow rate is governed by the maximum hydrogen that can be produced at full load, and the length is fixed. Unlike the infield cable layout in an electrical wind farm, the infield pipeline topology is simplified, where a single feeder connects all the turbines in a single column, and the total number of columns in the regular square layout determines the number of feeders. Hence, for the infield pipeline, the flow rate depends on the rated power of the turbine and the number of turbines in a given column, which depends on the farm layout. The maximum flow rate for the infield pipeline ($Q_{infield}$) and the export pipeline (Q_{export}) can be derived using Equation (5.2) and is given by Equation (5.7) and Equation (5.8), respectively. For the infield pipeline, the maximum flow rate is

achieved when the turbine operates at its rated power, P. $N_{\mathrm{T,feeder}}$ is the number of turbines per feeder, which in turn depends on the number of turbines per column. For the export pipeline, the hydrogen produced per turbine at full-load is multiplied by the total number of turbines in the wind farm (N_{T}).

$$Q_{\mathrm{infield}} = \frac{P \cdot \eta_{\mathrm{electrolyzer}}(P)}{\mathrm{HHV}} \cdot N_{\mathrm{T,feeder}} \tag{5.7}$$

$$Q_{\mathrm{export}} = \frac{P \cdot \eta_{\mathrm{electrolyzer}}(P)}{\mathrm{HHV}} \cdot N_{\mathrm{T}} \tag{5.8}$$

Kuczynski et al. [86] show how the pipeline diameter, mass flow rate, and pipeline inlet pressure are related. For a fixed pipeline inlet pressure, the scaling relation between the diameter and flow rate can be given by Equation (5.9).

$$D_{\mathrm{pipeline}} \propto Q^{0.4} \tag{5.9}$$

For a flow rate of 0.3 kg/s and a pipeline inlet pressure of about 80 bar, the calculated diameter was about 90 mm [86]. Since a similar pipeline inlet pressure is used in this study, the diameter of 90 mm is used as a reference and is scaled w.r.t. the flow rate to evaluate the diameter of both infield and export pipelines.

5.4 Case study description

The section describes the baseline case and its underlying assumptions. The site conditions used to simulate the wind farm are already defined in **Chapter 2**. This section elaborates the research activities required to answer the research question.

- First, the turbine size needs to be optimized w.r.t. the LCoE for a representative case. This is already shown in **Chapter 4**, which sets the baseline LCoE case.
- Next, for the baseline LCoH case, the turbine size is optimized w.r.t. the LCoH. This is done for an initial set of assumptions for the electrolyzer costs and an electrolyzer-to-turbine capacity ratio ($\zeta_{\mathrm{electrolyzer}}$) of 1.
- The baseline analysis will be carried out using a variable electrolyzer efficiency curve where the efficiency is a function of the input load. To evaluate the effect of the nature of the efficiency curve on the optimum turbine size, a case with a flat efficiency will also be simulated.
- The drivers leading to the differences in design between the LCoE and the LCoH-optimized turbine are identified and elaborated.

- The same LCoH optimization is then performed for various electrolyzer-to-turbine capacity ratios to determine the optimal sizing ratio and the corresponding optimal turbine sizing.
- Lastly, since a large range of electrolyzer costs are reported in the literature, the sensitivity of the LCoH optimum w.r.t. the electrolyzer costs is carried out.

The assumptions used to optimize for the baseline LcoH case are summarized in Table 5.1. The cost assumptions are based on the estimates from van 't Noordende and Ripson [87], IRENA [18], and Mayyas et al. [88]. The additional cost factor includes additional indirect costs like profit margins, contingency, etc. [87] and costs for installation. Mayyas et al. [88] suggests a cost factor of about 1.3 for installation but that has been reduced and included in the total cost factor since most of the electrolyzer system installation can be performed along with the wind turbines. The Operations & Maintenance (O&M) costs of the electrolyzer system are expressed as a fraction of the electrolyzer system CAPEX ($C_{\text{electrolyzer}}$). A stack lifetime of 10 years is assumed [18], and the number of stack replacements would depend on the wind farm lifetime, assumed to be 25 in this study.

Table 5.1: Electrolyzer system costs

Variable	Value
Electrolyzer-to-turbine capacity ratio ($\zeta_{\text{electrolyzer}}$)	1
Electrolyzer stack costs	400 $/kW
Electrolyzer BoP costs	200 $/kW
Battery backup costs	10 M$
Additional cost factor	1.6
Electrolyzer O&M costs	2% of $C_{\text{electrolyzer}}$
Stack lifetime	10 years

5.5 Results & sensitivity

This section discusses the results for the baseline case and also shows the sensitivity of the optimum to changes in the inputs.

5.5.1 Baseline results

Figure 5.4 show the cost breakdown for electricity production and hydrogen production respectively, for a 1 GW farm using the LCoE optimized design (a rated power of 15.5 MW and rotor diameter of 230 m). The cost breakdowns include all the capital expenditures, discounted O&M expenditures over the lifetime, and

the decommissioning costs. As seen, for the hydrogen production configuration, the cost of the pipelines is much lower than the cost of the electrical equipment. However, the electrolyzer system costs (including stack replacement costs) take up a huge share. The slight increase in the O&M cost share for the hydrogen configuration is because of the additional costs of maintaining the electrolyzer facility.

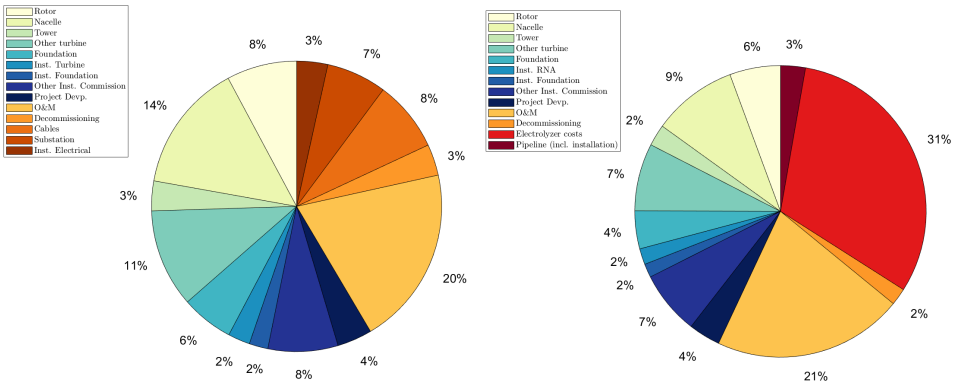

Figure 5.4: (a) Electricity production cost breakdown (b) Hydrogen production cost breakdown

The LCoH over the entire design space is shown in Figure 5.5. The figure also shows the difference in the optimum designs for electricity and hydrogen production. Section 2.9 defines a change of 5% or more in the objective as significant. Within the analysed domain of the design variables, the change in LCoH is significant in the direction of changing specific power, while it is insignificant in the direction of constant specific power. This is similar to the LCoE variations across the design space (as shown in Chapter 3), which can be attributed to how costs and the AEP change w.r.t. both design variables. It can also be seen that the design optimized for hydrogen production has a larger rotor, and hence, a lower specific power than that of the design optimized for electricity production.

The differences in the optimum design can be explained via LCoH gradients at the LCoE optimum. The gradient formulation for LCoE and its deconstruction into cost and AEP gradients is explained in Section 3.3. The gradients for LCoH can be similarly obtained. In simplified terms, the LCoH can be expressed as total lifetime costs (C_{H2}), which is the sum of total CAPEX, discounted OPEX, and decommissioning costs, divided by the discounted hydrogen production over the lifetime (m_{H2}). The gradient of LCoH w.r.t. the rotor diameter and rated power is shown in Equation (5.10) and Equation (5.11), respectively. It is expressed in the form of cost and hydrogen production gradients along with their weights.

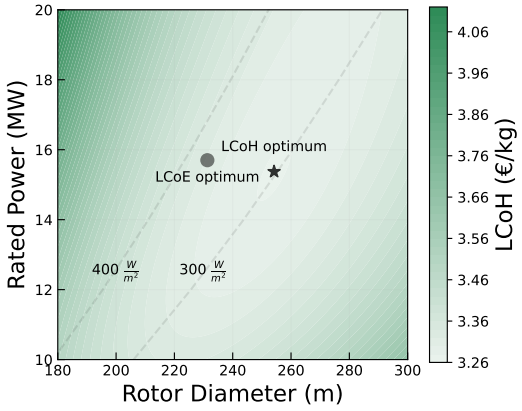

Figure 5.5: LCoH across the entire design space for the baseline case

$$\frac{\partial \text{LCoH}}{\partial D} = \frac{1}{{m_{\text{H2}}}^2}\left(m_{\text{H2}} \cdot \frac{\partial C_{\text{H2}}}{\partial D} - C_{\text{H2}} \cdot \frac{\partial m_{\text{H2}}}{\partial D}\right) = A \cdot \frac{\partial C_{\text{H2}}}{\partial D} - B \cdot \frac{\partial m_{\text{H2}}}{\partial D} \tag{5.10}$$

$$\frac{\partial \text{LCoH}}{\partial P} = \frac{1}{{m_{\text{H2}}}^2}\left(m_{\text{H2}} \cdot \frac{\partial C_{\text{H2}}}{\partial P} - C_{\text{H2}} \cdot \frac{\partial m_{\text{H2}}}{\partial P}\right) = A \cdot \frac{\partial C_{\text{H2}}}{\partial P} - B \cdot \frac{\partial m_{\text{H2}}}{\partial P} \tag{5.11}$$

The weights A and B are shown in Equation (5.12).

$$A = \frac{1}{m_{\text{H2}}} \quad \text{and} \quad B = \frac{C_{\text{H2}}}{{m_{\text{H2}}}^2} \tag{5.12}$$

The overall cost gradient is simply a summation of the gradients of various costs like turbine, O&M, installation, other farm costs, etc., as shown, only w.r.t. the rotor diameter, in Equation (5.13). The gradients w.r.t. the rated power can be similarly obtained. The components of cost gradients for electricity production and hydrogen production are shown in Figure 5.6 (a) and Figure 5.6 (b), respectively. For the hydrogen production, the pipeline costs replace the cost of the electrical system. It can be seen that the pipeline cost gradient points towards larger power ratings, as opposed to the cost gradient for the electrical equipment. Larger ratings reduce the number of turbines and the overall infield cable/pipeline length. However, larger ratings also result in more current through the cables and a higher flow rate, in the case of pipelines. For cables, the costs are dominated by the current in the cables, resulting in a gradient pointing towards smaller ratings. However, for pipelines, the costs scale less than linearly with the flow rate. Hence, the pipeline length has a dominating effect resulting in the cost gradient pointing towards larger ratings.

The cost of the electrolyzer system is fixed across the design space since the farm power is constant, and hence, has no gradient component. The other costs comprise other turbine costs related to profit margins and additional farm costs related to contingency, project development, and decommissioning. The other farm costs are a function of the total farm CAPEX, which includes costs for pipelines for hydrogen production and cables in case of electricity production. Since the cost gradients for pipelines and cables point in opposite directions, that effect is also seen in the slight rotation of the cost gradient vector.

$$\frac{\partial C_{\mathrm{H2}}}{\partial D} = \frac{\partial}{\partial D}(C_{\mathrm{turbine}} + C_{\mathrm{other}} + C_{\mathrm{support}} + C_{\mathrm{installation}} + C_{\mathrm{OPEX}} + C_{\mathrm{pipeline}}) \tag{5.13}$$

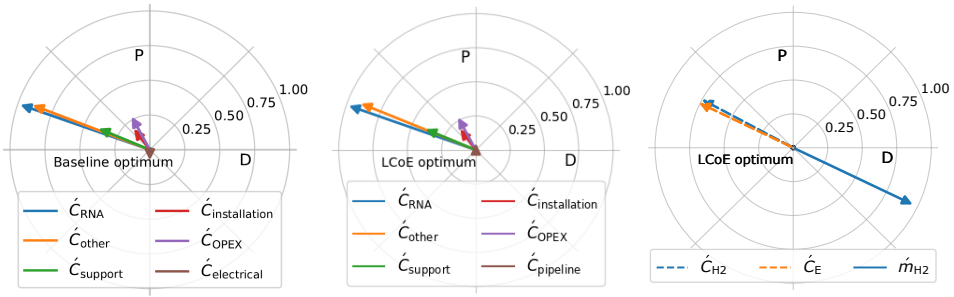

Figure 5.6: (a) LCoE gradient components of costs (b) LCoH gradient components of costs (c) Cost and hydrogen production gradients

The instantaneous electricity consumption of the electrolyzer (E) depends on the instantaneous efficiency ($\eta_{\mathrm{electrolyzer}}$), as shown in Equation (5.14). However, the hydrogen production can be expressed in the form of AEP and average electricity consumption ($\bar{E}_{\mathrm{avg}}$), as shown in Equation (5.15). The instantaneous electricity consumption of the electrolyzer varies because of the variations in instantaneous farm power. The average electricity consumption also varies across the design space. This is because every turbine design has a different power curve, resulting in not only a different AEP but also different instantaneous power values for the same wind speed and hence, different electricity consumption values.

$$E = \frac{\mathrm{HHV}}{\eta_{\mathrm{electrolyzer}}} \tag{5.14}$$

$$m_{\mathrm{H2}} = \frac{\mathrm{AEP}}{\bar{E}_{\mathrm{avg}}} \tag{5.15}$$

However, it is observed that the variations of $\bar{E}_{\mathrm{avg}}$ across the design space are minor, as shown in Table 5.2. The design with the highest specific power has the

least average consumption for the electrolyzer while the design with the lowest specific power has the highest average consumption for the electrolyzer. This is because an electrolyzer coupled to the higher specific power design operates at a lower input load, and hence, higher efficiency, for a relatively high number of hours.

Table 5.2: Variations of $\bar{E}_{\text{avg}}$ across the design space

	Value (kWh/kg)	Design point
Max. $\bar{E}_{\text{avg}}$	55.45	20 MW-180 m
Min. $\bar{E}_{\text{avg}}$	56	10 MW-300 m

Hence, the average electricity consumption can be assumed to be a constant across the design space, and the hydrogen production gradient can be simply expressed in the form of AEP gradients. The simplified LCoH gradient can hence be expressed as shown in Equation (5.16) and Equation (5.17).

$$\frac{\partial \text{LCoH}}{\partial D} = \frac{\bar{E}_{\text{avg}}}{\text{AEP}^2}\left(\frac{\text{AEP}}{\bar{E}_{\text{avg}}}\cdot\frac{\partial C_{\text{H2}}}{\partial D} - \frac{C_{\text{H2}}}{\bar{E}_{\text{avg}}}\cdot\frac{\partial \text{AEP}}{\partial D}\right) = A\cdot\frac{\partial C_{\text{H2}}}{\partial D} - B\cdot\frac{\partial \text{AEP}}{\partial D} \tag{5.16}$$

$$\frac{\partial \text{LCoH}}{\partial P} = \frac{\bar{E}_{\text{avg}}}{\text{AEP}^2}\left(\frac{\text{AEP}}{\bar{E}_{\text{avg}}}\cdot\frac{\partial C_{\text{H2}}}{\partial P} - \frac{C_{\text{H2}}}{\bar{E}_{\text{avg}}}\cdot\frac{\partial \text{AEP}}{\partial P}\right) = A\cdot\frac{\partial C_{\text{H2}}}{\partial P} - B\cdot\frac{\partial \text{AEP}}{\partial P} \tag{5.17}$$

The new weights A and B are shown in Equation (5.18).

$$A = \frac{1}{\text{AEP}} \quad \text{and} \quad B = \frac{C_{\text{H2}}}{\text{AEP}^2} \tag{5.18}$$

These expressions are similar to weighted LCoE gradients, except that total costs for hydrogen production (C_{H2}) are used instead of total costs for electricity production (C_{E}). This results in a difference in the unweighted cost gradient and the weight for the AEP gradient. At the LCoE optimum, the weighted gradients for costs and AEP are in balance. For hydrogen production, the gradients are out of balance, as shown in Figure 5.6 (c). The change in the direction of the cost gradient is explained by the differences between infield cables and pipelines. However, the magnitude of the hydrogen cost gradient is much smaller than that of the hydrogen production gradient. From Figure 5.6 (c), it is clear that the magnitude of the cost gradient for both electricity ($\frac{\partial C_{\text{E}}}{\partial D}$ and $\frac{\partial C_{\text{E}}}{\partial P}$) and hydrogen production ($\frac{\partial C_{\text{H2}}}{\partial D}$ and $\frac{\partial C_{\text{H2}}}{\partial P}$) are similar in magnitude. Hence, the only difference in magnitudes between the cost and hydrogen production gradient can be attributed to the higher CAPEX of the hydrogen production system compared to the CAPEX of the electricity production

system. The high CAPEX stretches the hydrogen production gradient much more compared to the electricity production case, causing the gradients to be out of balance at the LCoE optimum. As a consequence, the difference in magnitude of the gradients drags the solution for the hydrogen turbine in the direction of the hydrogen-production gradient. The final solution is moved up a little bit, compared to that gradient, because of the upward directional change to the cost gradient.

A marginal difference in the values of $\bar{E}_{\text{avg}}$ across the design space also implies that the hydrogen production obtained using the fixed efficiency curve assumption is similar to the production with the variable efficiency curve. It is also observed that the optimum turbine sizes obtained using the two different efficiency curve assumptions differ insignificantly, as shown in Table 5.3. The variable efficiency curve drives the optimum towards higher specific power turbines, to attain a higher electrolyzer efficiency. However, the difference is insignificant. Hence, it can be concluded that the nature of the electrolyzer efficiency curve does not play a significant role from a turbine sizing perspective.

Table 5.3: Difference in LCoH optimum for a variable and a fixed efficiency curve

Efficiency curve	Design point
Variable eff.	15.4 MW-254 m
Fixed eff.	15.3 MW-256 m

5.5.2 Optimum electrolyzer sizing ratio

For the baseline case, the electrolyzer ratio ($\zeta_{\text{electrolyzer}}$) was set to 1 and for all the designs, the electrolyzer rating was equal to the turbine rated power. However, that may not always be the optimum. Hence, sensitivity w.r.t. the electrolyzer ratio is carried out where the ratio is varied between 0.8 and 1.2. Undersizing the electrolyzer reduces the costs at the expense of curtailing some electricity while oversizing increases the production due to efficiency gains at the expense of added electrolyzer costs.

This trade-off is shown in Figure 5.7 (a) for the LCoH baseline optimum design. The change in cost w.r.t. the sizing ratio is linear since the costs are a function of the rated power of the electrolyzer. For undersized electrolyzers, the drop in hydrogen production due to curtailment is steeper than the decrease in costs. For oversized electrolyzers, hydrogen production does not increase significantly due to marginal gains in the efficiency. As a result, the LCoH increase for over-sizing is much higher than the LCoH increase due to under-sizing, as shown in Figure 5.7 (b). It is also clear that the LCoH for an electrolyzer ratio of 1 is also the overall optimum LCoH. The optimum turbine designs for electrolyzer ratio values of 0.8, 1, and 1.2 are also mentioned in the figure, where the optimum for an undersized electrolyzer has

much higher specific power than the optimum design for an oversized electrolyzer. This is further illustrated and explained next.

For the same electrolyzer ratio, each turbine design performs differently. This is because, even for a sizing ratio of 1, each design has a different number of full load hours for the electrolyzer. High-specific power designs have fewer full load hours and lower utilization of the electrolyzer compared to low-specific power designs.

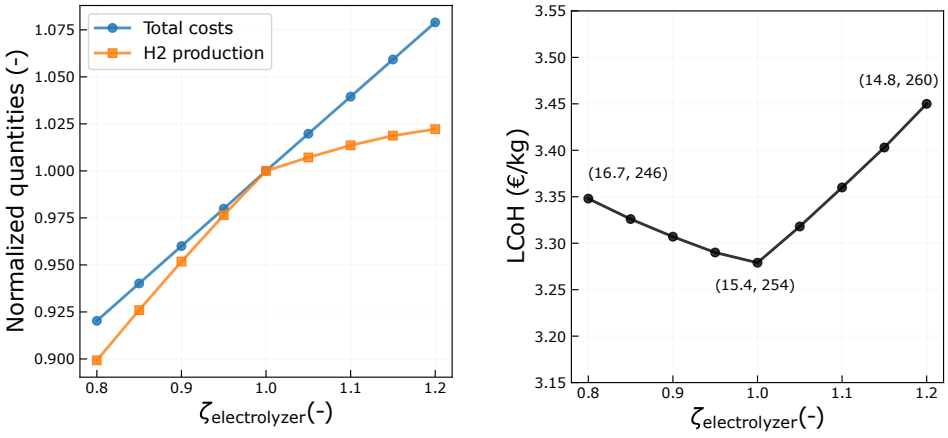

Figure 5.7: (a) Variations in discounted lifetime cost and hydrogen production for the LCoH baseline optimum for different electrolyzer ratios (b) LCoH (optimum) as a function of electrolyzer ratio

This implies that, although the optimum sizing ratio for the optimum design is 1, the optimum electrolyzer ratio for different (non-optimum) designs may differ. An example of this is shown in Figure 5.8 (a) where the low specific power design has a rating of 10 MW and a rotor diameter of 300 m while the high specific power design has a rating of 20 MW and a rotor diameter of 180 m. The high-specific power design has a much lower utilization of the electrolyzer compared to the low-specific power design. Hence, it is beneficial to undersize the electrolyzer. For the low specific power design, undersizing results in a relatively large loss of hydrogen production, quickly increasing the LCoH. Oversizing increases the operating efficiency of the electrolyzer but still does not pay off for the added costs. However, the increase in LCoH is not as steep as in the case of under-sizing. The optimum design for electrolyzer ratios in the range 0.8-1.2 is shown in Figure 5.8 (b) where the design with the highest specific power (largest rating and smallest rotor diameter) is the optimum for an electrolyzer ratio of 0.8. Also, the global LCoH optimum is marked which corresponds to an electrolyzer ratio of 1.

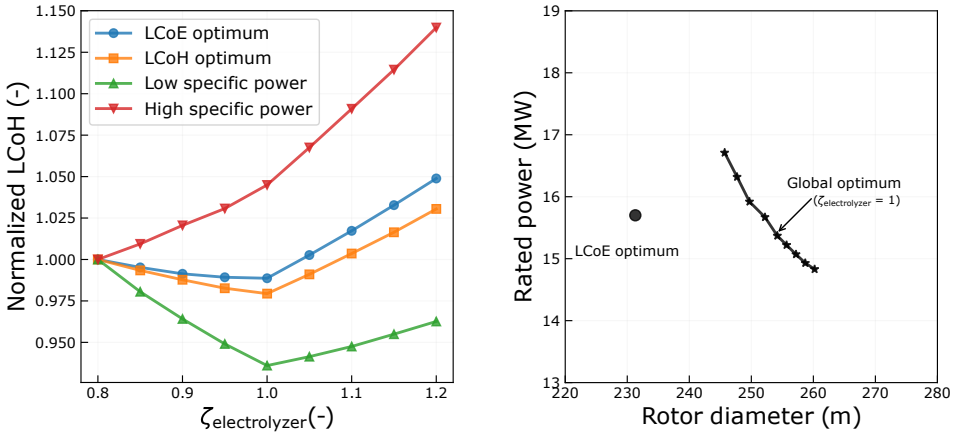

Figure 5.8: (a) Performance of various designs for different electrolyzer ratios (b) Optimum designs for different electrolyzer ratios

5.5.3 Sensitivity to electrolyzer costs

The baseline case assumes a given cost for the electrolyzer system. However, a wide range of values for electrolyzer costs have been reported in the literature. To evaluate the impact of electrolyzer costs on the optimum, the CAPEX of the electrolyzer system is varied between 100 \$/kW and 700 \$/kW, and the O&M costs, expressed as a fraction of the electrolyzer CAPEX, are varied in the range of 1-3% of CAPEX. Since the electrolyzer costs are fixed and do not vary with turbine design, the only effect is on the weight of the hydrogen production gradient, as shown in Equation (5.12).

A higher electrolyzer cost and/or O&M cost share increases the overall hydrogen system cost (C_{H2}), stretching the hydrogen production gradient. This drives the optimum in the direction of lower specific powers, and vice-versa for a lower electrolyzer cost, as shown in Figure 5.9. The difference in specific power of the LCoH-optimized design and LCoE-optimized design depends on future developments of the electrolyzer system costs. The color bar shows the difference in LCoH values for the LCoE-optimized design and LCoH-optimized designs, for various electrolyzer system costs. A maximum difference of about 3% is observed for high electrolyzer system costs, which results in a design with a specific power much lower than that of the LCoE-optimized design. It is also observed that for the entire range of variations for the electrolyzer system costs, the optimum electrolyzer sizing ratio is still found to be 1. This implies that oversizing in the case of low electrolyzer costs or undersizing in the case of high electrolyzer costs, is not optimal.

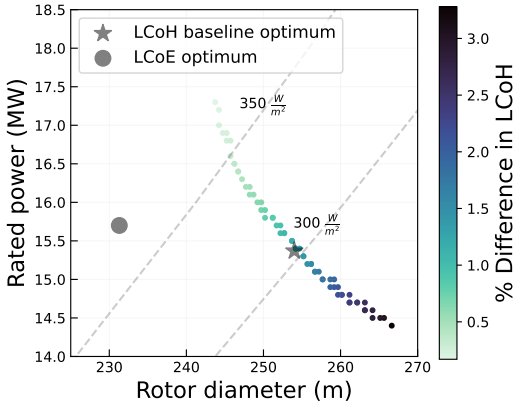

Figure 5.9: Sensitivity of optimum to electrolyzer system costs

5.6 Discussion

Chapter 5 explores a sizing study for both electricity and hydrogen production and also presents the possibility of a global optimum for both configurations, which is within reach of current turbine sizes. The relevance of these global optima to the current study is that the comparisons between hydrogen and electricity turbines hold all the way up to the scale at which these are reached. This indicates a strong general validity of the conclusions presented below, also for future developments that may cause the global optimum to shift. However, the absolute value of these global optima depends on the case setup, the cost modelling of various elements, their scaling, and on how these costs evolve in the future. The key insights that can be drawn from this study are listed below:

1. Optimizing the turbine size for hydrogen production results in a low specific power turbine relative to the turbine sized for electricity production. The change in configuration eliminates the substation and export cable costs while adding electrolyzer costs that take up a significant share of the LCoH. The addition of these high fixed costs, which do not vary much with the turbine sizing, makes the hydrogen production with low specific power turbines more valuable.

2. Due to the similarity in scaling up of the costs of most wind farm components for both electricity and hydrogen production, the LCoH values for LCoH-optimized and LCoE-optimized designs do not show a significant deviation. As a result, the LCoE-optimized turbine designs are already well-suited for hydrogen production. Depending on the price of the electrolyzers, turbines designed for LCoH may have a similar or lower specific power compared

to LCoE-optimized turbines. However, the maximum difference in LCoH between an LCoE-optimized design and an LCoH-optimized design is about 3%.

3. The nature of the efficiency curve of the electrolyzer has an insignificant impact on the optimum turbine size. This is because the average electricity consumption of the electrolyzer does not vary much with the turbine design. A change in the electrolyzer costs shifts the optimum in the direction of changing specific power. High electrolyzer costs make hydrogen production from low-specific power turbines more valuable, while low electrolyzer costs shift the optimum towards high-specific power turbines. Also, an electrolyzer with nearly the same power rating as the turbine is found to be optimal for a wide range of electrolyzer system costs.

Currently, there is a marginal advantage in resizing a turbine specifically for hydrogen production. The sensitivity of the optimum values to the electrolyzer costs suggests that it is difficult for an academic study to pinpoint the absolute best design. However, the difference between a hydrogen and an electricity producing turbine remains marginal under a wide range of cost assumptions and conditions. This is caused by the large part that the systems for both applications have in common. Therefore, LCoE-optimized turbines with an electrolyzer sizing ratio of about one are well suited to cater to the current hydrogen market. The next generation of turbines for electricity, however, will arguably be optimized for the fluctuating market prices and for system flexibility, which may lead to lower specific power designs [89]. On the other hand, an expected decrease in the cost of electrolyzers will shift the specific power of the hydrogen-optimized turbines closer to that of the turbines optimized for LCoE. Consequently, the market may see two differing trends in turbine designs regarding specific power.

6

Conclusions

Affordable clean energy is not just an economic opportunity but a social and environmental necessity

Michael Liebreich

This chapter provides a brief overview of the methodology and results presented in this thesis followed by some conclusions w.r.t. optimal turbine sizing. The chapter ends by pointing out some limitations of the research and their consequences on the conclusions.

This research explored various drivers of wind turbine sizing in an offshore wind farm in the form of objectives, constraints, and design inputs. The study first described a multi-disciplinary design framework that coupled various low-fidelity models to capture all the trade-offs that occur in a system as complex as an offshore wind farm. The purpose of the models was to capture all the variations in the costs and production of the wind farm w.r.t. the turbine size. A methodology was provided to visualize and understand the drivers for turbine sizing in the form of gradients. The shift in optimum turbine sizing can be well understood if the impact of the input, objective, constraint, etc. on the gradients is known. The research also looked at objectives beyond LCoE by coupling a simplified market pricing model. The purpose was to capture the variations in the prices w.r.t. the local wind speed instead of accurately predicting the spot prices, which would be a completely different study. The simplified market model was parameterized using the mean spot price, correlation between spot prices and wind speeds, and the price volatility, such that a change in any of these parameters represents a specific scenario. The model was used to then create several future possibilities and its influence on the optimum turbine sizing, for several profitability indicators, was evaluated. Lastly, turbine sizing for hydrogen production was explored by coupling a simplified hydrogen production and cost module to the existing offshore wind farm-level framework developed for electricity production.

6.1 Key findings

Chapter 3 first established the optimum turbine size for a conventional offshore wind farm with representative constraints and site conditions that was designed for LCoE. The sensitivity of this optimum to various design inputs, model assumptions, and constraints were discussed in detail. The key drivers of turbine sizing with respect to LCoE were identified, and a baseline optimum was established as a reference for the subsequent chapters, which focused on objectives beyond LCoE. Chapters 4 and 5 looked at how a change in the objective drives turbine design compared to the baseline established in Chapter 3. The chapters discuss possible differences that drive the optimum in a certain direction and also evaluate the magnitude of the change. Some conclusions that can be drawn based on the entire research are summarized as follows:

- For a typical offshore wind farm with a grid constraint, turbines with a low specific power (larger rotors for a smaller generator) will almost always lead to a higher production and revenues while turbines with a higher specific power (smaller rotors for a larger generator) will almost always result in a cost decrease at a farm level. A shift in turbine design in the direction of changing specific power leads to a maximum rate of change in any objective

function whereas any shift in the direction of constant specific power leads to marginal differences. For instance, upscaling from a 10 MW-190 m turbine to the LCoE optimum of around 16 MW-236 m resulted in an LCoE drop of less than 5%.

- For any given objective, there exists an optimum and none of the results point towards continued upscaling of turbines. The results for the optimum size are, of course, sensitive to the modeling assumptions, design inputs, and constraints. The drivers for turbine sizing can be better understood with the help of cost and production or revenue gradients. Using a better model or different assumptions may result in a change in the magnitude and direction of one of the gradient components. For instance, any uncertainties in cost modelling assumptions or future RNA cost reductions due to a change in materials mainly alter how these (variable) costs scale with the rated power or rotor diameter. This affects the gradient magnitude of an individual cost component, hence impacting both the direction and the magnitude of the overall cost gradient. As a consequence, the optimum turbine size might shift along the direction of constant specific power, resulting in potential upscaling where the LCoE gradient is relatively low due to a flat response surface in that direction. On the other hand, changes that stretch the overall gradients without affecting their direction, like fixed costs (that do not vary with the design variables) or wind conditions, drive the optimum along the direction of changing specific power, where the LCoE gradient is steep.

- Turbine sizing w.r.t. revenue-based metrics (like MIRR) is primarily driven by market conditions: spot price variation, anti-correlation between wind speed and spot prices, and the mean spot price level. This is in addition to the drivers for turbine sizing w.r.t. LCoE. For a given market scenario, the overall gradients of MIRR across the power-diameter design space are found to be similar to that of LCoE. The mean spot price level shifts the turbine in the direction of constant specific power, where MIRR has a relatively smaller gradient due to a flat response surface in that direction. The anti-correlation and spot price variation drive the turbine in the direction of changing specific power, where MIRR has a relatively steep gradient. Even for an extreme scenario in the future with high price volatility and strong wind-spot anti-correlation, a turbine designed specifically for maximizing revenues (MIRR) achieves a 0.1-0.2%pt higher MIRR compared to an LCoE-optimized design, which is insignificant.

- Turbine sizing in order to minimize LCoH is primarily driven by the electrolyzer costs, with secondary effects arising from variations in costs between

cabling (for electricity) and piping (for hydrogen) systems. Also, the shape of the electrolyzer efficiency curve (whether flat or variable) is found to have an insignificant impact on the optimum turbine size. This is in addition to the drivers for turbine sizing w.r.t. LCoE. For a given market scenario, the overall gradients of LCoH across the power-diameter design space are found to be similar to that of LCoE. Compared to the conventional configuration for electricity production, the added (fixed) costs of the electrolyzer system stretch the hydrogen production gradient, making the additional production from a lower specific power design much more valuable. However, as electricity costs comprise over 70% of hydrogen production costs, the difference in LCoH between an LCoE-optimized design and an LCoH-optimized design is minimal.

- The shift in optimum towards lower specific power turbines for low wind speed regions, profitability or for hydrogen production, have similar underlying mechanics. Essentially, it is how the production or revenue is valued relative to the costs. In the case of low wind, even a minor absolute gain in production, at the expense of extra costs, is highly valuable. For profitability, the value of every kWh is not the same and the power produced at lower wind speeds is valued much more due to higher spot prices. This effect becomes more pronounced, and the relative gain increases further, when there is a strong anti-correlation between spot prices and wind speed, and the variation in prices is significant. For hydrogen production, the high fixed costs of the electrolyzer system make the extra hydrogen production from low specific power turbines much more valuable.

In conclusion, this research explored various drivers for turbine sizing for an offshore wind farm for different objective functions, constraints, and applications. A methodology to understand these drivers and quantify the impact on the optimum via gradients is also provided. This is helpful in identifying how modelling uncertainties, design inputs, constraints, or objectives drive both the direction and magnitude of the optimum. The upscaling of turbines have indeed helped in reducing the cost of energy so far. However, arguments about further upscaling have mostly been qualitative without enough evidence showing the benefits from a developer's perspective using a comprehensive economic metric. This work provides a systematic way of conducting such a study while also providing several insights that can be helpful for both developers and OEMs.

NedZero (formerly the Netherlands Wind Energy Association (NWEA)) has proposed a new standard to limit the tip height of offshore wind turbines to 1000 feet, corresponding to a maximum rotor diameter of approximately 300 m [90]. Given the economic challenges faced by the offshore wind sector, this approach

promotes the standardization of turbine components, installation vessels, and related infrastructure, potentially leading to significant cost savings. This research highlights the marginal benefits of upscaling, as indicated by a low LCoE gradient value due to a relatively flat response surface along the direction of constant specific power. By evaluating the techno-economic trade-offs at a farm level, such studies can help identify key drivers of turbine sizing and provide a basis for setting design standards, ultimately enabling further reductions in the cost of offshore wind energy.

6.2 Limitations & implications

These conclusions are based on the methodology, assumptions, and design inputs used in this research. However, it is also important for a thesis to highlight the shortcomings of the models or methods used and to be aware of the consequences on the results and conclusions. Some limitations of this research and the expected implications are listed as follows:

- No change in rotor performance is assumed across the design space. The change in the Reynolds number across the design space is expected to significantly alter the airfoil polars and hence, the rotor performance. However, the airfoils and aerodynamic profiles (chord, twist, tip speed ratio) of the rotor are expected to be redesigned for each configuration such that optimal performance is achieved. Hence, this assumption is not expected to change the conclusions of the research. There might also be technical constraints when designing rotors of around 280-300 m, which are not considered in this research. For instance, [91] and [92] indicate the possibilities of transonic flow under certain operating conditions for large turbines. Accounting for those would probably make the case for upscaling worse.

- Although an MDAO-based framework and a methodology are provided, the necessary level of fidelity required for each model is not demonstrated. It is also not known or validated whether the modelled fidelity captures the dependencies accurately. However, the individual models are either validated (energy production), use standard scaling principles (rotor mass), or are calibrated based on real data (O&M, installation). Also, the overall performance of the model can be evaluated based on the absolute values of the economic metrics used and those seem to align well with industry trends. Lastly, there are no real data (for costs or performance) for some of the turbine design points included in this research, making it even more difficult to validate the performance of the framework at that scale.

- The market model used in this study is simplified in order to quickly generate hundreds of future price scenarios. The spot prices are sampled from a normal distribution with a certain mean spot price and standard deviation such that the prices have a certain anti-correlation with the wind speed. In reality, the market prices are influenced by various factors (other generating sources, demand, etc.) and do not necessarily follow a normal distribution. The simplified model misses out on certain extreme events. However, the model captures the variation of spot prices as a function of wind speed as well as the absolute yearly revenues, making it suitable for the given application. Also, the prices are expected to decrease in the long term with more renewable penetration, and will hence result in a yearly revenue decreasing over the lifetime. However, since this research looks at hundreds of scenarios, it is expected that the true optimum, based on a more comprehensive market model and realistic future build-out assumptions, would lie somewhere within the spread of optimum designs evaluated in this research.

- The electrolyzer system model used in this research does not include an operational strategy that can optimize the electrolyzer performance to maximize efficiency while minimizing electrolyzer degradation. The results from the research show that the implications of the nature of the efficiency curve on turbine design is insignificant. However, if the efficiency curve (as a function of input load) deviates a lot from the one used in this research, or if the electrolyzer degradation varies significantly across the turbine design space, then the results may differ. However, this would not change the conclusions, as the primary factor driving the difference in the optimum compared to an LCoE-based design would still be the additional cost of the electrolyzer system.

- This research focuses solely on economically driven design objectives. However, sustainability-oriented metrics—such as life cycle emissions, material consumption, and system compatibility (benefits to the electricity grid or energy system)—could gain increasing importance. Preliminary studies already highlight trade-offs between costs and emissions for turbine designs [14] and demonstrate the advantages of very low-specific-power turbines for the system [25]. However, achieving broader adoption may require internalizing these societal benefits and implementing market policy instruments to encourage behaviors that benefit both the energy system and developers.

As discussed, most limitations are unlikely to affect the conclusions. However, the uncertainty associated with scaling various cost elements for large-scale turbines represents the most critical limitation that could impact the conclusions

(particularly regarding the second bullet point). Switching to high-fidelity modeling for different aspects of the wind farm could better capture certain scaling effects. Nonetheless, value-based pricing factors, such as vessel costs driven by limited supply for larger turbines, would still contribute to the overall uncertainty. This also highlights the need for more data points regarding various farm costs and turbine parameters for large-scale turbines.

References

References

[1] IEA, "Offshore Wind Outlook 2019," International Energy Agency, Paris, Tech. Rep., 2019, (last access: 24 March 2025). [Online]. Available: https://www.iea.org/reports/offshore-wind-outlook-2019

[2] International Renewable Energy Agency (IRENA), "Future of wind: Deployment, investment, technology, grid integration and socio-economic aspects (A Global Energy Transformation paper)," International Renewable Energy Agency, Tech. Rep., 2019. [Online]. Available: https://www.irena.org/-/media/files/irena/agency/publication/2019/oct/irena_future_of_wind_2019.pdf

[3] S. Lensink and I. Pisca, "Costs of offshore wind energy 2018," PBL Netherlands Environmental Assessment Agency, The Hague, Tech. Rep., 2019. [Online]. Available: https://www.pbl.nl/sites/default/files/downloads/pbl-2019-costs-of-offshore-wind-energy-2018_3623.pdf

[4] Wind & water works, "Dutch offshore wind guide: Your guide to dutch offshore wind policy, technologies and innovations," Tech. Rep., 2022. [Online]. Available: https://www.rvo.nl/sites/default/files/2021/10/Dutch%20Offshore%20Wind%20Guide%202022.pdf

[5] E. Lantz, M. Hand, and R. Wiser, "WREF 2012: Past and future cost of wind energy," National Renewable Energy Lab (NREL), Golden, CO (United States), Tech. Rep., 2012. [Online]. Available: https://escholarship.org/content/qt9161j61q/qt9161j61q.pdf

[6] P. Veers, K. Dykes, E. Lantz, S. Barth, C. L. Bottasso, O. Carlson, A. Clifton, J. Green, P. Green, H. Holttinen *et al.*, "Grand challenges in the science of wind energy," *Science*, vol. 366, no. 6464, p. eaau2027, 2019.

[7] N. Mangat, J. G. Zinderenn van, L. F. Hansen, and F. Sevilla, "Optimal offshore wind turbine size and standardisation study," DNV Services UK, Tech. Rep. March, 2022. [Online]. Available: https://topsectorenergie.nl/documents/334/20220519_RAP_DNV_Optimal_Offshore_Wind_Turbine_Size_and_Standardisation_F.pdf

[8] S. Andrew Ning, R. Damiani, and P. J. Moriarty, "Objectives and constraints for wind turbine optimization," *Journal of Solar Energy Engineering*, vol. 136, no. 4, 2014.

[9] A. Chehouri, R. Younes, A. Ilinca, and J. Perron, "Review of performance optimization techniques applied to wind turbines," *Applied Energy*, vol. 142, pp. 361–388, 3 2015.

[10] K. Dykes, "Optimization of wind farm design for objectives beyond LCoE," in *Journal of Physics: Conference Series*, vol. 1618, no. 4, 2020, p. 042039.

[11] RVO, "Hollandse kust (noord) wind farm zone, site v," https://english.rvo.nl/information/offshore-wind-energy/hollandse-kust-noord-wind-farm-zone-v, 2020, (last access: 24 March 2025).

[12] J. López Prol, K. W. Steininger, and D. Zilberman, "The cannibalization effect of wind and solar in the california wholesale electricity market," *Energy Economics*, vol. 85, p. 104552, 2020.

[13] E. Loth, C. Qin, J. G. Simpson, and K. Dykes, "Why we must move beyond lcoe for renewable energy design," *Advances in Applied Energy*, vol. 8, p. 100112, 2022.

[14] H. Canet, A. Guilloré, and C. L. Bottasso, "The eco-conscious wind turbine: bringing societal value to design," *Wind Energy Science Discussions*, pp. 1–30, 2022.

[15] A. Schnettler, V. Pflug, E. Zindel, O. R. Zimmermann Gerhard, Olvera, I. Pyc, and C. Trulley, "Power-to-X: The crucial business on the way to a carbon-free world [White Paper]," Siemens Energy, Tech. Rep., 2021.

[16] A. van Wijk and F. Wouters, *Hydrogen–The Bridge Between Africa and Europe*. Cham: Springer International Publishing, 2021, pp. 91–119.

[17] C. Gulli, B. Heid, J. Noffsinger, M. Waardenburg, and M. Wilthane, "Global Energy Perspective 2023: Hydrogen outlook," McKinsey & Company: Chicago, IL, USA, Tech. Rep. March, 2024. [Online]. Available: https://safety4sea.com/wp-content/uploads/2023/11/McKinsey-Sustainability-%E2%80%93-Global-Energy-Perspective-2023_11.pdf

[18] IRENA, "Green Hydrogen Cost Reduction: Scaling Up Electrolysers to meet the 1.5°C Climate Goal," International Renewable Energy Agency, Abu Dhabi, Tech. Rep., 2020. [Online]. Available: https://www.irena.org/-/media/Files/IRENA/Agency/Publication/2020/Dec/IRENA_Green_hydrogen_cost_2020.pdf

[19] J. I. Levene, M. K. Mann, R. M. Margolis, and A. Milbrandt, "An analysis of hydrogen production from renewable electricity sources," *Solar Energy*, vol. 81, no. 6, pp. 773–780, jun 2007.

[20] A. Spyroudi, D. Wallace, G. Smart, and K. Stefaniak, "OSW-H2: Solving the Integration Challenge," ORE Catapult, Tech. Rep., 2020. [Online]. Available: https://cms.ore.catapult.org.uk/wp-content/uploads/2020/09/Solving-the-Integration-Challenge-ORE-Catapultr.pdf

[21] A. Babarit, J. C. Gilloteaux, G. Clodic, M. Duchet, A. Simoneau, and M. F. Platzer, "Techno-economic feasibility of fleets of far offshore hydrogen-producing wind energy converters," *International Journal of Hydrogen Energy*, vol. 43, no. 15, pp. 7266–7289, apr 2018.

[22] T. Ashuri, M. B. Zaaijer, J. R. Martins, and J. Zhang, "Multidisciplinary design optimization of large wind turbines—Technical, economic, and design challenges," *Energy Conversion and Management*, vol. 123, pp. 56–70, 9 2016.

[23] G. Sieros, P. Chaviaropoulos, J. D. Sørensen, B. H. Bulder, and P. Jamieson, "Upscaling wind turbines: theoretical and practical aspects and their impact on the cost of energy," *Wind Energy*, vol. 15, no. 1, pp. 3–17, 1 2012.

[24] M. Shields, P. Beiter, J. Nunemaker, A. Cooperman, and P. Duffy, "Impacts of turbine and plant upsizing on the levelized cost of energy for offshore wind," *Applied Energy*, vol. 298, p. 117189, 9 2021.

[25] P. Swisher, J. P. M. Leon, J. Gea-Bermúdez, M. Koivisto, H. A. Madsen, and M. Münster, "Competitiveness of a low specific power, low cut-out wind speed wind turbine in north and central europe towards 2050," *Applied Energy*, vol. 306, p. 118043, 2022.

[26] J. J. Thomas, C. Irmas, G. Starke, Z. Tully, E. Grant, N. Riccobono, K. Nagasawa, and C. J. Bay, "Wind turbine design optimization for hydrogen production," National Renewable Energy Laboratory, Tech. Rep., 2024. [Online]. Available: https://docs.nrel.gov/docs/fy25osti/92347.pdf

[27] S. Sanchez Perez Moreno, K. Dykes, K. O. Merz, and M. B. Zaaijer, "Multidisciplinary design analysis and optimisation of a reference offshore wind plant," *Journal of Physics: Conference Series*, vol. 1037, no. 4, p. 042004, 6 2018.

[28] K. L. Dykes, R. R. Damiani, P. A. Graf, G. N. Scott, R. N. King, Y. Guo, J. Quick, L. Sethuraman, P. S. Veers, and A. Ning, "Wind turbine optimization with wisdem," National Renewable Energy Lab

(NREL), Golden, CO (United States), Tech. Rep., 2018. [Online]. Available: https://docs.nrel.gov/docs/fy18osti/70652.pdf

[29] P. Bortolotti, C. Bay, G. Barter, E. Gaertner, K. Dykes, M. McWilliam, M. Friis-Moller, M. Molgaard Pedersen, and F. Zahle, "System Modeling Frameworks for Wind Turbines and Plants: Review and Requirements Specifications," Tech. Rep. March, 2022. [Online]. Available: https://www.nrel.gov/docs/fy22osti/82621.pdf.

[30] S. Sanchez Perez Moreno, "A guideline for selecting MDAO workflows with an application in offshore wind energy," Ph.D. dissertation, Delft University of Technology, 2019. [Online]. Available: https://pure.tudelft.nl/ws/portalfiles/portal/51093403/PhD_thesis_S_Sanchez_Perez_Moreno.pdf

[31] P. Bortolotti, H. C. Tarres, K. L. Dykes, K. Merz, L. Sethuraman, D. Verelst, and F. Zahle, "IEA Wind TCP Task 37: Systems Engineering in Wind Energy - WP2.1 Reference Wind Turbines," 6 2019. [Online]. Available: http://www.osti.gov/servlets/purl/1529216/

[32] G. Serafeim, D. Manolas, V. Riziotis, and P. Chaviaropoulos, "Multidisciplinary aeroelastic optimization of a 10MW-scale wind turbine rotor targeting to reduced LCoE," *Journal of Physics: Conference Series*, vol. 2265, no. 4, p. 042051, 5 2022.

[33] Rijkswaterstaat, "Hollandse kust (zuid) wind farm zone including offshore wind farm luchterduinen (lud)," https://www.noordzeeloket.nl/en/functions-and-use/offshore-wind-energy/free-passage-shared-use/hollandse-kust-zuid-wind-farm-zone-including/, 2021, (last access: 24 March 2025).

[34] T. Tanmay, "Multi-disciplinary optimization of rotor nacelle assemblies for offshore wind farms," Master's thesis, Delft University of Technology, 2018. [Online]. Available: https://repository.tudelft.nl/islandora/object/uuid:d7e2b321-adf8-4a64-97b5-7bad5f644a1f?collection=education

[35] M. Mehta, "mihir0210/window_static: v2.0_turbine_scaling," Apr. 2023. [Online]. Available: https://doi.org/10.5281/zenodo.7817565

[36] P. Bortolotti, D. S. Berry, R. Murray, E. Gaertner, D. S. Jenne, R. R. Damiani, G. E. Barter, and K. L. Dykes, "A detailed wind turbine blade cost model," 6 2019. [Online]. Available: https://www.osti.gov/biblio/1529217

[37] D. T. Griffith and W. Johanns, "Large Blade Manufacturing Cost Studies Using the Sandia Blade Manufacturing Cost Tool and Sandia

100-meter Blades," Tech. Rep. March, 2013. [Online]. Available: https://energy.sandia.gov/wp-content/gallery/uploads/dlm_uploads/SAND_SNLLargeBladeManufacturingCostTrendsAnalysis_SAND2013-2734.pdf

[38] D. T. Griffith and W. Johanns, "Carbon design studies for large blades: performance and cost tradeoffs for the sandia 100-meter wind turbine blade," in *54th AIAA/ASME/ASCE/AHS/ASC Structures, Structural Dynamics, and Materials Conference*, 2013, p. 1554.

[39] NREL, "DrivetrainSE — WISDEM 2.0 documentation," https://wisdem.readthedocs.io/en/master/wisdem/drivetrainse/index.html, 2015, (last access: 24 March 2025).

[40] M. Bastankhah and F. Porté-Agel, "A new analytical model for wind-turbine wakes," *Renewable energy*, vol. 70, pp. 116–123, 2014.

[41] M. M. Pedersen, P. van der Laan, M. Friis-Møller, J. Rinker, and P.-E. Réthoré, "Dtuwindenergy/pywake: Pywake (v1.0.10)," Feb. 2019. [Online]. Available: https://doi.org/10.5281/zenodo.2562662

[42] M. B. Zaaijer, "Great expectations for offshore wind turbines," Ph.D. dissertation, 2013. [Online]. Available: https://repository.tudelft.nl/islandora/object/uuid%3Afd689ba2-3c5f-4e7c-9ccd-55ddbf1679bd

[43] M. Dicorato, G. Forte, M. Pisani, and M. Trovato, "Guidelines for assessment of investment cost for offshore wind generation," *Renewable energy*, vol. 36, no. 8, pp. 2043–2051, 2011.

[44] M. J. Kaiser and B. Snyder, *Offshore wind energy cost modeling: installation and decommissioning*. Springer Science & Business Media, 2012, vol. 85.

[45] I. Dinwoodie, O.-E. V. Endrerud, M. Hofmann, R. Martin, and I. B. Sperstad, "Reference cases for verification of operation and maintenance simulation models for offshore wind farms," *Wind Engineering*, vol. 39, no. 1, pp. 1–14, 2015.

[46] G. Smart, A. Smith, E. Warner, I. B. Sperstad, B. Prinsen, and R. Lacal-Arantegui, "IEA wind task 26: offshore wind farm baseline documentation," National Renewable Energy Lab (NREL), Golden, CO (United States), Tech. Rep., 2016. [Online]. Available: https://docs.nrel.gov/docs/fy16osti/66262.pdf

[47] BVG Associates, "Guide to an offshore wind farm," https://guidetoanoffshorewindfarm.com/guide, 2019, (last access: 5 December 2024).

[48] E. Gaertner, J. Rinker, L. Sethuraman, F. Zahle, B. Anderson, G. Barter, N. Abbas, F. Meng, P. Bortolotti, W. Skrzypinski, G. Scott, R. Feil, H. Bredmose, K. Dykes, M. Shields, C. Allen, and A. Viselli, "Definition of the IEA Wind 15-Megawatt Offshore Reference Wind Turbine," Tech. Rep. March, 2020. [Online]. Available: https://www.nrel.gov/docs/fy20osti/75698.pdf

[49] H. Hersbach, B. Bell, P. Berrisford, G. Biavati, A. Horányi, J. Muñoz Sabater, J. Nicolas, C. Peubey, R. Radu, I. Rozum *et al.*, "ERA5 hourly data on single levels from 1979 to present," *Copernicus climate change service (c3s) climate data store (cds)*, vol. 10, no. 10.24381, 2018.

[50] Rijksdienst voor Ondernemend Nederland (RVO), "Hollandse kust (zuid) wind farm zone (wind farm sites iii & iv)," Tech. Rep., 2018. [Online]. Available: https://offshorewind.rvo.nl/file/download/ce29c209-818e-4727-9c44-68c4902e7caa/1540220273rvo%20hkz%20iii%20and%20iv%20maindocument_october_2018_lowres_web.pdf

[51] M. Mehta, M. B. Zaaijer, and D. von Terzi, "Drivers for optimum sizing of wind turbines for offshore wind farms," *Wind Energy Science*, vol. 9, no. 1, pp. 141–163, 2024.

[52] ——, "Designing wind turbines for profitability in the day-ahead market," *Wind Energy Science*, vol. 9, no. 12, pp. 2283–2300, 2024.

[53] A. Mills and R. Wiser, "Changes in the economic value of variable generation at high penetration levels: a pilot case study of california," Lawrence Berkeley National Lab (LBNL), Berkeley, CA (United States), Tech. Rep., 2012. [Online]. Available: https://www.osti.gov/servlets/purl/1183176

[54] L. Hirth, "The market value of variable renewables: The effect of solar wind power variability on their relative price," *Energy economics*, vol. 38, pp. 218–236, 2013.

[55] E. Loth, C. Qin, J. G. Simpson, and K. Dykes, "Why we must move beyond LCOE for renewable energy design," *Advances in Applied Energy*, vol. 8, p. 100112, 12 2022.

[56] L. Hirth and S. Müller, "System-friendly wind power. How advanced wind turbine design can increase the economic value of electricity generated through wind power," *Energy Economics*, vol. 56, pp. 51–63, 2016.

[57] P. Chen and T. Thiringer, "Analysis of energy curtailment and capacity overinstallation to maximize wind turbine profit considering electricity price–wind

correlation," *IEEE Transactions on Sustainable Energy*, vol. 8, no. 4, pp. 1406–1414, 2017.

[58] W. S. de Oliveira, A. J. Fernandes, and J. J. B. Gouveia, "Economic metrics for wind energy projects." *International Journal of Energy & Environment*, vol. 2, no. 6, 2011.

[59] J. Simpson, E. Loth, and K. Dykes, "Cost of Valued Energy for design of renewable energy systems," *Renewable Energy*, vol. 153, pp. 290–300, 6 2020.

[60] K. Dykes, "Optimization of wind farm design for objectives beyond lcoe," *Journal of Physics: Conference Series*, vol. 1618, p. 042039, 2020.

[61] Rijksdienst voor Ondernemend Nederland, "Hollandse Kust (noord) Wind Farm Zone, Site V," https://english.rvo.nl/information/offshore-wind-energy/hollandse-kust-noord-wind-farm-zone-v, 2020, (last access: 25 July 2023).

[62] V. Delapedra-Silva, P. Ferreira, J. Cunha, and H. Kimura, "Methods for financial assessment of renewable energy projects: A review," *Processes*, vol. 10, no. 2, p. 184, 2022.

[63] J. S. González, A. G. G. Rodriguez, J. C. Mora, J. R. Santos, and M. B. Payan, "Optimization of wind farm turbines layout using an evolutive algorithm," *Renewable energy*, vol. 35, no. 8, pp. 1671–1681, 2010.

[64] S. Shamshirband, D. Petković, Ž. Ćojbašić, V. Nikolić, N. B. Anuar, N. L. M. Shuib, M. L. M. Kiah, and S. Akib, "Adaptive neuro-fuzzy optimization of wind farm project net profit," *Energy Conversion and Management*, vol. 80, pp. 229–237, 2014.

[65] A. W. Ciavarra, R. V. Rodrigues, K. Dykes, and P.-E. Réthoré, "Wind farm optimization with multiple hub heights using gradient-based methods," in *Journal of Physics: Conference Series*, vol. 2265, no. 2, 2022, p. 022012.

[66] R. Joshi, M. Kruijff, and R. Schmehl, "Value-driven system design of utility-scale airborne wind energy," *Energies*, vol. 16, no. 4, p. 2075, 2023.

[67] S. Pookpunt, W. Ongsakul, and N. Madhu, "A comprehensive techno-economic analysis for optimally placed wind farms," *Electrical Engineering*, vol. 102, pp. 2161–2179, 2020.

[68] H. Habbou, J. P. M. Leon, and K. Das, "Profitability of hybrid power plants in european markets," in *Journal of Physics: Conference Series*, vol. 2507, no. 1, 2023, p. 012009.

[69] A. de Souza Rangel, J. C. de Souza Santos, and J. R. F. Savoia, "Modified profitability index and internal rate of return," *Journal of International Business and Economics*, vol. 4, no. 2, pp. 13–18, 2016.

[70] F. Wiese, R. Bramstoft, H. Koduvere, A. P. Alonso, O. Balyk, J. G. Kirkerud, Å. G. Tveten, T. F. Bolkesjø, M. Münster, and H. Ravn, "Balmorel open source energy system model," *Energy strategy reviews*, vol. 20, pp. 26–34, 2018.

[71] L. Hirth, O. Ruhnau, and R. Sgarlato, "The european electricity market model emma-model description," *Kiel, Hamburg: ZBW-Leibniz Information Centre for Economics*, 2021.

[72] P. Verstraten and A. H. van der Weijde, "The case for simple simulation: Stochastic market simulation to assess renewable business cases," *Current Sustainable/Renewable Energy Reports*, pp. 1–7, 2023.

[73] European Network of Transmission System Operators for Electricity (ENTSO-E), "ENTSO-E Transparency platform," https://transparency.entsoe.eu/, 2023, (last access: 25 July 2023).

[74] A. Singlitico, J. Østergaard, and S. Chatzivasileiadis, "Onshore, offshore or in-turbine electrolysis? Techno-economic overview of alternative integration designs for green hydrogen production into Offshore Wind Power Hubs," *Renewable and Sustainable Energy Transition*, vol. 1, p. 100005, aug 2021.

[75] G. Glenk and S. Reichelstein, "Economics of converting renewable power to hydrogen," *Nature Energy*, vol. 4, no. 3, pp. 216–222, 2019 Economics of converting renewable power to hydrogen.

[76] O. S. Ibrahim, A. Singlitico, R. Proskovics, S. McDonagh, C. Desmond, and J. D. Murphy, "Dedicated large-scale floating offshore wind to hydrogen: Assessing design variables in proposed typologies," *Renewable and Sustainable Energy Reviews*, vol. 160, p. 112310, 2022.

[77] M. Mehta, M. B. Zaaijer, and D. von Terzi, "Optimum turbine design for hydrogen production from offshore wind," in *Journal of Physics: Conference Series*, vol. 2265, no. 4, 2022, p. 042061.

[78] M. Kopp, D. Coleman, C. Stiller, K. Scheffer, J. Aichinger, and B. Scheppat, "Energiepark Mainz: Technical and economic analysis of the worldwide largest Power-to-Gas plant with PEM electrolysis," *International Journal of Hydrogen Energy*, vol. 42, no. 19, pp. 13 311–13 320, may 2017.

[79] P. Lettenmeier, "Siemens ag efficiency - electrolysis [white paper]," Siemens Energy, Tech. Rep., 2019, (last access: 25 November 2024). [Online]. Available: https://assets.new.siemens.com/siemens/assets/api/uuid:a5fa8257-6c71-496f-a324-454241f1df71/version:1626351542/white-paper-effizienz-de.pdf

[80] S. M. Saba, M. Mü, M. Robinius, and D. Stolten, "The investment costs of electrolysis - A comparison of cost studies from the past 30 years," *International journal of hydrogen energy*, vol. 43, no. 3, pp. 1209–1223, 2018.

[81] H. Groenemans, G. Saur, C. Mittelsteadt, J. Lattimer, H. Xu, Y. Yan, and W. Li, "Techno-economic analysis of offshore wind pem water electrolysis for h2 production," *Current Opinion in Chemical Engineering*, vol. 37, p. 100828, 2022.

[82] A. Christensen, "Assessment of hydrogen production costs from electrolysis: United states and Europe [white paper]," International Council on Clean Transportation, Tech. Rep., 2020. [Online]. Available: https://theicct.org/wp-content/uploads/2021/06/final_icct2020_assessment_of-_hydrogen_production_costs-v2.pdf

[83] N. Parker, "Using natural gas transmission pipeline costs to estimate hydrogen pipeline costs," Institute of Transportation Studies, University of California, Tech. Rep., 2004. [Online]. Available: https://escholarship.org/uc/item/9m40m75r

[84] M. Reuß, L. Welder, J. Thürauf, J. Linßen, T. Grube, L. Schewe, M. Schmidt, D. Stolten, and M. Robinius, "Modeling hydrogen networks for future energy systems: A comparison of linear and nonlinear approaches," *International journal of hydrogen energy*, vol. 44, no. 60, pp. 32 136–32 150, 2019.

[85] Néstor González Díez, Simone van der Meer, Jorge Bonetto, and Arend Herwijn, "Technical assessment of hydrogen transport, compression, processing offshore," North Sea Energy (TKI Offshore Wind & TKI New Gas), Tech. Rep., 2020. [Online]. Available: https://north-sea-energy.eu/static/f9c806827555f23ec1bcdc92c510b7af/5.-FINAL-NSE3-D3.1-Final-report-technical-assessment-of-Hydrogen-transport-compression-processing-offshore.pdf

[86] S. Kuczynski, M. Łaciak, A. Olijnyk, A. Szurlej, and T. Włodek, "Thermodynamic and technical issues of hydrogen and methane-hydrogen mixtures pipeline transmission," *Energies*, vol. 12, no. 3, 2019.

[87] H. van 't Noordende and P. Ripson, "Baseline design and total installed costs of a GW green hydrogen plant," Institute for Sustainable Process Technology (ISPT), Tech. Rep., 2020. [Online]. Available: https://ispt.eu/media/ISPT-public-report-gigawatt-green-hydrogen-plant.pdf

[88] A. Mayyas, M. Ruth, B. Pivovar, G. Bender, and K. Wipke, "Manufacturing Cost Analysis for Proton Exchange Membrane Water Electrolyzers," National Renewable Energy Laboratory, Tech. Rep., 2019. [Online]. Available: https://www.nrel.gov/docs/fy10osti/72740.pdf.%0Ahttps://www.nrel.gov/docs/fy10osti/72740.pdf

[89] P. Swisher, J. P. Murcia Leon, J. Gea-Bermúdez, M. Koivisto, H. A. Madsen, and M. Münster, "Competitiveness of a low specific power, low cut-out wind speed wind turbine in North and Central Europe towards 2050," *Applied Energy*, vol. 306, p. 118043, jan 2022.

[90] NedZero, "The North seas standard enable growth with wind turbine standardization," https://www.nedzero.nl/en/news/the-north-seas-standard-enable-growth-with-wind-turbine-standardization, 2023, (last access: 24 March 2025).

[91] M. Vitulano, D. De Tavernier, G. De Stefano, and D. von Terzi, "Numerical analysis of static and dynamic wind turbine airfoil characteristics in transonic flow," in *Journal of Physics: Conference Series*, vol. 2767, no. 2, 2024, p. 022013.

[92] A. Aditya, D. De Tavernier, F. Schrijer, B. Van Oudheusden, and D. von Terzi, "Experimental investigation of the occurrence of transonic flow effects on the ffa-w3-211 airfoil," in *Journal of Physics: Conference Series*, vol. 2767, no. 2, 2024, p. 022031.

Curriculum Vitæ

Mihir Kishore Mehta

02-10-1994	Born in Gujarat, India

Education

2010–2012	**Higher secondary education** Gokalibai P.P. High school, Mumbai, India
2012–2016	**Bachelor of Technology, Mechanical Engineering** VJTI, India
2017–2019	**Master of Science, Sustainable Energy Technology** Delft University of Technology, Netherlands
2019–2023	**PhD researcher, Wind energy** Delft University of Technology, Netherlands

Experience

2024–Present	**Senior cost & value engineer, Onshore wind** Vattenfall, Netherlands

List of Publications & Presentations

1. *Mihir Mehta, Michiel Zaaijer, and Dominic von Terzi*: Designing wind turbines for profitability in the day-ahead market. Wind Energy Science 9.12 (2024): 2283-2300

2. *Mihir Mehta, Michiel Zaaijer, and Dominic von Terzi*: Drivers for optimum sizing of wind turbines for offshore wind farms. Wind Energy Science 9.1 (2024): 141-163.

3. *Mihir Mehta*: Optimum turbine design for offshore wind farms, optimizing for economic value, in EAWE Wind Energy Science Conference Glasgow, 2023.

4. *Mihir Mehta, Michiel Zaaijer, and Dominic von Terzi*: Optimum turbine design for hydrogen production from offshore wind. Journal of Physics: Conference Series. Vol. 2265. No. 4. IOP Publishing, 2022.

5. *Mihir Mehta, Gijs van Holthoon, Dominic von Terzi, and Michiel Zaaijer*: Technical and economic value of utility-scale wind-storage hybrid power plants in Hybrid Power Sytems Conference, 2021.